Compression wood formation in *Pinus strobus* L. following ice storm damage in southwestern Virginia

Benjamin A. Hook

Thesis submitted to the faculty of the Virginia Polytechnic Institute and State University in partial fulfillment of the requirements for the degree of

Master of Science

In

Forestry

APPROVED:

Carolyn A. Copenheaver, Chairperson

Audrey Zink-Sharp, Committee Member

Shepard M. Zedaker, Committee Member

April 22nd, 2010

Blacksburg, VA, USA

Keywords: Compression wood, reaction wood, ice storms, forest ecology, Appalachian Mountains, eastern white pine, northern white pine, freezing rain, wood anatomy, light microscopy, tracheid size, lumen size, tracheid shape

Copyright 2010, Benjamin A. Hook

Compression wood formation in *Pinus strobus* L. following ice storm damage in southwestern Virginia

Benjamin A. Hook

ABSTRACT

To evaluate the compression wood response in eastern white pine (*Pinus strobus* L.) following a severe ice storm in 1994, 47 trees were felled in 2007 and cross-sectional samples were collected at 0.5 (±0.2) m stem height. The disks were sanded and digitally scanned, and the cross-sectional area (mm^2) of compression wood within each tree-ring was quantified using image analysis software. Topographic data (slope, aspect, and elevation) were also recorded for each *P. strobus* tree, along with a modified competition index. Wood anatomical features were also quantified in the three years before and after the storm along a tree diameter gradient. Although tree age was relatively constant in this stand, tree size was influenced by topographic position; larger trees grew in the valley while smaller trees were found growing in thin soils at the mid-slope position. When the cohort was about 25 years old, ice deposition caused a heterogeneous compression wood response which was highly related to tree size. In the thirteen years following the ice storm, the 6 – 9 cm (2007) diameter class formed significantly more compression wood area than any other, followed by the 10 – 13 cm (2007) diameter class. The tree diameter range that formed the most post-storm compression wood was 4 – 8 cm at the time of the storm, suggesting that this diameter range was most affected by 8.5 cm of ice loading in *P. strobus*. Trees > 18 cm in 1994 did not form any compression wood after the storm, but many experienced a growth release to fill canopy gaps. Topographic variables did not influence compression wood formation directly, but only one plot was

sampled so these results are tenuous. However, topography did influence tree size which was the most important predictor in compression wood. There was no relationship between compression wood area and competition index. Due to compression wood formation after the ice storm, cell wall thickness and cell circularity were significantly higher in the 1994 tree-ring than in other rings examined (1991 – 1993, 1995, and 1996). Tracheid and lumen diameters were significantly smaller in compression wood cells (30.5 and 19.5 µm, respectively) than in normal wood (36.8 and 28.4 µm, respectively); opposite wood cells were intermediate in size (32.4 and 24.4 µm, respectively). Due to small tracheid size, compression wood contained significantly more cells mm^{-1} (33) than normal wood (27), but no significant differences in cell wall area. Therefore, cumulative cell wall area occupied 47% of the cross-section in compression wood tissue on average, compared to 31% in normal wood. Dispersing tree weight across a greater surface area may help compression wood to prop up a bent tree, but reduced lumen area may also impact hydraulic conductivity in the stem.

Acknowledgements

I would like to thank my committee members for their assistance throughout this project. My committee chair and major advisor, Dr. Carolyn Copenheaver, has been extremely helpful. She has wisely guided my research, helping me to remove unimportant details and focus on what truly matters in this document. Thanks to my funding source, the Sustainable Engineered Materials Institute (SEMI), and to its director, Dr. Audrey Zink-Sharp. Dr. Zink-Sharp was a valuable committee member, very helpful in matters of microscopy as well as wood anatomy. Thanks also to Dr. Shepard Zedaker who was helpful in suggesting approaches for the field component of my research, and in data analysis methods.

My love goes out to my family, whose constant support throughout my life has made me what I am today. My parents, Martin and Sally Hook, have been a source of stability for me; I know I can always count on them, and I will always be there for them. My brother Joey has been a great friend to me, but I miss him; I can feel his love all the way from Texas – it's that big. I will visit you soon brudder… However, the person who deserves my deepest gratitude is my wife, Kara Hicks. Her calm, rational nature has kept me going these past two years. Throughout my thesis writing process, she has been there; bringing me coffee, food, band-aids… She has seen the worst of it and lived to tell the tale – without her support and patience I would probably go insane. I am so blessed to have her in my life –and although she laughed when I finally finished it and asked if she'd like to read it, this work is dedicated to her.

Table of Contents

List of Tables

List of Figures

I. Introduction

Ice storms are one of the most common yet unpredictable, types of natural disturbance in the eastern deciduous forest biome (Lemon 1961, Lafon et al. 1999). Ice storms can be severe in eastern North America, due to the confluence of factors that favor freezing rain formation (Lafon 2004). In ice storms liquid precipitation freezes on impact with objects (Lemon 1961). Also referred to as "glaze" or "rime" ice accretion on branches can increase the load many times their original weight causing a great deal of breakage or bending. Two separate components work in concert to produce the damage seen after the event: the meteorological event itself and the response of the individual tree species (Bragg et al. 2003). Similar levels of ice loading will trigger different responses in trees depending upon their species, diameter, foliage surface area and disease (Warrillow and Mou 1999, Rhoades and Stipes 2007). Small-diameter conifer stems are more likely to bend than break and will subsequently form denser compression wood to re-straighten the stem and grow toward the canopy (Timell 1986). Trees in the seedling to pole stage experience the highest rates of growth, so understanding compression wood dynamics in this smallest size class is important knowledge for future growth and yield of trees (Zedaker et al. 1987).

Compression wood formation lowers the quality of softwood lumber and pulpwood so it is important to understand how ice storm disturbances affect its formation. Softwoods are the most important group of trees in the pulp and lumber industries, but to date, no study has quantified the amount of compression wood formation due to an ice storm (Rhoads et al. 2002). Therefore, the purpose of this project is to quantify the amount of compression wood formation in eastern white pine (*Pinus strobus* L.) trees and evaluate the influence of age, size,

location, and competition on its formation. The range of *P. strobus* extends over much of the eastern deciduous forest, from the Appalachian Mountains, USA, into Canada, and its wood is prized for its workability and light weight, characteristics which are hindered by compression wood formation (Wendel and Smith 1990, Donaldson et al. 2001). Therefore, this study will benefit the wood products industry adding a unique perspective to the growing body of literature on ice storm damage, which has previously focused on external tree damage and stand dynamics, but has not examined wood anatomy.

My research objectives were to quantify the cross-sectional area of compression wood formed in *Pinus strobus* trees before and after a major ice storm in relation to tree age, size (diameter, height, and crown class), topographic factors (slope, elevation, and aspect), and a modified competition index. A second objective was to quantify physical characteristics of wood cells (cross-sectional diameter and area of tracheids and lumina, and cell circularity) formed in the three years before and after ice storm damage in 1994 along a tree diameter gradient. Measurements were evaluated with respect to cell type (compression, normal, or opposite wood cells), tree diameter, and year of cell formation.

II. Literature Review

Ice Storms

Ice storm occurrence and magnitude is highly unpredictable. Minor ice storms occur nearly every year in some portion of the eastern United States (Lemon 1961). Their damage to forests is usually minor; clearing away dead and diseased limbs from otherwise healthy trees (Timell 1986). Truly severe ice storms leave a strong and lasting impression on forests and people, for many years after the event, and are the subject of great interest. Ice storm publications appear in the literature as sporadically as the events themselves, and can sometimes offer conflicting silvicultural recommendations. This conflicting advice is due to the rarity of ice storms; they are the subjects of observational case studies, each in a different location with unique climates, topographies, and forest communities.

Freezing rain is caused by rain falling through a super-cooled layer of air near the earth's surface and freezing on impact with objects on the ground (Lemon 1961). The thickness of the layer of cold air beneath an overriding layer of warm, moist air determines the type of precipitation that reaches the ground. Only a specific mix of conditions will produce icing: thinner layers of cold air produce rain because the water does not freeze, while thicker layers of cold air produce sleet, ice pellets, or snow (Lemon 1961).

While ice storms occur nearly every year in some portion of the eastern deciduous forest (Lemon 1961), estimates of return intervals vary from two years (Rhoads et al. 2002) to 20 years (Whitney and Johnson 1984). In southwest Virginia during the period 1925 – 1953 there were 7 – 13 recorded glaze storms; the local ice storm return interval is about one storm

every three years (Nelson and Zillgitt 1969). Much of the damage that is reported is due to ice loading on tree limbs that causes breakage, indirectly impacting utility lines, and damaging public and private property (Irland 2000). Geographic and climatic variables as well as species-specific traits of trees combine to produce the patchy distribution of ice storm damage across the forest landscape. The patchiness is due to the random ice deposition of a moving weather front stochastically influenced by wind and temperature over varied topography (Table 1).

Table 1. *Geographic, climatic, and tree-specific factors contributing to ice damage to trees in the eastern deciduous forest biome (Table modified from Panshin and de Zeeuw 1980, Amateis and Burkhart 1996, Lafon et al. 1999, Warrillow and Mou 1999, Mou and Warrillow 2000, Rhoads et al. 2002, Bragg et al. 2003, Darwin et al. 2004, Lafon 2004, Millward and Kraft 2004, Lafon 2006, Rhoades and Stipes 2007, Stueve et al. 2007)*

Geographic	Climatic	Tree-Specific
Latitude / Longitude	Air temperature (at different atmospheric strata)	Species
Elevation	Ground temperature	Diameter
Aspect	Precipitation Type	Leaf Surface Area
Slope	Precipitation Amount	Growth Form: Excurrent vs. Decurrent
Landform Type	Duration of Storm	Presence of Rot or Disease
Edaphic conditions	Number of Repeated Storms	Specific Gravity
Surrounding Topography	Wind Speed	Modulus of Elasticity
Surrounding Vegetation	Wind Direction	Modulus of Rupture

As trees are immobile, their location on the landscape determines their fate before, during, and after an ice storm. Topography not only influences species composition on different aspects and landforms, but also influences climatic patterns (Stueve et al. 2007). Furthermore, certain sites could be predisposed to damage due to characteristics of the soils, such as shallow depth to bedrock or poor soil structure leading to inadequate rooting potential. Poor rooting stability was found to be an important factor in uprooted trees in a review of ice storm literature (Bragg et al. 2003).

Damage to individual trees depends on species-specific properties of their wood, and defects in their wood. Factors such as modulus of elasticity, modulus of rupture, specific gravity, leaf/needle surface area, and growth form all play a role in how much ice a healthy tree can support (Panshin and de Zeeuw 1980). Diseased or hollow trees are more likely to experience breakage under ice loads than healthy trees (Rhoades and Stipes 2007).

Finally, the stand-level response of the forest to icing depends upon the pre-storm composition of the forest, which has been shaped by past disturbances and site conditions (Whitney and Johnson 1984, Mou and Warrillow 2000, Copenheaver et al. 2006). Therefore, many of the factors involved are correlated with other factors leading to a complex system, e.g. aspect influences species composition, as well as amount of precipitation (Bragg et al. 2003). Due to this complexity, most observational studies produce highly varied results concerning species-specific responses to glazing.

A meteorological phenomenon known as cold-air damming causes many glazing events in the ridge-and-valley physiographic region of the Appalachian Mountains (Lafon et al. 1999,

Bragg et al. 2003). Cold-air damming occurs when a layer of sub-zero air becomes trapped between one side of a mountain and an overriding layer of warm, moist air (Forbes et al. 1987). The differences in air temperature on either side of a mountain produce different amounts of ice accretion on opposing aspects. This leads to the spatially localized patterns of disturbance observed on eastern slopes in the Appalachians (Lafon et al. 1999, Steuve et al. 2007). Similarly behaving "frost-pockets", in which masses of cold air become trapped in low-elevation areas, serve as a contributing factor to ice formation (Boerner et al. 1988).

Forest Stand Dynamics Related to Ice Storms

The impact of ice storms on forest succession varies according to the condition of the forest when the icing occurs. For example, ice storms can accelerate forest succession by unduly damaging early-successional species such as Virginia pine (*Pinus virginiana* Mill.) or pitch pine (*Pinus rigida* Mill.), compared to late successional species (Lemon 1961, Whitney and Johnson 1984, Boerner et al. 1988, Lafon et al. 1999, Warrillow and Mou 1999, Brommit et al. 2004, Lafon 2006, Rhoades and Stipes 2007). In other forest conditions, ice damage can slow succession by letting more light penetrate through the canopy, thus allowing shade-intolerant early-successional species to establish (Rebertus et al. 1997, Irland 1998, Rhoads et al. 2002, Lautenschlager et al. 2003a, Lautenschlager et al. 2003b, Lafon 2004, Millward and Kraft 2004). Other forests experience no alteration of succession because the replacement vegetation that established after the ice storm closely matches current overstory species (Mou and Warrillow 2000, Copenheaver et al. 2006).

In general, conifers exhibit poorer re-sprouting ability after stem breakage than hardwoods, which could put them at a disadvantage in late succession forests (Whitney and Johnson 1984, Brommit et al. 2004, Dietze and Clark 2008). On the other hand, their excurrent tree form distributes the ice load more evenly than the decurrent form of many hardwoods (Irland 2000). Limbs that are diseased or infected with rot fungi are likely predisposed to breakage during an ice storm regardless of an excurrent form (Rhoades and Stipes 2007). By breaking structurally weaker limbs and letting more light into the understory, ice storms may be deleterious for overstory trees but beneficial for suppressed trees. Such smaller trees, if undamaged by falling limbs, actually experience a release from light suppression.

Overall, light ice deposition creates diffuse canopy damage, accelerates succession by unduly damaging early-successional species, and favors growing conditions for late-successional species. On the other hand, heavy ice deposition causes canopy gaps due to tree falls and could slow or reverse succession by letting in enough light to allow establishment of early-successional species (Mou and Warrillow 2000, Smolnik et al. 2006). If disturbances disproportionately affect certain geographical locations more than others, future patterns in succession and species composition could be influenced by topography (Lafon et al. 1999).

Forest Management Implications of Ice Storms

Following an ice storm event, the trees left standing are temporarily released from competition and quickly grow to fill in gaps in the canopy (Lemon 1961). Ice storms cause a sudden increase in the amount of light penetration in forests, but one study found that within

seven years light levels may actually be lower than before the storm due to canopy regrowth (Beaudet et al. 2007). Six years after an ice storm in Quebec, Canada, sugar maple (*Acer saccharum* L.) had recovered pre-storm growth rates while less dominant species declined during this period (Pisaric et al. 2008). In other forest types regeneration of the canopy may take up to 25 years to recover (Duguay et al. 2001). Time for canopy recovery is influenced by differences in storm intensity, soil factors, geographical location, and microtopography.

Silvicultural recommendations for dealing with ice storms often conflict due to the irregular spatial distribution of icing and the unpredictable timing of the storms. For instance, ice-caused stem breakage was greater in thinned plantations of loblolly pine (*P. taeda* L.) than un-thinned plantations, and fusiform rust (*Cronartium fusiforme* Hedg. & Hunt ex Cumm.) was weakly associated with branch breakage (Belanger et al. 1996). At another site, tree spacing did not influence ice storm damage on *P. taeda* plantations, but trees with forked branching patterns were more likely to break than non-forked trees (Amateis and Burkhart 1996).

After a severe ice storm breaks tree tops and weighs smaller trees to the ground a common reaction of many landowners is to consider the stand lost and perform a salvage logging operation to recover perceived timber losses (Irland 1998). This is probably the worst approach to take; ice storm hysteria often leads to excessive harvesting, which floods the timber market, thus lowering the price of timber (Irland 2000). Such operations are difficult to conduct quickly and healthy trees must often be harvested along with damaged trees to make the operation economically viable (Bragg et al. 2003). Many of these salvage operations remove the large trees with broken tops, leaving the smaller non-merchantable stems bent by

the ice, believing that they are doing right by leaving the advanced regeneration in place. However, the compression wood they will form is economically undesirable.

Trees have a surprising ability to rebound from breakage, as long as branches are still intact on the tree; if bole breakage occurs below the crown the tree will not be able to produce photosynthate and regenerate (Timell 1986). The most frequent recommendation in the ice storm literature is to thin from below and remove severely bent stems, so that available resources will be allocated by larger trees with intact branches (Shepard 1975).

In pine plantations equal spacing of trees is recommended to help trees develop symmetric crowns. Row or strip-thinning techniques should not be used because trees on row edges will grow toward the canopy gap through phototropism and develop asymmetrical crowns; making them more vulnerable to severe breaking or bending under heavy glaze (Timell 1986). One study found that row-thinned plots had six times as much damage as those that were thinned from below, and three times as much damage as un-thinned plots (Shepard 1975). After ice storm damage, early removal of irregular or crooked stems is suggested while maintaining regular tree spacing (Johnston 1962).

The timing of the thinning operation is also important, or the timing of the ice storm, depending on your viewpoint (Bragg et al. 2003). Recently thinned stands are more vulnerable to ice and wind damage because tree roots are not as developed as in stands thinned 8 – 12 years before rime deposition (Shepard 1975). If repeated ice storms occur two or more years in a row in the same location, the effects can be especially devastating to trees that were bent by

the previous storm. In one study, stands that had been thinned from below only received minor damage from the second consecutive ice storms (Shepard 1978).

It is impossible to predict the timing of future ice storms, so a proactive silvicultural plan should be used in ice-prone areas, combined with targeted thinning treatments following severe ice events. In addition to proper thinning, the spacing of trees in plantations can influence the amount of compression wood they may form. Close spacing (5' x 5') of pine trees reduces their tendency to branch, thereby decreasing their compression wood content in knot wood, and the likelihood of basal crook formation (Timell 1986).

Severe Winter Weather in Southwest Virginia

In 1994, two major ice storms hit the ridge and valley region of southwest Virginia: February 9 – 13, and March 1 – 3, (Lott and Ross 1994, Lafon et al. 1999). The weather patterns that created these ice storms were typical for this area; a stationary front to the southeast produced freezing rain near the surface to the north of the front (Lott and Ross 1994). The only differences in the ice storm of 1994 were the high amounts of precipitation that fell from repeat events between January and March. An ice layer 3 – 8 cm thick was deposited across central and western Virginia (Watson 1999). Ten to twenty percent of trees in this area were damaged, and ninety percent of residents were without power due to downed utility lines (Watson 1999).

Another notable ice storm in recent history occurred on February 18 – 19, 1979; a local snow-and-ice storm known as the "President's Day Storm." At the time is was the worst storm

in 57 years, depositing about 2.5 cm of ice in southwestern Virginia (Watson 1999). Significant damage to forests occurred in the area due to the ice (Whitney, 1984). Most other winter storms in the area produce large amounts of snow rather than ice such as in the "Superstorm of '93" in which 76 – 107 cm of snow were dropped across southwestern Virginia between March 13 – 14, 1993 (Watson 1999).

While an average return interval for minor ice storms is 3 years, severe storms are much less common (Nelson and Zillgitt 1969). Each winter storm is different, and variable climatic and topographic conditions lead to different damage responses in trees. In addition, the tree response is also largely governed by size; larger-diameter trees are able to support greater loads of ice, but when a critical weight load is reached their limbs or tops tend to break, whereas smaller-diameter trees undergo plastic deformation and then form compression wood in the years following the storm to re-straighten the trunk (Bragg et al. 2003).

Compression Wood

Compression wood is a type of reaction wood, which is primarily a gravitropic response to an exterior force that moves a tree from an optimal, usually upright, position (e.g., ice, wet snow, heavy wind, rock falls, tree falls, or landslides) (Timell 1986). There are two types of reaction wood: compression wood and tension wood. Most gymnosperms form compression wood on the lower side of the stem to "push" the tree up to a more favorable position for gathering light; angiosperm species use an opposite strategy and form tension wood on the upper side of the stem to "pull" the stem up to a better position (Timell 1986). Looking at a

stem cross-section reveals which way and when a tree was leaning from the mean direction of compression wood and the year of its formation (Figure 1). Dendrochronologists have long made use of its presence in determining the timing and return interval of any number of external bending stimuli, including hurricanes, avalanches, landslides, and even thermokarst dynamics resulting from climate change (Pillow 1931, Douglass 1940, Agafonov 2004).

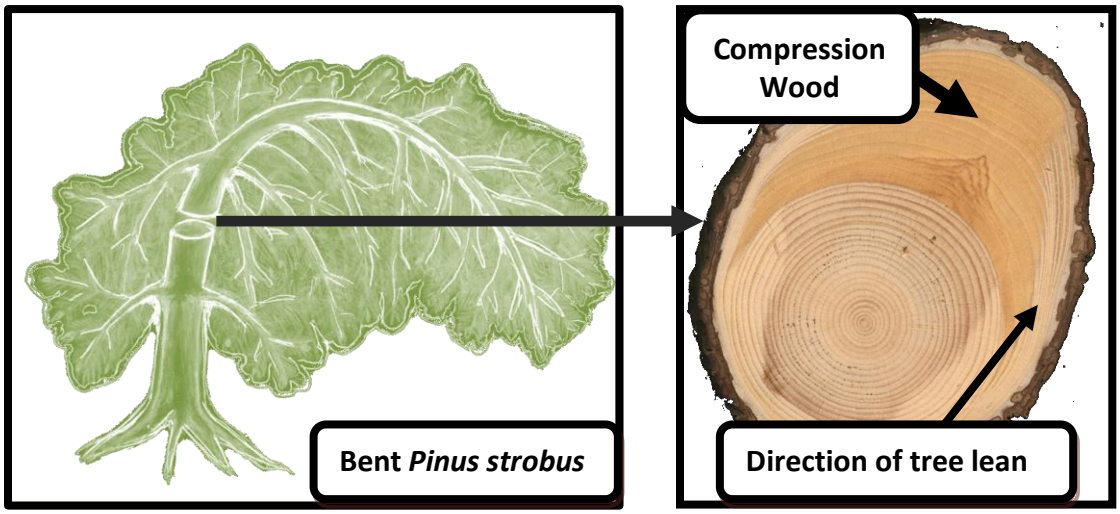

Figure 1. *An eastern white pine (P. strobus) tree showing location of a cross-section containing severe compression wood formation. The direction and timing of when a tree was leaning can be determined by the presence of compression wood.*

While most ice storm studies focus on the effects of glaze on limb breakage or forest succession, little research has examined the quantity of compression wood formation that results specifically from ice-caused stem bending (Lafon and Speer 2002, Smolnik 2004). In most cases, conifer stems are bent downhill due to ice loading, causing compression wood formation on the underside of the tree. However one study found compression wood on the

uphill side of trees on a southwest aspect, presumably due to a prevailing uphill southwesterly wind (Duncker and Spiecker 2008). In rare cases, spiraled compression wood has been discovered in some cross-sections although the causes are still unknown (Douglass 1940, Timell 1986).

Compression Wood Formation

Trees use chemical signals to adapt to exogenous and endogenous influences (Plomion et al. 2000, Cosgrove 2005). When a pine leader or branch is displaced from a genetically determined optimal position, it forms compression wood cells to push the tree section back into chemical equilibrium (Du and Yamamoto 2007). Auxins (e.g. indole-3-acetic acid, IAA) and ethylene are known to be associated with compression wood formation, but the actual causes of compression wood are still unclear; auxins are likely involved in its formation (Du and Yamamoto 2007). It is thought that auxins concentrate near amyloplasts, which accumulate on the under stem side of the cambium due to gravity, leading to a high auxin/photosynthate ratio possibly triggering compression wood formation (Yamaguchi et al. 1983). It has been observed that sap-sucking insects such as balsam woolly adelgid (*Adelges piceae* Ratzeburg) can induce local pseudo-compression wood formation by lowering tree-sugar levels locally in the cambium, thus raising the auxin/photosynthate ratio in that area (Yamaguchi et al. 1983). A half-year lag time was found in photosynthate transport in *L. gmelinii*, accounting for autocorrelation of tree-ring parameters with past-year environmental signals (Kagawa et al. 2006).

Originally it was assumed that the side of the tree experiencing compressive stress formed compression wood, resulting in the name "compression wood" (Bowyer et al. 2007). However, around the turn of the 20th century, Robert Hartig found that in trees suspended upside down and then bent upwards, compression wood formed on the lower stem side, rather than the inner concave side of the bend where compressive stresses were generated (Du and Yamamoto 2007). Recent tree experiments in earth's orbit have found that mechanical stress may also be a factor in compression wood formation, which occurred on the concave side of stems of Douglas-fir (*Pseudotsuga menziesii* (Mirb.) Franco) bent to 45° in the microgravity environment onboard the space shuttle Columbia (Kwon et al. 2001).

Compression wood can also be artificially induced by exogenously applied auxin or auxin inhibitors. Experiments with morphactin, a known auxin inhibitor, applied to the circumference of tilted Japanese larch (*Larix leptolepis* Gordon) stems resulted in compression wood growth around the entire stem just above the morphactin treatment, while the control group formed compression wood only on the underside of the stem; abnormal amounts of extra compression wood formed above the morphactin blockage due to the increased auxin/sugar ratio (Yamaguchi et al. 1983). Growth hormones caused compression wood formation in Japanese black pine (*Pinus thunbergii* Lamb.) saplings injected with ferulic acid and indoleacetic acid (a type of auxin) (Terashima 1979).

Compression wood forms in lateral branches under apical control to hold them at genetically determined branch angles, which vary by species (Timell 1986). However, when released from apical control, branches form extra compression wood under the branch to bend

upward and replace the apical stem around the end of June (Wilson and Archer 1981). Loss of the apical leader stem interrupts its production of auxin which keeps lateral branches from turning upward and becoming dominant stems (Wilson and Archer 1982). Lateral branches of girdled trees treated with auxin do not form extra compression wood and bend upward to replace the leader, due to auxin suppression (Wilson 1986). If a branch is intentionally bent upwards, compression wood will form on the upper side to bend it back down to an optimal position (Du and Yamamoto 2007).

Auxin is thought to travel basipetally, from shoot tip to root, activating the cambium as it travels through it, but no lag time was found in cambial activation of balsam fir (*Abies balsamea* L.) and black spruce (*Picea mariana* Mill.) (Thibeault-Martel et al. 2008). That is, wood in all parts of the tree began growing simultaneously at the start of the growing season, suggesting that auxin is already present in all parts of the stem when the cambium reactivates (Thibeault-Martel et al. 2008). Both root and stem wood of white spruce (*Picea glauca* Moench.) experienced an immediate pulse in growth when a forest edge was created by road building (Urban et al. 1994).

Wet wood tissue and individual tracheid cells undergo a plastic deformation process when bent, in which a Velcro-like action theoretically takes place at the molecular level; once the cell walls are bent from their original position they form chemical bonds with their new neighbor cells, thus holding the stem in a bent position (Keckes et al. 2003, Kretschmann 2003). Compression wood must act against these chemical bonds, slowly bending the stem upward over time through longitudinal swelling (Du and Yamamoto 2007). It follows that larger bent

trees may require more force to right themselves than smaller bent trees and may require more compression wood formation.

Trees often allocate resources differently to various parts of the plant depending on growing conditions (Pisaric et al. 2008). Severely bent trees may form a great deal of compression wood at the expense of growth of other parts of the tree. A study comparing stem growth to root growth of Dahurian larch (*Larix gmelinii* Rupr.) found twice as much radial growth in stem wood as in root wood of a tree containing compression wood, compared to trees without compression wood which formed relatively equal amounts of wood in the stem and roots (Kagawa et al. 2006). There seems to be a tilting threshold for compression wood induction, in that trees tilted > 10° form significantly more compression wood than those tilted < 10° from vertical (Lachenbruch et al. 2010).

Physical Properties of Compression Wood

For compression wood tissue to push a tree back to an upright position after displacement, it expands in the longitudinal direction on the underside of the stem (Archer 1987, Du and Yamamoto 2007). Compression wood tracheids have different physical properties than normal tracheids: thicker cell walls and high angle in the cellulose microfibrils with respect to the longitudinal cell axis. The higher microfibril angle causes a higher shrink-swell potential in compression wood than normal wood (Table 2) (Panshin and de Zeeuw 1980, Timell 1986).

Table 2. *Differences in physical properties of compression and normal woods at the cellular level. Table modified from Panshin and de Zeeuw 1980 and Timell 1986.*

Physical Properties	Compression Wood	Normal Wood
Tracheid shape in cross-section	Rounded/Circular	Boxy/Hexagonal
Intercellular spaces	Present	Absent
Tracheid diameter	Shorter	Longer
Cell wall thickness (*P. strobus*)	Thicker	Thinner
Layers within secondary cell wall	S_1, S_2 (modified)	S_1, S_2, S_3
Microfibril angle within S_2 layer	~45° to longitudinal axis of tracheid cell	~30°
Helical checks and cavities in S_2	Present	Absent

Compression wood tracheids are more circular than the box-shaped tracheids of normal wood (Figures 2 & 3). Cylindrical structures are more capable at load-bearing than box-shaped structures, which tend to buckle at the corners during structural failure. In addition, the extra mass supplied by increased numbers of compression wood cells with higher cell wall thickness gives it greater stability than normal wood. Due to this thickened cell wall, it is possible that hydraulic conductivity is impaired through this tissue (Spicer and Gartner 2002).

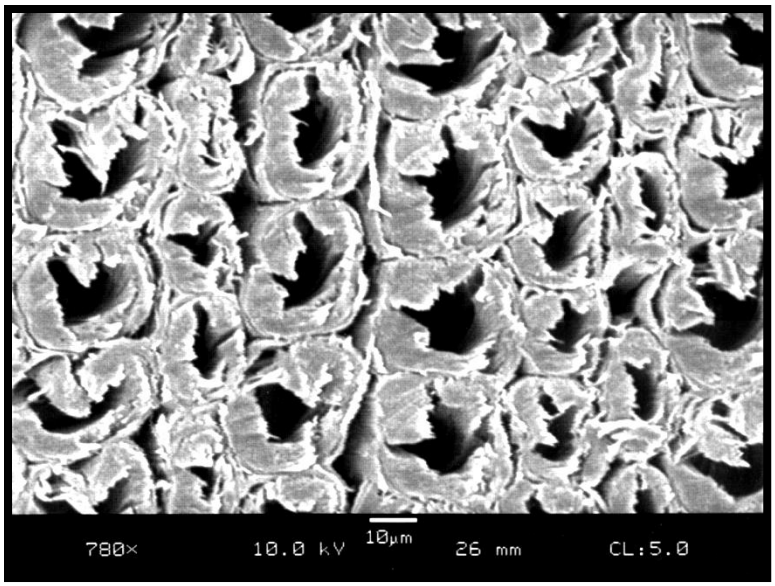

Figure 2. *Scanning electron microscope image of a cross-section of Pinus strobus compression wood cells. Note the thick-walled circular tracheids with intercellular spaces. Some splitting occurred along helical checks in the cell walls during sample preparation. Measurement bar equals ten microns.*

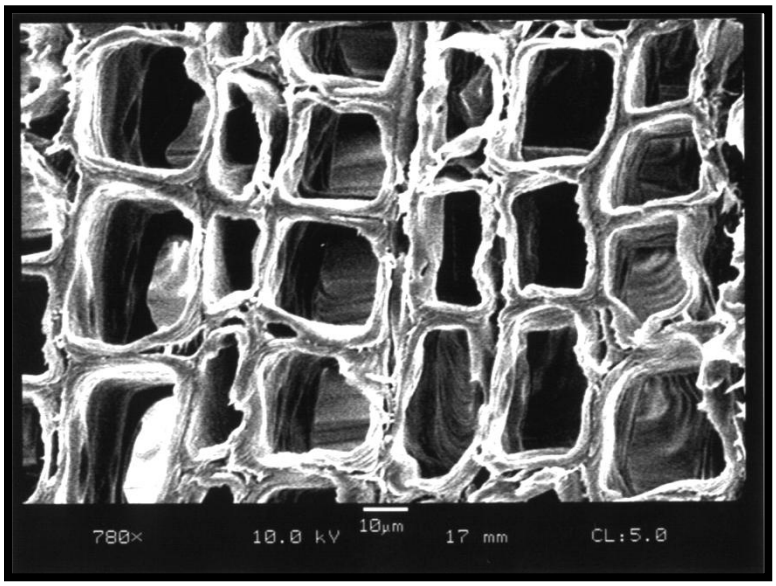

Figure 3. *Scanning electron microscope image of a transverse section of Pinus strobus normal earlywood cells. Note the box-shaped, thin-walled tracheids with no intercellular spaces. Intercellular pitting is visible on the inner walls of tracheids in the lower left corner of the image. Measurement bar equals ten microns.*

Compressive stress, defined as the total compression force divided by cross-sectional area, is one of three stresses trees experience in bending stress. Bending stress (σ) includes compressive, tensile, and shear stresses, which cause distortion in tissues known as strain (ϵ) (Panshin and de Zeeuw 1980). The amount of stress a material can withstand depends on its modulus of elasticity (*E*) (Panshin and de Zeeuw 1980).

Wood tissues are elastic and will return to their original position as long as stress levels do not exceed the proportional limit (Panshin and de Zeeuw 1980). Beyond this limit, irreparable bending or breaking will occur. Specific gravity, the ratio of a material's weight to an equal volume of water, has a strong influence on wood strength and is considered one of the best predictors of modulus of rupture, or the amount of weight wood can withstand before failure in bending (Panshin and de Zeeuw 1980). The specific gravity of compression wood is higher than normal wood (e.g. ponderosa pine (*Pinus ponderosa* C. Lawson) compression wood specific gravity is 0.467, while the specific gravity of normal wood is 0.354) (Timell 1986).

The larger microfibril angle of compression wood serves two functions: greater longitudinal shrink-swell potential (but lower transverse shrinkage) than normal wood tissue and greater support for the cell wall radially and tangentially (Cave 1972, Timell 1986). A helix of parallel rows of cellulose microfibrils, which are hydrophobic, spiral around the inside of the cell wall embedded within a three-dimensional matrix of lignin, which is hydrophobic (Meylan 1972). Therefore, when water molecules soak into the cell they cause it to swell elongating the cell longitudinally (Boyd 1972, Cave 1972). A theoretical model predicting stresses in wood cells

found that microfibril angles greater than 30.94° create compressive stresses (compression wood), and angles less than 30.94° create tensile stresses (normal wood) (Archer 1987).

In most tree diameter classes, compression wood rings are significantly wider, tracheids are shorter, and the specific gravity higher than opposite wood on the upper stem side (Jain and Seth 1980). However, in larger diameter classes, ring widths on opposite stem sides are more similar than in smaller diameter classes (Jain and Seth 1980). Radial eccentricity of growth rings and compression wood are not necessarily caused by the same mechanism because they do not always co-occur, although they do in over 99% of samples (Duncker and Spiecker 2008).

Chemical Properties of Compression Wood

There is a greater percentage of lignin and galactose in compression wood and less cellulose, glucose and mannose than in normal wood (Table 3) (Mukoyoshi et al. 1981, Timell 1986). In addition, the compression wood lignin molecule contains higher proportions of condensed p-hydroxyphenylpropane units than any other lignin (Nimz et al. 1981). Hence, it is termed a guaiacyl-p-hydroxyphenyl, or GH-lignin, while normal gymnosperm wood contains a guaiacyl, or G-lignin (Timell 1982). The higher number of condensed GH-lignin units give the compression wood cell wall greater rigidity (Yasuda and Sakakibara 1981). Compression wood also contains 1.4 times as much Klason lignin and more carbon-carbon bonds as normal wood lignin (Nimz et al. 1981, Hatfield and Fukushima 2005).

Table 3. *Differences in chemical properties of compression and normal woods. All values in percent extractive free sapwood of P. strobus, table modified from Timell (1986).*

Chemical Constituent	Compression Wood (%)	Normal Wood (%)
Lignin	39.4	29.0
Acetyl	0.8	1.2
Uronic Anhydride	4.8	5.2
Galactose	11.0	3.8
Glucose	32.2	43.6
Mannose	3.8	8.1
Arabinose	1.0	1.7
Xylose	6.7	7.0
Cellulose	28.9	40.9

The smaller percentage of cellulose is likely due to the increased lignification of the cell wall. In compression wood cells there is more lignin matrix surrounding the scaffold of cellulose microfibrils than in normal wood. Another consequence of the increased amount of lignin is the slow decay process of compression wood compared to normal wood. Decaying fungi consume the cellulose component of wood, not lignin, so compression wood tissues, including knot wood, will commonly remain in the forest long after normal wood tissues in the same tissue have deteriorated (Timell 1986).

The lignin of compression wood fluoresces under ultraviolet (UV) light. The amount and type of lignin in the woody cell wall determines its UV light absorption (Timell 1982). Specifically, a 1,3-glucan in compression wood may give rise to the fluorescence that is not seen in normal wood of similar cell wall thickness. This specific type of lignin is a natural

fluorophore, which when hit with UV light, the electrons within enter an excited state causing the material to glow; this glucan is most likely located on or in the helical ribs of the S_2 layer of the secondary wall, which is the most fluorescent area of the cell wall (Timell 1982). Normal wood, by contrast, is more lignified in the compound middle lamella causing this area to be more fluorescent than the cell wall (Donaldson et al. 2010).

Researchers have employed epifluorescence microscopy to determine the amount and type of lignin present in a variety of wood types (Timell 1982, De Micco and Aronne 2007). This modified layer, named the S_2(L) layer, exhibits unusually high UV absorbance due to its high lignin content (Timell 1982). Hydrofluoric acid has been used to remove polysaccharides from compression woods of balsam fir (*Abies balsamea* (L.) Mill), red spruce (*Picea rubens* (Sarg.)), and tamarack larch (*Larix laricina* (Du Roi) K. Koch), to create "lignin skeletons" of tracheids. These skeletons reveal the presence of the highly lignified middle lamella and primary wall, the S_1, S_2(L), and S_2 layers, with the branching network of cellulose and holocellulose removed (Timell 1982). The ratio of blue to UV fluorescence may be a better way to quantify compression wood severity than total fluorescence of a sample (Donaldson et al. 2010).

Detection and Classification of Compression Wood

In addition to detecting compression wood using epifluorescence microscopy, other methods include radiation densitometry, hyperspectral image analysis, and histological staining (Cown and Clement 1983, Timell 1986, De Micco and Aronne 2007, Duncker and Spiecker 2009). Different approaches may be necessary with different tree species, as the dark color of

compression wood varies among species. The color of wood is a result of both light-scattering and light-absorbing characteristics; dark compression wood scatters less light than normal wood due to its physical qualities (thicker cell walls), and absorbs more light due to its chemical properties (higher lignin content) (Timell 1986). Detection is relatively easy in *P. strobus* wood with the naked eye, because its darker color contrasts the light blonde color of the normal wood tissue.

Detection is also possible using a transmitted-light microscope if ultra-thin samples of wood are cut with a microtome and mounted on glass slides. In unstained slides, compression wood is more opaque than normal wood in transmitted light (Timell 1986). Selective stains such as safranin, malachite green, and astra blue may also used to bring out the contrast between cellulose and lignin (Timell 1986, De Micco and Aronne 2007). Samples can be viewed in transmitted light, reflected light, UV light, polarized light, and through a variety of filters and lenses (Timell 1986). Epifluorescence microscopy combined with histological staining reveals more details within cell walls than autofluorescence of unstained sections or transmitted light microscopy of counterstained samples (De Micco and Aronne 2007). Scanning electron microscopes (SEM) and transmitted electron microscopes (TEM) can also be used to visualize the cellular structure of wood cells (Fromm et al. 2003).

Researchers have created many different classification systems for classifying the severity of compression wood in tree rings. Yumoto et al. (1983) created a six-class system of compression wood severity, based on qualitative observation of anatomical features that characterize compression wood, including cell circularity, presence of intercellular spaces, UV

absorbance, and other attributes. This system requires that microtome sections be prepared and observed with a transmitted-light microscope (Timell 1986).

Other researchers have proposed simpler systems requiring less preparation, such as a four-class rating system designed by Harris (1977). This method requires only surface sanding of stem cross-sections and then classification of the rings as severe (class 3), moderate (class 2), or mild (class 1) compression wood, or normal wood (class 0) (Table 4) (Harris 1977). The advantage of this system is that the only tools needed are a handsaw, several grades of sandpaper, and a hand lens. However, a quick and simple classification system may produce coarser results. Measurement precision should reflect the objectives and needs of the study.

Table 4. *Four-class compression wood rating system modified from Harris (1977).*

Grade	Description of amount of compression wood in a tree-ring
3	Dark wood tissue occupying the whole width of a growth increment
2	Dark wood tissue occupying at least 45° of an arc, and more than half of the tree ring's radial measurement
1	Small areas of dark wood tissue occupying less than 45° of an arc, and less than half of the tree ring's radial measurement
0	Rings not containing compression wood

More recently, researchers have begun to make use of image analysis software to quantify the area and volume of compression wood in logs. Some have used existing software packages to select areas of compression wood in cross-sections (Wernsdörfer et al. 2004).

Others have designed software specifically to model the three-dimensional extent of compression wood in logs based on linking several cross-sections (Pont et al. 2007).

Problems Associated with Compression Wood in Wood Products

While compression wood is an essential adaptation in living gymnosperms that helps them compete for light in the forest canopy, its formation lowers the quality of timber because it causes warping in lumber products (Plomion et al. 2001). This is due to differences in density and shrink-swell potential between compression wood and normal woods, which causes excessive warping between the two tissues when the wood is dried (Panshin and de Zeeuw 1980). Greatest amounts of warping when dying wood are found in boards that contain both normal and compression woods (Xu et al. 2009).

Cellular properties scale-up to properties of the wood tissue. The higher shrink-swell potential of compression wood is largely due to the greater microfibril angle of the cellulose spirals in cell walls as measured from the longitudinal axis. This gives water molecules more influence on the longitudinal shrinkage of the tissue (Panshin and de Zeeuw 1980). Pulpwood quality is also poorer in compression wood due to increased lignin and shorter, stouter wood cells than in normal wood (Watson and Dadswell 1957). Increased cell density and decreased lumen diameter associated with compression wood lowers water permeability in the stem, but the effect is minor relative to root and leaf limitations on water conductivity (Spicer and Gartner 2002). Historically, compression wood was used for the runners on Scandinavian sleighs, but there are few modern-day uses (Timell 1986).

Silvics of Eastern White Pine

Eastern white pine (*Pinus strobus* L.), also known as northern white pine, is a common North American conifer (Wendel and Smith 1990). Its native range spans most of the eastern deciduous forest biome, stretching across southern Canada, the northern Great Lakes and New England states, and extending southward into the Appalachian Mountains. A common pioneer species, it was a successful old-field invader on many abandoned farms in the eastern United States. It out-competes hardwoods on well-drained sandy soils of lower site quality, attaining merchantable value where there is little competition from the hardwoods. In the southern Appalachians, *P. strobus* grows best between 370 – 1070 m above sea level, mostly on northern aspects, and attains its greatest growth along low slopes near streams. In a species comparison study in the southern Appalachians, it outranked all other gymnosperm species in diameter growth, and was outranked in height only by yellow-poplar (*Liriodendron tulipifera* L.) (Wendel and Smith 1990).

Shady conditions can aid *Pinus strobus* establishment, which is one reason why more *P. strobus* recruitment is found on northern aspects (Wendel and Smith 1990). Intermediate in shade-tolerance, *P. strobus* is influenced by competition for light from neighboring trees. When subjected to conditions of over 80% shade, growth is reduced. In competition with broadleaf species such as oaks, growth stagnates and the tree eventually dies. It is most susceptible to light stress in its early development as a seedling. Stands of *P. strobus* can be regenerated by a variety of silvicultural methods including clearcuts, seed tree, shelterwood, and group selection. (Wendel and Smith 1990).

Pinus strobus trees have been used for a variety of purposes in history, although today as a forest product, they have been largely replaced by western white pine (*P. monticola* (Douglas ex D. Don)) and sugar pine (*P. lambertiana* (Douglas)). However, increased population will put pressure on timber markets in the future and *P. strobus* will likely increase in economic importance once *P. monticola* and *P. lambertiana* resources are used. The wood of *P. strobus* is prized for its light weight, ease of cutting, medium texture, straight-grain, and its light color, which is good for stenciling or dyeing (Panshin and de Zeeuw 1980). Its uses include crates, boxes, patterns, and millwork. Because compression wood causes warping of window frames and other interior wood products it is important to study its formation in *P. strobus,* which is used for such interior wood products (Donaldson and Turner 2001).

III. Methods

Study Area

Fishburn Forest, an education and research forest owned by Virginia Tech, encompasses most of the western side of Price's Mountain (37°11'N, 80°30'W) in Montgomery County, Virginia. The area is in the Ridge-and-Valley physiographic region of the central Appalachian Mountains. Plot elevation ranges from 600 to 620 m above sea level (m.a.s.l.). Slopes range from 15% to 65%. Soils are sandy Inceptisols, with the south ridge top in the Berks-Groseclose complex, the north ridge top in the Berks-Clymer complex, and mid-slopes and valleys in Berks and Weikert series (Creggar and Hudson 1985). Soil profiles were used as a measure of soil depth to bedrock because if the soil depth is shallow, then the tree may have greater potential

to be uprooted than if it had grown in deeper soil (Moore et al. 2008). On the northeast aspect depth was highest at the base of the slope and shallowest at the mid-slope position (Table 5).

Table 5. *Summary of depth to bedrock data at five slope positions along the northeast aspect.*

Slope Position	Depth to Bedrock (m)	Elevation (m.a.s.l.)
Ridge Top	1.05	607
Upper Mid-slope	0.40	603
Mid-slope	0.35	599
Lower Mid-slope	0.65	595
Bottom of slope	1.2	591

In addition to *P. strobus*, the site also included white oak (*Quercus alba* L.), northern red oak (*Q. rubra* L.), scarlet oak (*Q. coccinea* Muenchh.), chestnut oak (*Q. prinus* L.), American beech (*Fagus grandifolia* Ehrh.), sugar maple (*Acer saccharum* Marsh.), red maple (*A. rubrum* L.), downy serviceberry (*Amelanchier arborea* Michx. f.), pignut hickory (*Carya glabra* Mill.), mockernut hickory (*C. alba* L. Nutt.), blackgum (*Nyssa sylvatica* Marsh.), sourwood (*Oxydendrum arboreum* L.), sassafras (*Sassafras albidum* Nutt.), dogwood (*Cornus florida* L.), black birch (*Betula lenta* L.), and Virginia pine (*Pinus virginiana* Mill.).

Before Virginia Tech bought the property in the early 1960's, the area was selectively cut by the previous owners (Copenheaver et al. 2006). Removal of the merchantable timber opened up the canopy and let in more light, which allowed a cohort of intermediately shade-tolerant species such as *P. strobus* to flourish. Copenheaver et al. (2006) cross-dated *P. strobus*

trees in the Fishburn Forest understory and found that most recruited into the stands during the 1960s.

Average climate is temperate: yearly average temperature for the region is 10.8°C, and ranges from a monthly January mean of -0.6°C to a monthly July mean of 21.7°C. Annual precipitation averages 102 cm, with most rainfall in April and September (Mou and Warrillow 2000). Minor ice storms occur every 1 – 2 years in this area, but most are too light to do much damage to the forests; these storms can benefit the forest by clearing away dead branches and accelerating carbon cycling within forest ecosystems.

In 1994, four ice storms hit Price's Mountain (intermittently, February 9th – March 18th) and deposited an estimated total of 8.5 cm of ice (Rhoades and Stipes 2007). Some ice melting could have occurred between the events. However, once smaller trees were bent to the ground, additional ice deposition would not induce further bending, but merely adhere to completely bent trees. There would likely be increased danger from broken branches above; a study from Quebec found that only 22% of sub-canopy trees escaped damage from broken canopy branches; however, ice deposition levels in that storm were as high as 9 – 13 cm. (Duguay et al. 2001).

A study of forest damage from the 1994 ice storm in nearby Wythe and Bland counties found that highest tree damage occurred on south and east slopes, which were the windward sides of mountains in the Ridge and Valley region (Stueve et al. 2007). Our study plot was on the leeward side of Price's Mountain, and neither aspect was southeast facing, so an assumption of homogenous ice distribution within the plot is justified.

Field Work

A 50 x 100 m plot was established at Fishburn Forest with the long axis (100 m) oriented north – south, and the short axis (50 m) oriented east – west. The plot spanned a northeast aspect, an ephemeral stream, and a southwest aspect. For each *P. strobus* tree within the plot, data for tree size (diameter, height, and crown class), location (in 3 dimensional space), and a modified competition index were collected. Slope percent and aspect were measured at each tree's location. Depth to bedrock was measured at five locations along the northeast aspect.

Three measures of size were collected for all *P. strobus* trees (> 1 cm DBH) in the field: DBH (cm), height (m), and crown class (three classes: dominant/co-dominant, intermediate, or suppressed). Dominant and co-dominant trees were grouped into one crown class because determination of intermediate and suppressed classes are repeatable among observers, but dominant and co-dominant trees are often interchanged (Nicholas et al. 1991).

After the trees were felled, their height was measured to the nearest 0.1 m using a distance tape. A few large trees that did not reach the forest floor when felled were measured using a clinometer (to measure vertical distance to the tree top) and distance tape (to measure horizontal distance from the base to the tip of the tree) to find the hypotenuse (which is the height of that portion of the tree). This section's height was added to any additional logs on the ground to find total tree height. Four tree height classes were used: < 4, 5 – 9, 10 – 14, and > 15 m. All *P. strobus* trees within the plot were destructively sampled and cross-sectional samples taken from the stem 50 cm (±30 cm) above the uphill side of ground-level (n = 130). All samples were marked with a north arrow and given a number.

The southwest plot corner was located with a Garmin Legend global positioning system (GPS) unit, using Universal Transverse Mercator (UTM) North American Datum (NAD) 1983, along with elevation. A stem map was produced for all *Pinus strobus* stem locations within the plot using a laser range finder. Slope and aspect were measured at each stem location, along with data needed to calculate the modified competition index including the focal tree diameter, the nearest neighbor tree diameter and the distance between the two trees (Figure 4).

For the stem map, we used an Impulse LR laser transit (Laser Technology Inc.) combined with an electronic compass (Map Star). The following data were recorded for each *P. strobus* tree: horizontal distance (m), vertical distance (m), and bearing (°) relative to the southwest corner. Trigonometric formulas were used to find spatial (x, y) coordinates for all trees in the plot. Elevation was found by adding the vertical distance (z coordinate) to the elevation of the plot corner (609 m.a.s.l.). Slope was measured at each *P. strobus* stem with a clinometer. Aspect (°) was measured at each stem's location using a compass.

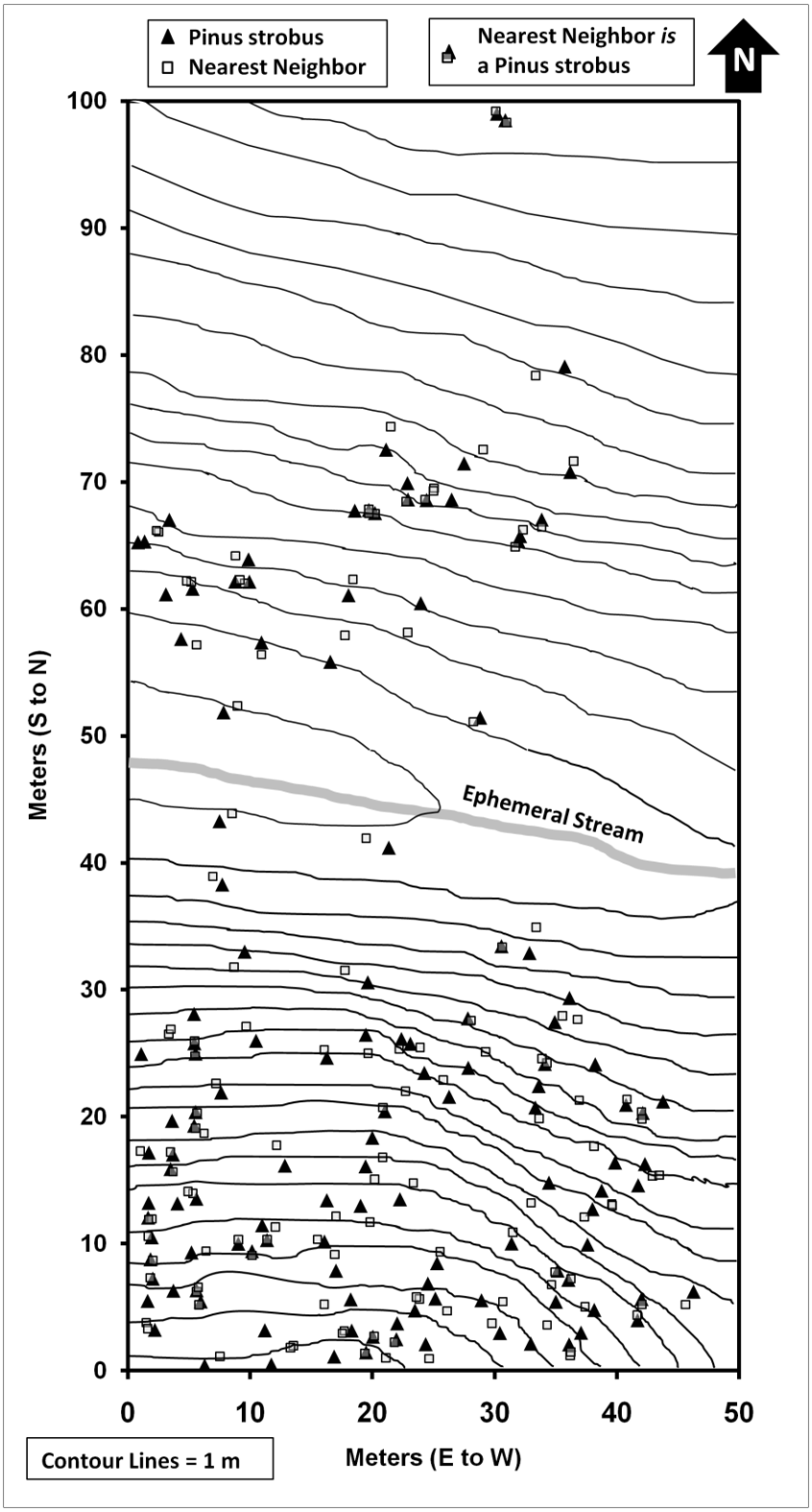

Figure 4. *Locations of all Pinus strobus and nearest neighboring trees on study plot. Contour lines represent 1 m increments. The southwest corner of the plot had the highest elevation at 609 m above sea level (m.a.s.l.), lowest plot elevation was 590 m.a.s.l.*

Laboratory Work

To produce a smooth sanding surface, the cross-sections were cut with a band saw, machine sanded with a belt sander (220 grit), and then hand sanded with progressively finer sandpaper (up to 2400 grit) until the wood cells were visible under a reflected-light microscope. The samples were visually cross-dated using the list year technique, in which tree rings were counted backwards from the known year of felling (2007), "list years" that were more narrow than the rings on either side were marked (Yamaguchi 1991). Certain years produced narrow rings in most trees, due to common climatic response in trees. Pattern-matching of tree-rings proved essential in some cases where some outer rings were absent due to recent (2005 – 2007) growth declines in trees in the 6 – 9 cm diameter range.

A sub-sample of forty-seven *P. strobus* cross-sections were randomly selected for detailed image analysis using Photoshop to quantify precise compression wood areas (Figure 5). Samples were stratified by aspect and diameter class, and then randomly selected within each diameter class using a random number generator (Appendix A1). Samples were not stratified by topographic location; however, plotting spatial locations of the samples selected for image analysis revealed that they were well-distributed spatially as well as by size. A higher percentage of samples were used from the largest two diameter classes out of necessity; there were fewer large trees on the plot. In addition, samples were limited on the exposed southwest aspect due to low *P. strobus* establishment.

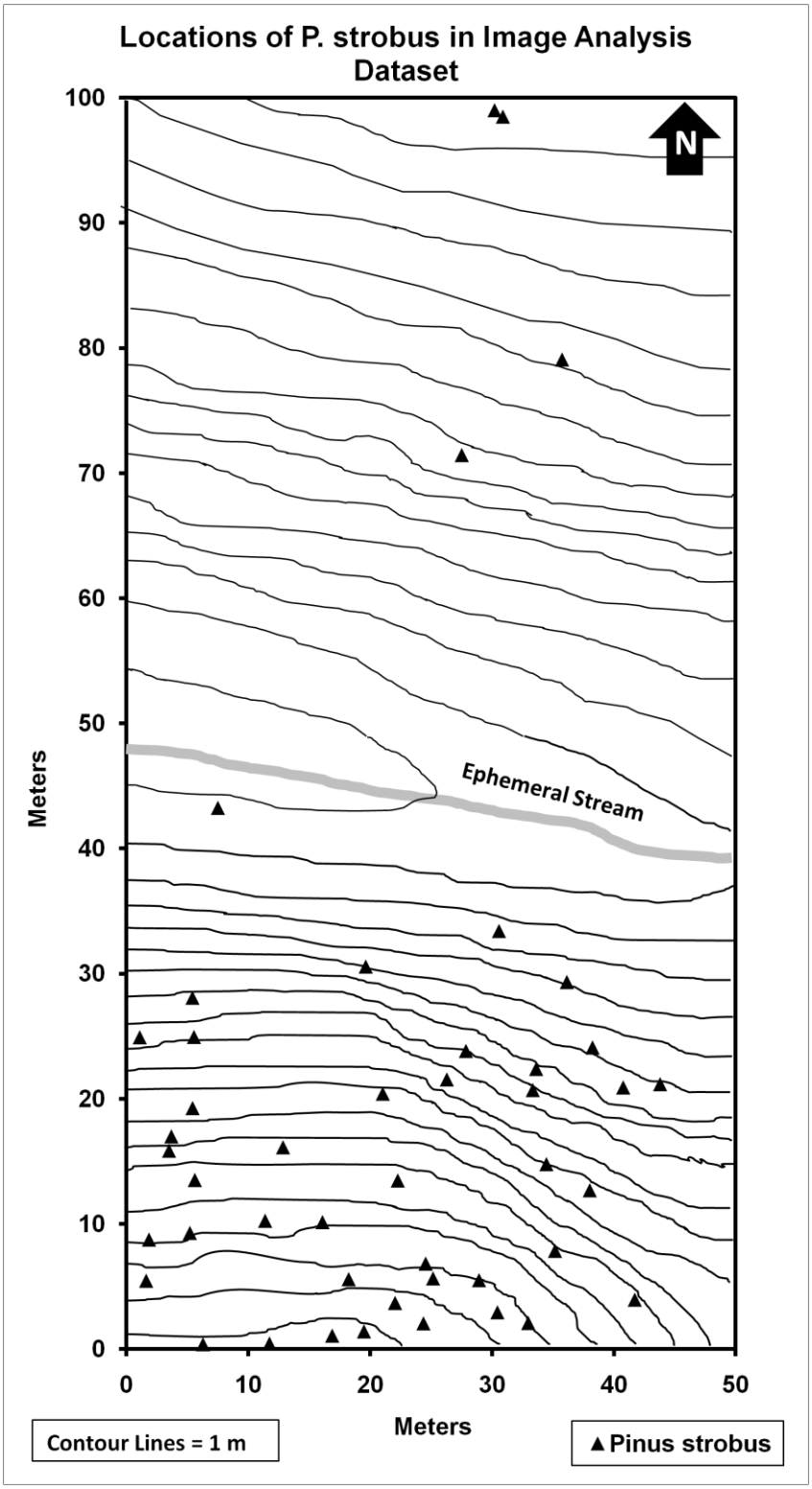

Figure 5. *Locations of P. strobus trees randomly selected for image analysis of compression wood area (n = 47). Contour lines represent 1 m increments. The southwest corner of the plot had the highest elevation at 609 m.a.s.l. and lowest plot elevation was 590 m.a.s.l.*

Images of the sanded cross-sections were scanned using an Epson Stylus Photo RX600, at 2400 pixels per inch (ppi) resolution and imported into Photoshop CS. The high-resolution scans enabled visualization of individual growth rings at high magnification. However, such scans created files that were very large, and the digital resolution had to be lowered (1200 or 600 ppi) for scans of many of the larger diameter disks to reduce file size. Lowering digital resolution did increase error in parameter-based measurements, but not radial measurements (Appendix A2); therefore, only radial measurements were used in the analysis.

All tree rings within the scanned images were virtually "cut" into Photoshop layers with the exception of some suppressed outer rings that did not contain compression wood (n = 1611). The magnetic lasso tool (in Photoshop) was used to cut each growth ring into its own layer, where it was analyzed independently of other growth rings. This image measurement tool works by affixing a digital line ("lasso") which sticks to differences in color contrast somewhat like a magnet. The software program allows the contrast tolerance settings to be altered (in this study, a 10 pixel search radius, 50% tolerance, and 77 anchors/inch produced the best results with this sample set). Working from the pith outward (and subtracting pith tissue from analysis), we used the magnetic lasso to "layer by cut" each tree ring into its own layer, and named layers by their year of formation.

Each layer was selected with the magic wand tool and measured with Photoshop CS4 Extended Analysis Pack. For each tree-ring layer, area, perimeter, image width (horizontal diameter), and image breadth (vertical diameter) were measured in pixels. Areas of compression wood within the rings were cut into their own layers and measured, as well any

large cracks in the wood. The bark was also cut into a separate layer, using the polygonal lasso tool to simulate a field measurement of bark diameter. This layer was used with the 2007 tree ring to create a simple linear regression equation to predict outer bark diameter based on inner bark diameter, or vice versa (Appendix A3).

It was observed that rings containing large amounts of compression wood were highly eccentric in cross section, so additional data were collected for an eccentricity metric. Each scanned image was rotated such that the mean direction of compression wood formation (or radial eccentricity) was oriented upwards in the monitor frame. In cases when compression wood was not apparent (e.g. large-diameter trees), the downhill side of the tree was used as a surrogate. Height and width of each layer were measured, and then each image was rotated 30° and 60° clockwise and re-measured, for a total of 6 diameter measurements per tree-ring (4833 total). Of these, the maximum and minimum lengths of each tree-ring were identified and averaged to find mean ring diameter, half of which equals the ring radius.

A quick and simple method of compression wood measurement was also used in the initial stages of the project but not in the final analysis. In this method, each tree ring is given a compression wood grade based on a classification system devised by Harris (1977) (Table 4). The average of all tree-ring grades over the lifespan of the tree is the compression wood index. A validation study found that this method was repeatable among observers, and provided an efficient and reliable, albeit coarser, estimate of relative compression wood area (Appendix B).

To measure the direction of tree lean in relation to aspect, a line was drawn through the mean direction of compression wood formation (the direction of greatest radial eccentricity) on

each sample with a black marker (Figure 1). Then a compass was used to measure the angle of deviation from the north arrow drawn on each sample in the field and the mean direction of compression wood formation, assumed to be the direction of tree lean. The direction of tree lean was compared to tree aspect measured at each tree's location in the field.

Microscopic Analysis

To quantify the impact of the ice storm on the cellular characteristics across a tree diameter gradient, microtome sections were cut from a stratified random sample of *P. strobus* cross-sections (n = 12) across a range of diameter classes (2 – 40 cm). Two trees in each of six tree-diameter classes (2 – 5, 6 – 9, 10 – 13, 14 – 17, 18 – 22, and > 23 cm) were randomly selected using a random number generator. Three tree-rings before (1991 – 1993) and after the ice storm (1994 – 1996) were sampled from two sides of each cross-section: compression wood (downhill side) and opposite wood (uphill side). A total of 72 tree-rings were examined in the 12 trees (6 years per tree). Compression wood samples were taken from the center of the arc of radial eccentricity (the center of the most severe compression wood), and opposite wood samples were taken 180° from the compression wood sample (Figure 6).

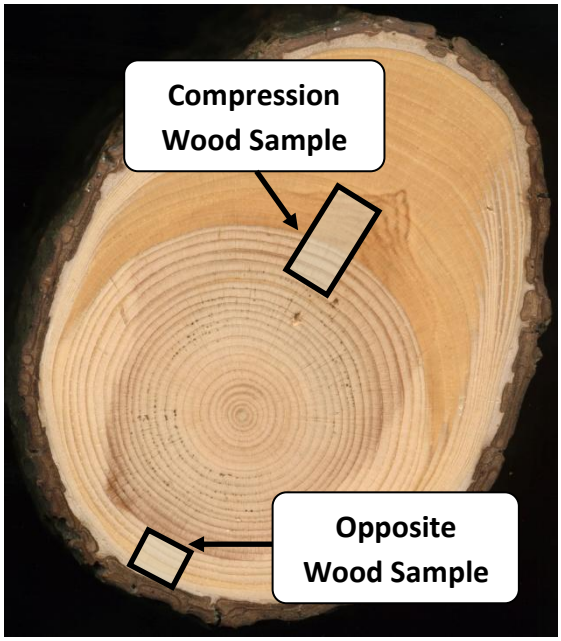

Figure 6. *The wood anatomy in the three years before and after the ice storm on compression wood and opposite wood sides of 12 P. strobus cross-sections was examined using transmitted light microscopy.*

In cases where no compression wood was discernable, the downhill tree side was used as a surrogate for the compression wood sample, and the opposite wood sample was taken 180° from the compression wood side. Sections were cut and soaked in water for 3 – 5 days before cutting with a microtome (Sledge Microtome G.S.L.1., Schenkug Dapples, Switzerland) (Gärtner and Nievergelt 2010). Sections were approximately 30-µm thick, stained in a 2% solution of Safranin O, and mounted in glycerin on glass slides for microscopic examination.

Nikon Image System Elements Basic Research (NIS Elements BR) software was used in conjunction with a Zeiss Axioskop transmitted light microscope and a Nikon Digital Sight DS-Fi1 camera to capture images of the stained *P. strobus* slides. Images were captured with the mounted digital camera, allowing digital resolutions as fine as 0.7µm/pixel in 400-x

magnification. The software is calibrated to automatically measure in actual units such as µm or μm^2, rather than pixels.

In each tree-ring cross-section, three randomly chosen ring widths were measured and all cells in a radial file were counted. In addition, three cells were randomly chosen along each radial file and their outer tangential diameters (perpendicular to the ring width line) measured with the length tool in NIS Elements BR at 25-x magnification (Appendix C1). Mean radial and tangential cell diameters were derived from these measurements.

Using 400-x magnification, finer cellular details such as the middle lamella and primary cell walls were visible (Figure 7). Three randomly selected tracheids per tree-ring were measured using a polygon area tool in NIS Elements BR (Appendix C1). Each outer (tracheid) and inner (lumen) cell wall was outlined with the selection tool, measuring the area, perimeter, diameter, and circularity (0 — 1) of each selection. In addition, we measured two transects of adjacent cell walls between a focal cell and a neighboring cell, thereby measuring four cell walls at once. Dividing this value by four yielded the mean cell wall thickness at a cell's location (Figure 7). As with macroscopic data, data from common samples measured with different methods were compared and we found that perimeter-based measurements systematically inflated diameter measurements compared to linear measures (Appendix C2).

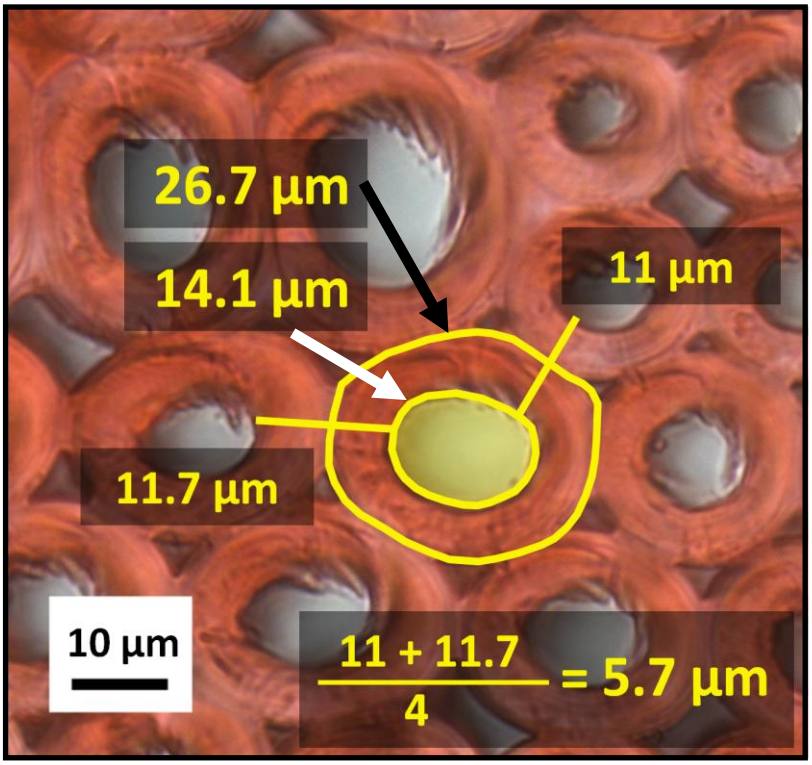

Figure 7. *Image of the 1994 tree-ring under 400-x magnification, showing P. strobus compression wood cells formed after freezing rain deposition. The tracheid (black arrow) and lumen (white arrow) cell dimensions were quantified, along with mean thickness of 4 cell walls. Measurement bar equals 10 microns.*

Data Analysis

The dependent variable, compression wood area, was calculated in both actual and relative terms. "Actual" in this study refers to the cross-sectional area of compression wood (mm^2), while "relative" refers to actual compression wood area as a percentage of total tree-ring area. To accomplish this, cross-sectional area increment (AI_t) was calculated for each tree-ring by subtracting the cross-sectional area of the previous year's growth layer (A_{t-1}) from the area of the focus layer (A_t), minus the area of any cracks that may be in the sample (A_{cracks}):

$$AI_t = (A_t - A_{t-1}) - A_{cracks}$$

Incremental compression wood area within each tree-ring (AI_{CW}) was measured directly from each Photoshop layer. Cumulative compression wood area was also calculated for each tree-ring, defined as the amount of compression wood in a focal ring and all previous rings.

$$A_{CW} = \sum AI_{CW}$$

By dividing the area in compression wood (AI_{cw}) by the cross-sectional area increment for a particular year (AI_t), the relative compression wood cross-sectional area per ring was obtained ($\%CW_R$):

$$\%CW_R = \frac{AI_{CW}}{AI_t}$$

Similarly, dividing the compression wood area by the total cross-sectional area in a disk equals the relative compression wood in the disk ($\%CW_D$).

Actual and relative compression wood data were calculated for each tree ring, along with other independent variables (diameter, height, crown class, elevation, slope, aspect, and competition index). The data were ordered by each independent variable in separate spreadsheets and broken up into independent variable classes. Compression wood areas were averaged by class. One-way Analysis of Variance (ANOVA) tests were used to test whether any differences existed among independent variable classes with respect to compression wood actual and relative area. If significant differences existed, Fisher's Least Significant Difference (LSD) multiple comparison tests were used to identify which classes contained significantly more or less compression wood before or after the ice storm ($\alpha = 0.05$).

To evaluate the influence of freezing rain deposition on compression wood formation, the ten years before and after the ice storm were examined in 42 samples on the northeast aspect. This eliminated juvenile growth rings from the dataset that may contain extra "juvenile" compression wood that young trees (< 10 years) must form to obtain rigidity. Ice storm induced compression wood was the focus of this study, so juvenile compression wood was avoided in the pre-storm and post-storm analysis. Within each independent variable class compression wood areas in the 10 years pre- and post-storm were averaged. Paired t-tests were used to test if any differences existed in actual or relative compression wood area between the 10 years before and after the ice storm ($\alpha = 0.05$).

To test the null hypothesis that all year and diameter classes formed equal amounts of compression wood a contingency table was constructed (χ^2 test for independence). To make sure that expected value cells were all > 5, it was necessary to create 4 groups of 5-year classes (1984-1988, 1989-1993, 1994-1998, and 1999-2003). Pearson's correlations were used to test relationships between compression wood height and crown class.

For each tree-ring, the longest diameter (D_L) and shortest diameter (D_S) were measured. The ratio of these two diameters, which could be measured on a living tree using calipers, equals the ratio of eccentricity (Timell 1986).

$$eccentricity\ ratio = \frac{D_L}{D_S}$$

Theoretically, this ratio ranges (1 – infinity), but a more practical range for this tree-ring dataset is (1 – 1.3). Tree rings that are more eccentric in shape have higher eccentricity ratios than those that are more circular in cross-section.

The mean diameter (D_2) of each tree-ring was found using the long and short diameter measurements:

$$D_2 = \frac{D_L + D_S}{2}$$

For the dataset listed by tree-rings (n = 1518), one-way ANOVA tests were used to identify if any of the eccentricity ratio classes were significantly different from the others. Fisher's LSD tests of multiple comparisons were used, which is a liberal test designed to detect differences among categories. The full tree-ring dataset was also used to test differences among tree-ring age classes. Pearson's correlation coefficient was used to test the relationship between cambial age class and compression wood formation.

Spatial (x, y) coordinates of *P. strobus* trees were obtained using the following trigonometric formulas:

$$\mathbf{x} = \mathbf{HD} \times \mathbf{sin}(\mathbf{radians}(\mathbf{azimuth}^\circ))$$

$$\mathbf{y} = \mathbf{HD} \times \mathbf{cos}(\mathbf{radians}(\mathbf{azimuth}^\circ))$$

Where x equals a focal tree's longitudinal position and y equals a focal tree's latitudinal position. Each tree's location was plotted on the maps, as well as the locations of nearest neighboring trees in relation to focal *P. strobus* trees. In addition, chi-squared tests of independence were used to test whether tree diameter depended on elevation and whether *P. strobus* establishment depended on aspect.

Slope degrees measured at each tree were transformed into slope percent by taking the tangent of degrees. Aspect measurements were cosine-transformed to resolve the problem that occurs in datasets with circular values (0 – 360°). Northeastern azimuth values are > 0°, while northwestern azimuths are < 360°. Even though 1° N is not significantly different from 359° N, their untransformed values lead to spurious results if inserted into a dataset without transformation. By taking the cosine of aspect, northern values approach +1, while the southern aspects approach -1.

To test whether compression wood formed on the downhill sides of trees on this site, data on aspect and mean direction of compression wood formation were collected. First, both datasets were transformed using cosine, to correct for the problem that arises in circular datasets. Pearson's correlation coefficient was used to test the relationship between the two datasets (Appendix D1).

Competition indices provide a numerical ranking system to evaluate the relative influence that neighboring trees have on a focal tree. An evaluation of several competition indices revealed that simpler indices were more predictive than excessively complicated models (Mugasha 1989). Therefore, a modified distance-dependant competition index was used to evaluate the influence of the nearest neighboring tree on a focal tree:

$$\boldsymbol{CI = \frac{D_j / D_i}{DIST_{ij}}}$$

where the influence of a neighboring tree on a focal tree (CI) equals the DBH (cm) of the neighboring tree (D_j) divided by the DBH (cm) of the focal tree (D_i) divided by the distance (m)

between the neighboring tree and the focal tree ($DIST_{ij}$), which may or may not be another *P. strobus* tree (Lorimer 1983). The higher the number, the more influence the neighbor tree has on the focal tree. Lorimer's original CI found the sum of all tree CI values within a specified search radius. The modified CI and a version of Lorimer's CI, which sums the CI values of all trees within 10 m of a focal tree, were compared using Pearson's correlation coefficient (Appendix D2).

For the microscopy data, random selections of cells were made using a random number generator to reduce bias in sample selection (Appendix C1). Ring width (µm) was divided by the number of cells (n_{cells}) in a radial file was equal to the average radial cell diameter for transect (D_{Radial}).

$$\overline{D_{Radial}} = \frac{RW}{n_{Cells}}$$

Cell count data were averaged by ring to calculate the mean number of cells produced by cambial initials over a growing season in a particular tree ring. In addition, tangential cell diameters of three random cells (D_A, D_B, and D_C) along each transect were measured and then averaged to find the mean tangential cell diameter of each transect ($D_{Tangential}$). Pearson correlation coefficients were used to compare mean radial cell diameter to mean tangential cell diameter along each transect (Appendix C2).

$$\overline{D_{Tangential}} = \frac{(D_A + D_B + D_C)}{3}$$

Measurements of cell diameter made using 25-x and 400-x magnification were compared using Pearson correlation coefficients. Means of cell diameter based on perimeter

(400-x) were compared to means of linear cell diameter measurements to test the amount of variation that arises from different methods (Appendix C2).

Tracheid and lumen diameter were measured directly with the perimeter tool, along with area of the selection. Pearson's correlation coefficients were used to test the relationships between tracheid diameter, tree diameter, tree-ring width, and number of cells in a radial file (Appendix C3). Subtracting the lumen area from the outer tracheid area equals the cell wall area ($A_{Cell\ Wall}$):

$$A_{Cell\ Wall} = A_{Tracheid} - A_{Lumen}$$

Dividing the number of cells in a radial file by the ring width equals the average number of cells per mm. Squaring this value and then multiplying by the mean cell wall area per wood cell type and multiplying by 100 equals the mean cell wall area per unit of wood cross-section in each type ($\%A_{Cell\ Wall}$):

$$\overline{\%A_{Cell\ Wall}} = \left(\frac{n_{Cells}}{RW}\right)^2 \times \overline{A_{Cell\ Wall}} \times 100\%$$

Cell wall thickness of two neighboring cells was also measured using the linear measurement tool in NIS-Elements BR. To find the average cell wall thickness, the lengths (L) of two cell walls were measured in each of two transects, and then divided by four to find the mean cell wall thickness in that cell's location.

$$\overline{L_{Cell\ Wall}} = \frac{2 \times (2\ L_{Cell\ Walls})}{4}$$

Circularity was calculated for each cell selection (tracheid or lumen). Circularity (0 – 1) is a shape metric, with 1 representing a perfect circle and lower values representing increasingly elongated polygons. Outer and inner circularity were averaged to find the mean cell circularity. Tracheid values using this shape metric were compared to the circularity rating of several geometric shapes to put the numbers in context (Appendix C4).

$$Circularity = \frac{4\pi \times area}{perimeter^2}$$

One-way ANOVA tests were conducted for each cell measurement (outer tracheid diameter, lumen diameter, cell wall thickness, tracheid area, lumen area, cell wall area, and mean circularity) for different independent variable classes of interest. Independent variable classes for microscopy data included cell types (compression, opposite, or normal wood on opposite sides of the stem), years of tree-ring formation (1991 – 1996), and diameter classes (2 – 5 cm, 6 – 9 cm, 10 – 13 cm, 14 – 30 cm, and over 30 cm). If groups were found to be significantly different, Fisher's LSD tests were used to see which years and sides of the stem had significantly higher or lower values than other categories ($\alpha = 0.05$). Paired t-tests were used to see if differences existed on opposite sides of the stem among year and diameter classes. Chi-squared goodness-of-fit tests were conducted for differences in cell counts among all independent variable classes.

IV. Results

Compression Wood Cross-Sectional Area

Tree Age

In 1994, heavy ice deposition caused large amounts of compression wood (CW) to form in this *Pinus strobus* stand (Figure 8). A significant increase in mean compression wood growth occurred in the ten years after ice storm damage, compared to the previous ten year mean (actual CW: $t = -4.83$, $P < 0.001$; relative CW: $t = -5.12$, $P < 0.001$).

Due to the relatively even age of the *Pinus strobus* cohort on the northeast aspect, cambial age showed a strong positive relationship with compression wood formation ($r = 0.24$, $P < 0.001$) (Figure 9). Most trees in this cohort were 21 – 27 years old at the time of the 1994 ice storm, resulting in significantly higher amounts of compression wood in this age class, as well as in the oldest age class ($F = 28.98$, $P < 0.001$).

Juvenile trees (< 7 age class) formed significantly more relative compression wood area than intermediate age classes to achieve early stability; however, the oldest age class still formed most relative compression wood ($F = 16.71$, $P < 0.001$) (Figure 9). Juvenile compression wood formation had begun to taper off in intermediate age classes until the ice storm caused severe bending in the 21 – 27 cambial age class. Although relative compression wood normally would decrease exponentially with time, heavy ice deposition in 1994 altered this pattern. Therefore, a significant positive relationship was found between age and relative compression wood rather than a negative exponential curve ($r = 0.13$, $P < 0.001$).

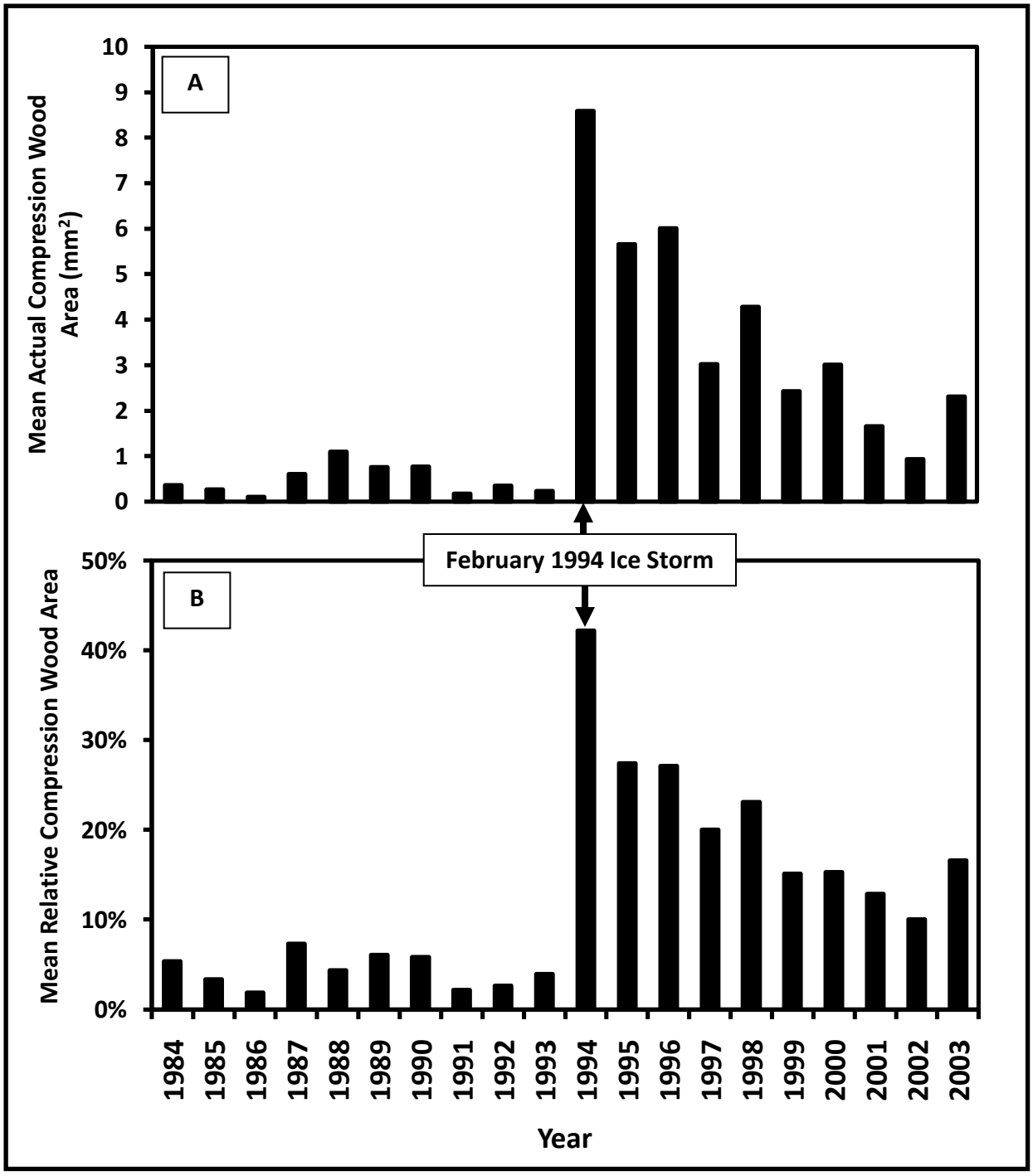

Figure 8. *There was a significant increase in mean actual* ***(A)*** *and relative compression wood* ***(B)*** *formation in the ten years after the ice storm of 1994.*

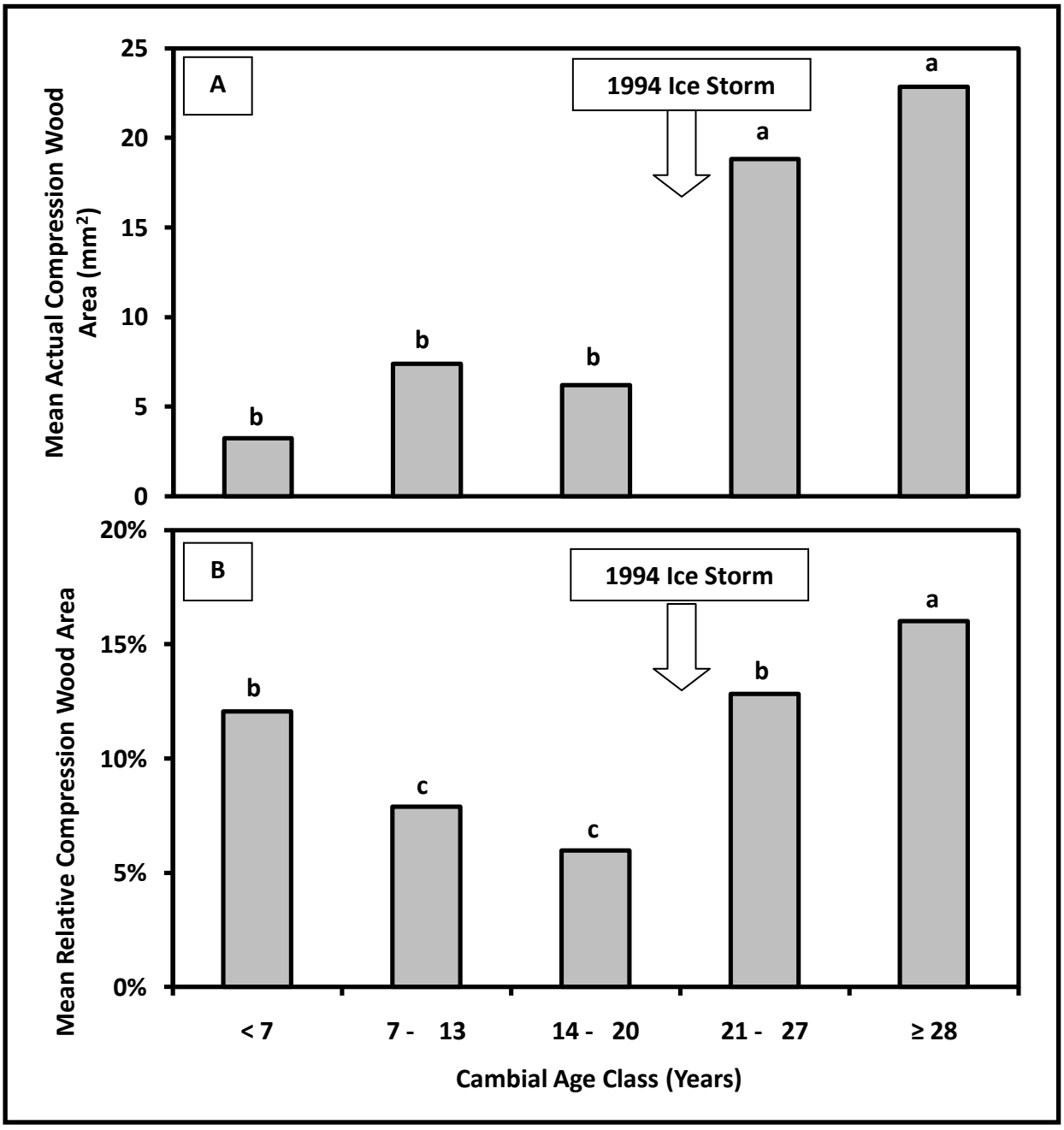

Figure 9. *Actual compression wood* ***(A)*** *and relative compression wood* ***(B)*** *cross-sectional area by cambial age class. Different lowercase letters indicate classes that were significantly different.*

Tree Size

Compression wood area was highly dependent on tree diameter and year of formation (χ^2 = 93.26, df = 12, P < 0.001) (Figure 10). Small-diameter trees at the mid-slope position and trees in the 6 – 9 cm diameter class along the ridge top formed the most compression wood. Diameter classes exhibited significant differences in actual and relative compression wood formation (actual F = 5.15, P = 0.002; relative F = 11.92, P < 0.001). The 6 – 9 cm class formed the most actual compression wood of any diameter class. The smallest diameter class contained a larger portion of relative compression wood formation, and was not significantly different from the 6 – 9 cm class. Trees > 10 cm had significantly less compression wood formation than small diameter stems.

In the ten years following ice storm damage, the 6 – 9 cm diameter class formed six times as much compression wood as before the storm (t = -5.18, P < 0.001) (Figure 11). The 2–5 cm class formed four times as much (t = -3.20, P = 0.011) and the 10 – 13 class formed 4.3 times as much post-storm compression wood (t =-2.43, P = 0.041). There were no significant differences in ten year pre- and post-storm compression wood formation in the 14 – 17 cm class (t = -0.68, P = 0.534) or the 18+ cm diameter class (t = -1, P = 0.363). The smallest two diameter classes experienced significant increases in relative compression wood after the ice storm (2 – 5 cm: t = -3.66, P = 0.005; 6 – 9 cm: t = -5.6, P < 0.001), but trees > 10 cm in diameter did not (10 – 13 cm: t = -1.87, P = 0.099; 14 – 17 cm: t = -0.6, P = 0.579; 18+ cm: t = -1, P = 0.363).

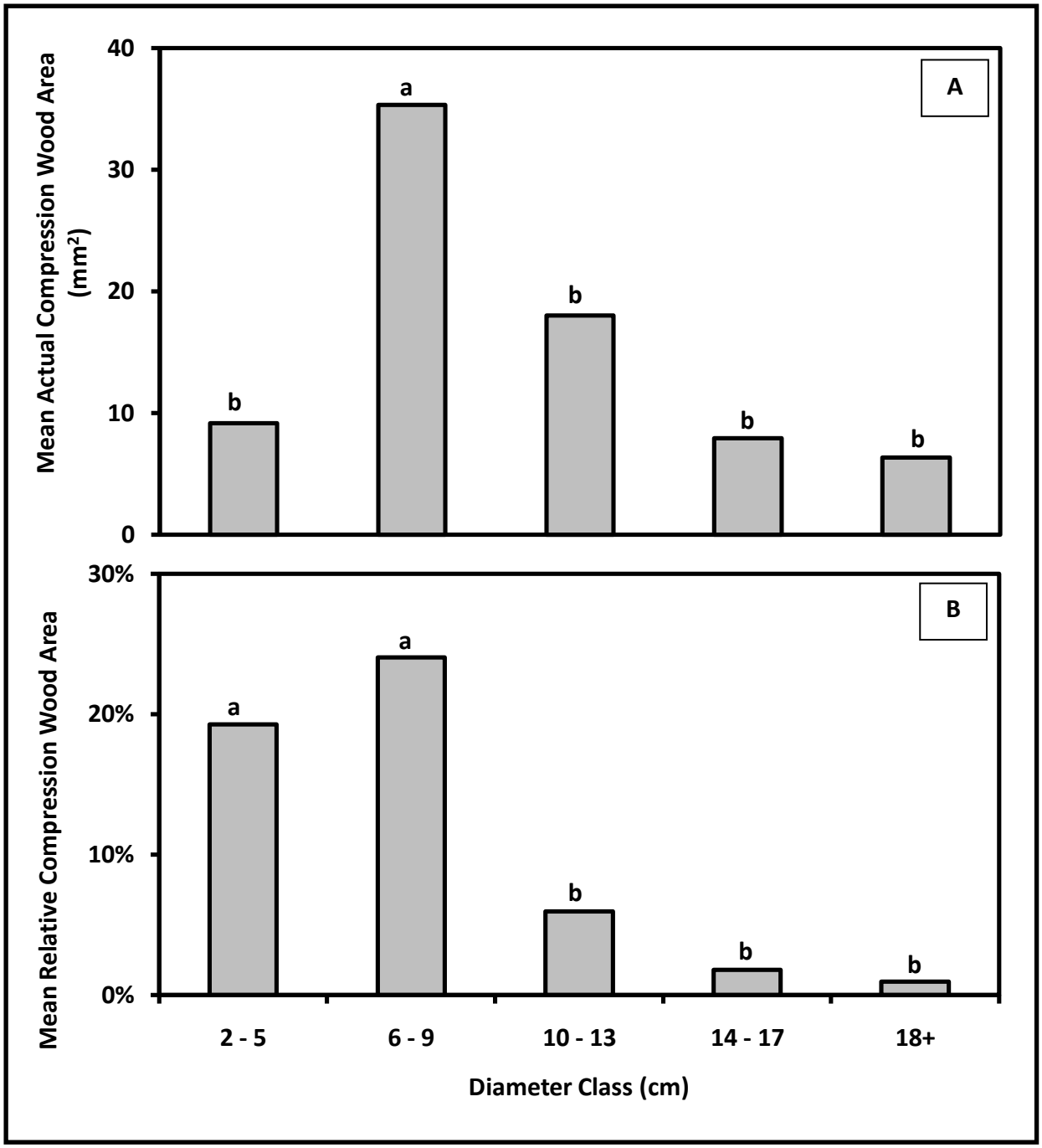

Figure 10. *Actual compression wood **(A)** and relative compression wood **(B)** cross-sectional area by diameter class. Different lowercase letters indicate classes that were significantly different.*

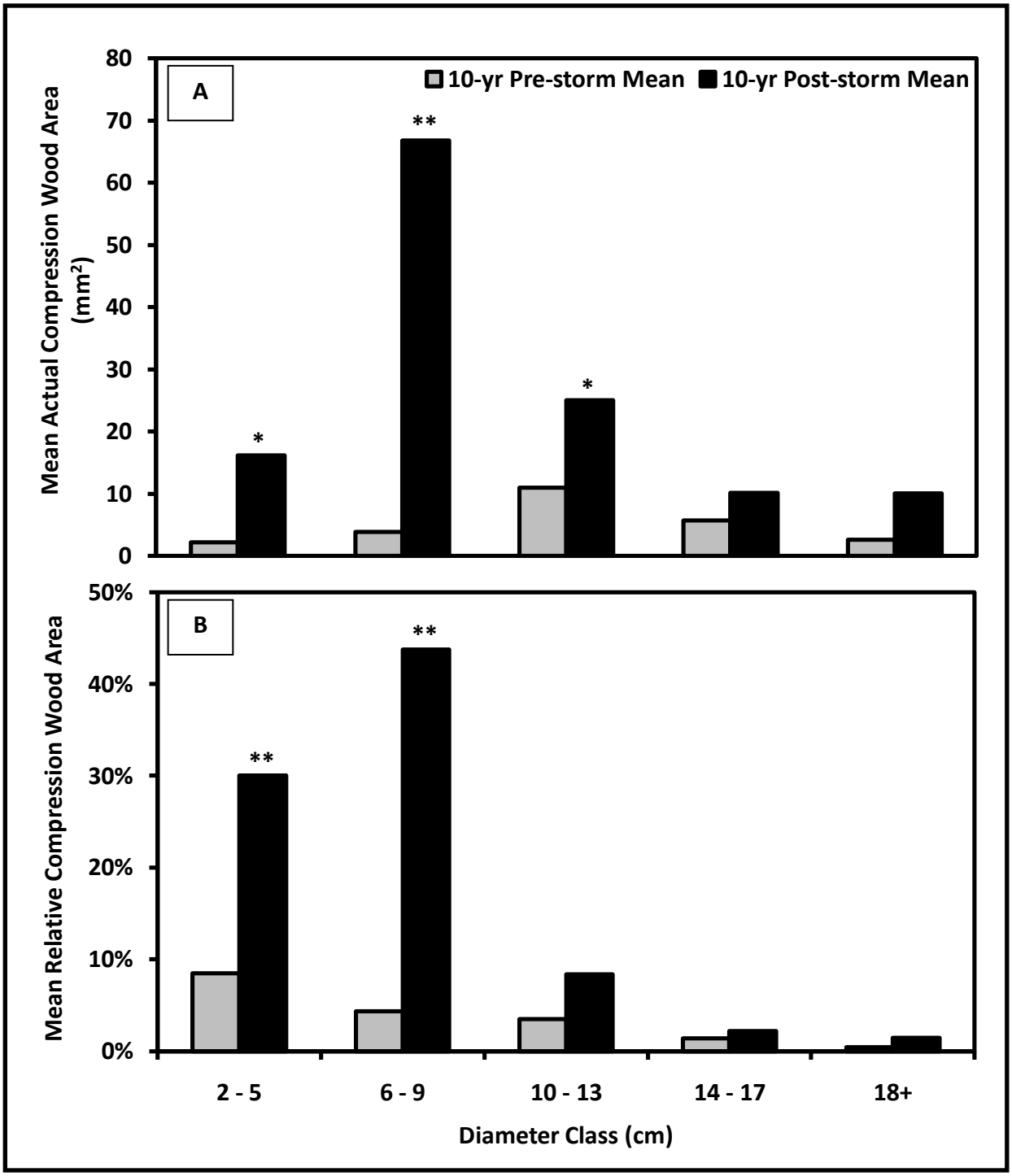

Figure 11. *Pre- and post-storm actual **(A)** and relative **(B)** compression wood by diameter class. Asterisks indicate diameter classes that formed significantly more compression wood after the ice storm (** = P < 0.01, * = P < 0.05).*

Diameter eccentricity ratio was positively related to compression wood formation, due to the highly eccentric nature of compression wood rings (Ratio vs. CW disk area $r^2 = 0.41$, $P < 0.000$). Mean percent compression wood area in tree-rings with eccentricity ratios > 1.15 was 33% (Figure 12). Most of the tree-rings that comprised this largest eccentricity ratio class were in the 6 – 9 cm diameter class. Actual compression wood area in tree-rings with eccentricity ratios < 1.1 was significantly higher than those with ratios > 1.1 ($F = 11.23$, $P < 0.001$) (Figure 12-A). Among relative data, significant differences were found between each of the eccentricity ratio classes ($F = 29.67$, $P < 0.001$) (Figure 12-B).

Compression wood did not form equally among height classes ($F = 5.71$, $P = 0.002$) (Figure 13). Significantly more compression wood was found in the 5 – 9 m height class than any other class. Relative compression wood area was negatively related to tree height ($r = -0.56$). The shortest two height classes formed significantly more relative compression wood area than the tallest two classes ($F = 9.53$, $P < 0.001$).

After the ice storm, significant increases in actual compression wood area were found in the shorter classes (< 5 m: $t = -4.1$, $P = 0.002$; 5 – 9 m: $t = -5.88$, $P < 0.001$), but not in the taller classes (10 – 14 m: $t = -1.69$, $P = 0.152$; > 14 m class formed no compression wood in the ten years pre- and post-storm) (Figure 14-A). Relative compression wood also increased in the shorter classes after the storm (< 5 m: $t = -4.37$, $P = 0.001$; 5 – 9 m: $t = -3.89$, $P = 0.001$). However, ice deposition did not significantly affect compression wood creation in the taller height classes (10 – 14 m: $t = -0.582$, $P = 0.59$; >14 m: $t = 2.32$, $P = 0.08$) (Figure 14-B).

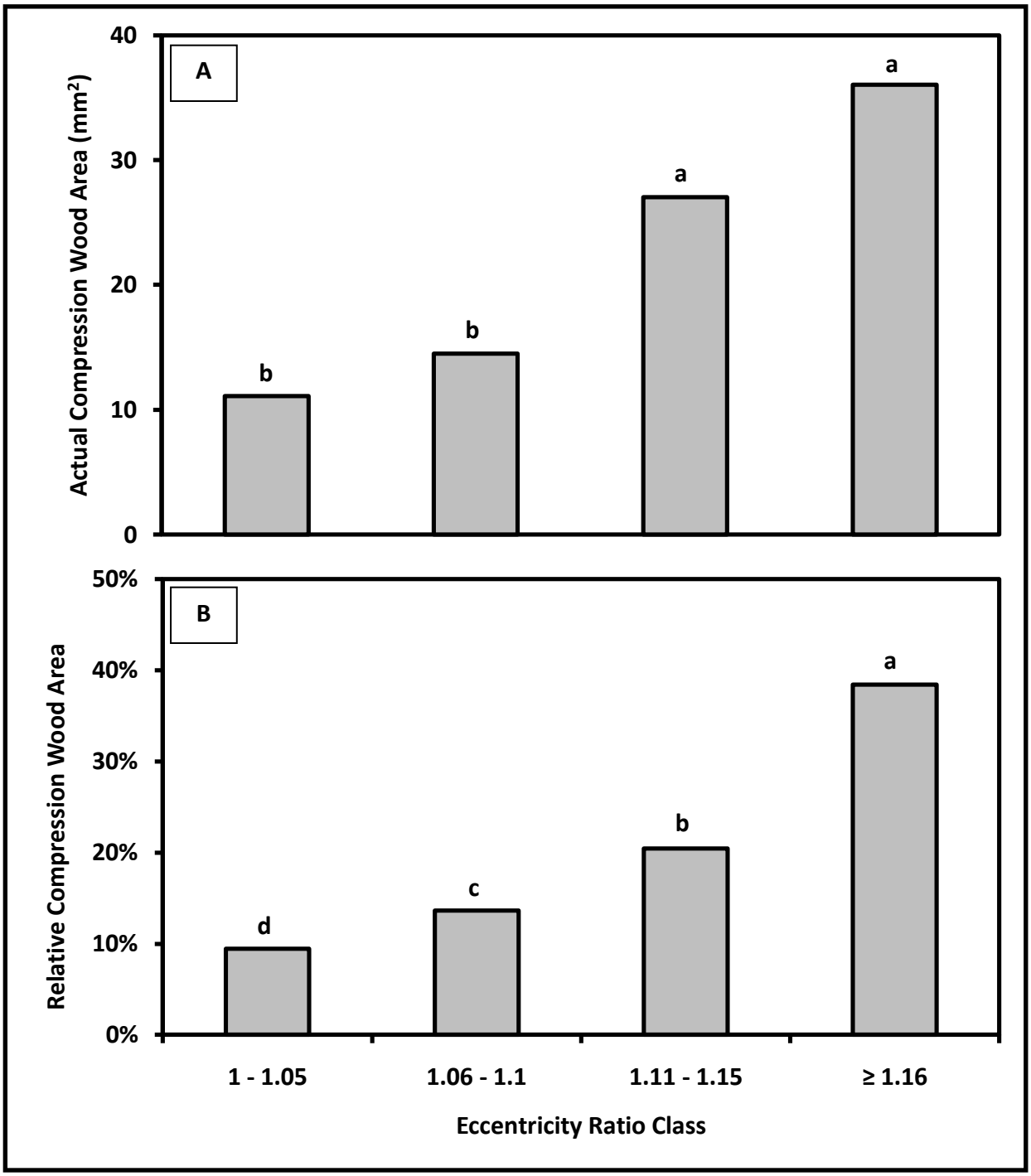

Figure 12. *Actual compression wood **(A)** and relative compression wood **(B)** cross-sectional area by eccentricity ratio class. Different lowercase letters indicate classes that were significantly different.*

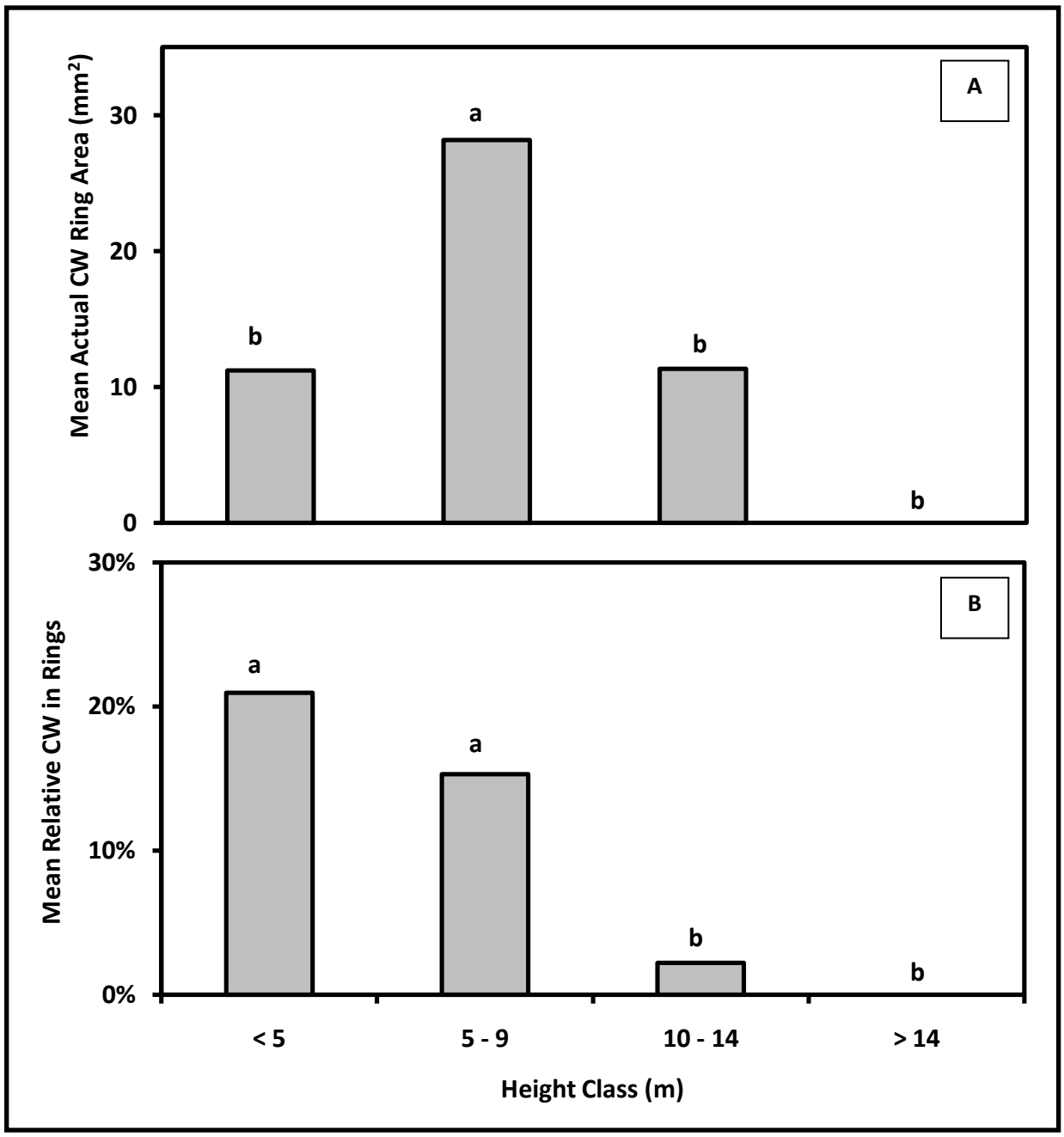

Figure 13. *Actual compression wood **(A)** and relative compression wood **(B)** cross-sectional area by height class. Different lowercase letters indicate classes that were significantly different.*

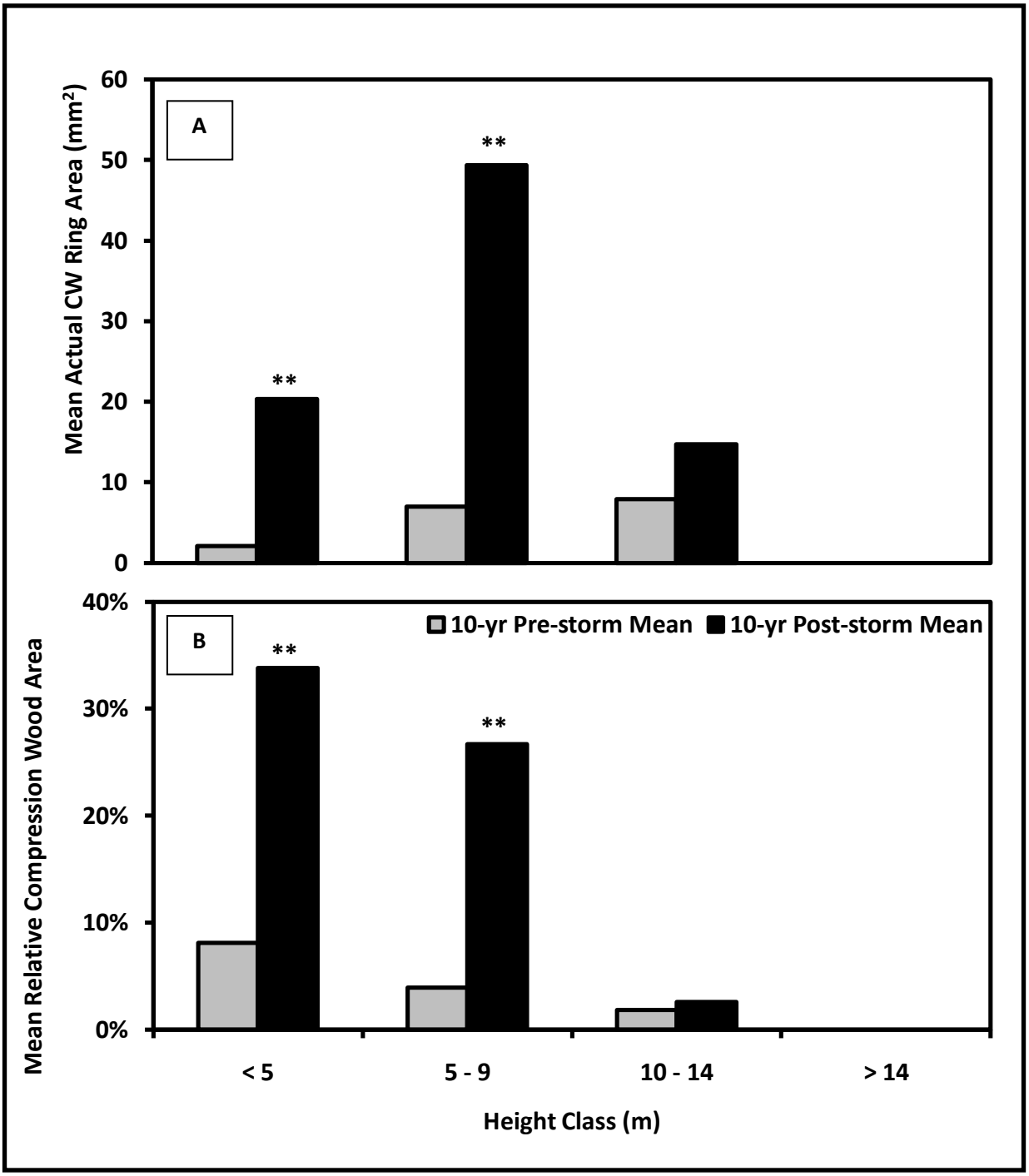

Figure 14. *Pre- and post-storm actual **(A)** and relative **(B)** compression wood by height class. Asterisks indicate height classes that formed significantly more compression wood after the ice storm (** = P < 0.01, * = P < 0.05).*

Crown class was negatively correlated with compression wood area ($r = -0.40$, $P < 0.000$) and its distribution was not equal among the crown classes ($F = 3.71$, $P = 0.034$) (Figure 15). The suppressed class formed significantly more actual compression wood than the (co-) dominant class. However, the intermediate class was not significantly different from the other crown classes. In relative compression wood formation, the suppressed class contained significantly larger amounts than the other classes ($F = 16.83$, $P < 0.001$).

The ice storm affected suppressed trees most severely, causing them to form nine times as much compression wood area in the ten years after the storm compared to the ten year pre-storm mean ($t = -5.04$, $P < 0.001$). The intermediate class formed about three times as much compression wood after the storm ($t = -2.76$, $P = 0.022$). There was no post-storm compression wood increase in the co/dominant class ($t = 1$, $P = 0.363$) (Figure 16-A). Ice deposition significantly affected relative compression wood formation in the suppressed crown class ($t = -6.07$, $P < 0.001$), but did not impact intermediate ($t = -2.22$, $P = 0.054$) or dominant trees ($t = 1$, $P = 0.363$) (Figure 16-B).

Comparing mean tree diameter to mean compression wood formation for each diameter class reveals that the 4 – 9 cm diameter range in *P. strobus* is most vulnerable to bending (Appendix E1). The 1979 ice storm deposited about 2.5 cm of glaze, causing highest compression wood formation in trees averaging 4.5 cm in diameter. In 1994, thicker ice deposition (8.5 cm) caused more severe compression wood formation in trees 4.6 – 8.6 cm in diameter. Large trees formed very little compression wood and actually experienced a minor release and growth pulse following both ice storms (Appendix E1).

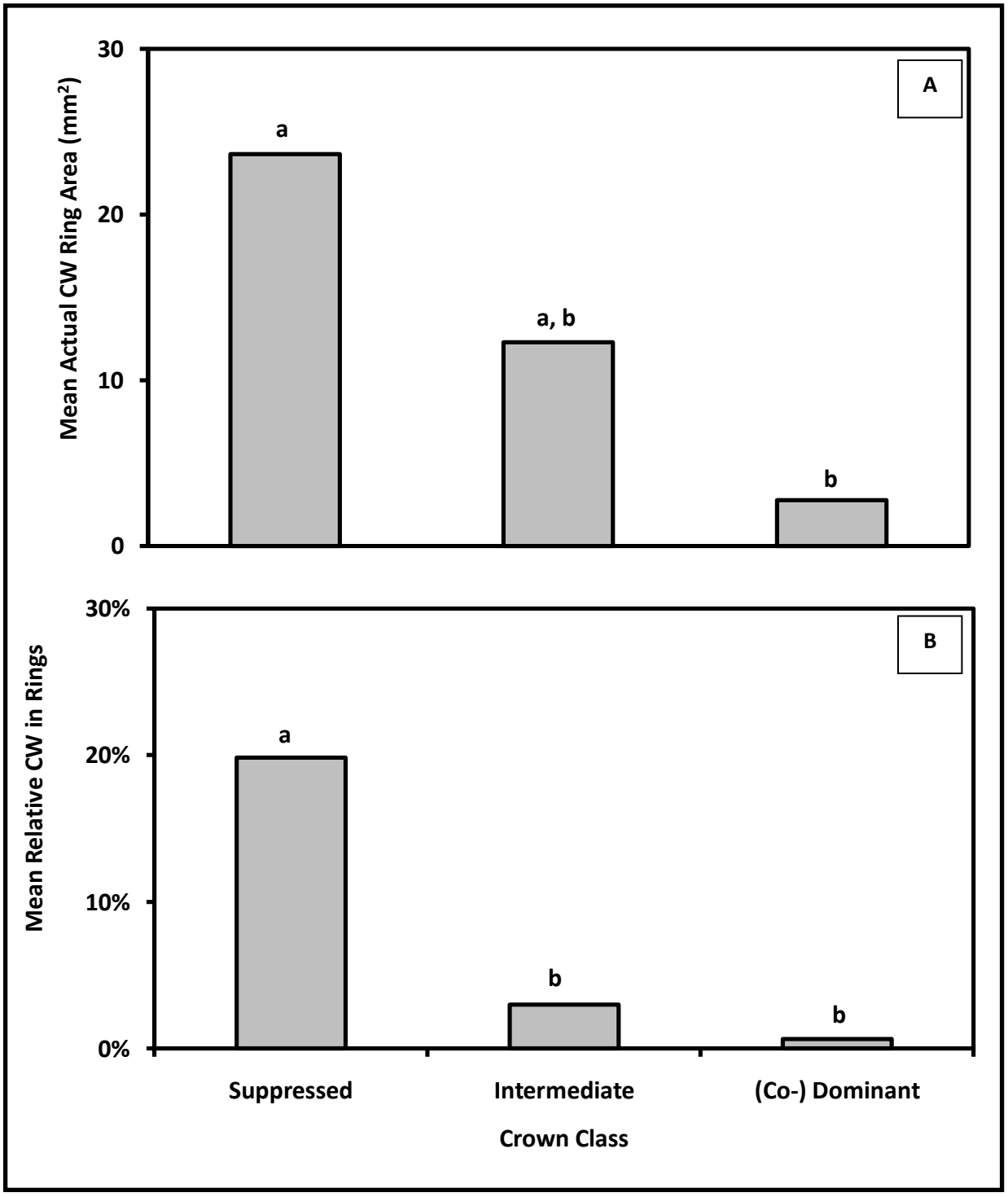

Figure 15. *Actual compression wood **(A)** and relative compression wood **(B)** cross-sectional area by crown class. Different lowercase letters indicate classes that were significantly different.*

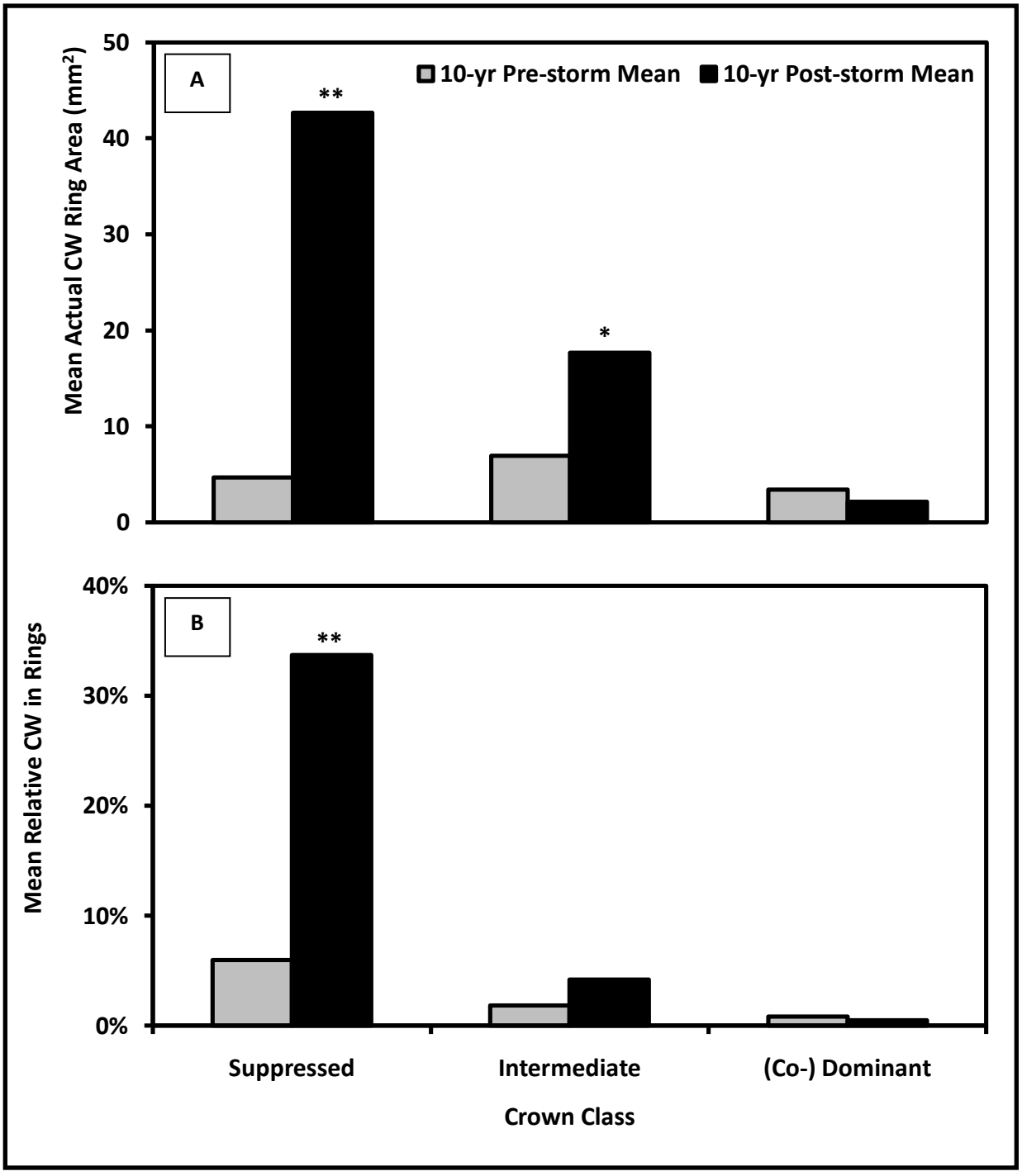

Figure 16. *Pre- and post-storm actual **(A)** and relative **(B)** compression wood by crown class. Asterisks indicate crown classes that formed significantly more compression wood after the ice storm (** = P < 0.01, * = P < 0.05).*

Topographic Factors

Because only one plot was sampled, there was low variation in tree elevation (range: 590 – 609 m.a.s.l.) and inferences about its relationship with compression wood are tenuous. On this plot, no significant relationships existed between elevation and compression wood areas (actual CW: F = 0.93, P = 0.434; relative CW: F = 1.97, P = 0.134) (Figure 17). Higher elevations contained the largest post-storm increases in compression wood area (class 1: t = -1, P = 0.391; class 2: t = -2.08, P = 0.071; class 3: t = -3.65, P = 0.004; class 4: t = -3.07, P = 0.007), and relative compression wood area was highest in the 600 – 604 m class after the storm (class 1: t = -1, P = 0.391; class 2: t = -2.49, P = 0.037; class 3: t = -3.44, P = 0.006; class 4: t = -2.82, P = 0.012) (Figure 18). While elevation had no significant relationship with compression wood distribution, tree diameter was highly dependent on elevation (χ^2 = 31.40, df = 9, P < 0.001).

No significant relationships existed among slope classes in actual (F = 1.54, P = 0.220) or relative compression wood area (F = 0.2, P = 0.894) (Figure 19). After the ice storm, largest increases in compression wood area occurred on slopes >30% (actual CW [class 1: t = -1.59, P = 0.150; class 2: t = -3.63, P = 0.010; class 3: t = -3.62, P = 0.002], relative CW [class 1: t = -1.56, P = 0.157; class 2: t = -3.09, P = 0.008; class 3: t = -3.97, P = 0.001]) (Figure 20). One tree on the northeast aspect grew on a very steep (>60%) mid-slope position and formed unusually high amounts of compression wood for its size. It was removed from other analyses due to high leverage, but is included in these graphs to evaluate slope steepness. Even with this outlier included, however, slope was not a significant factor in compression wood distribution (Appendix D3).

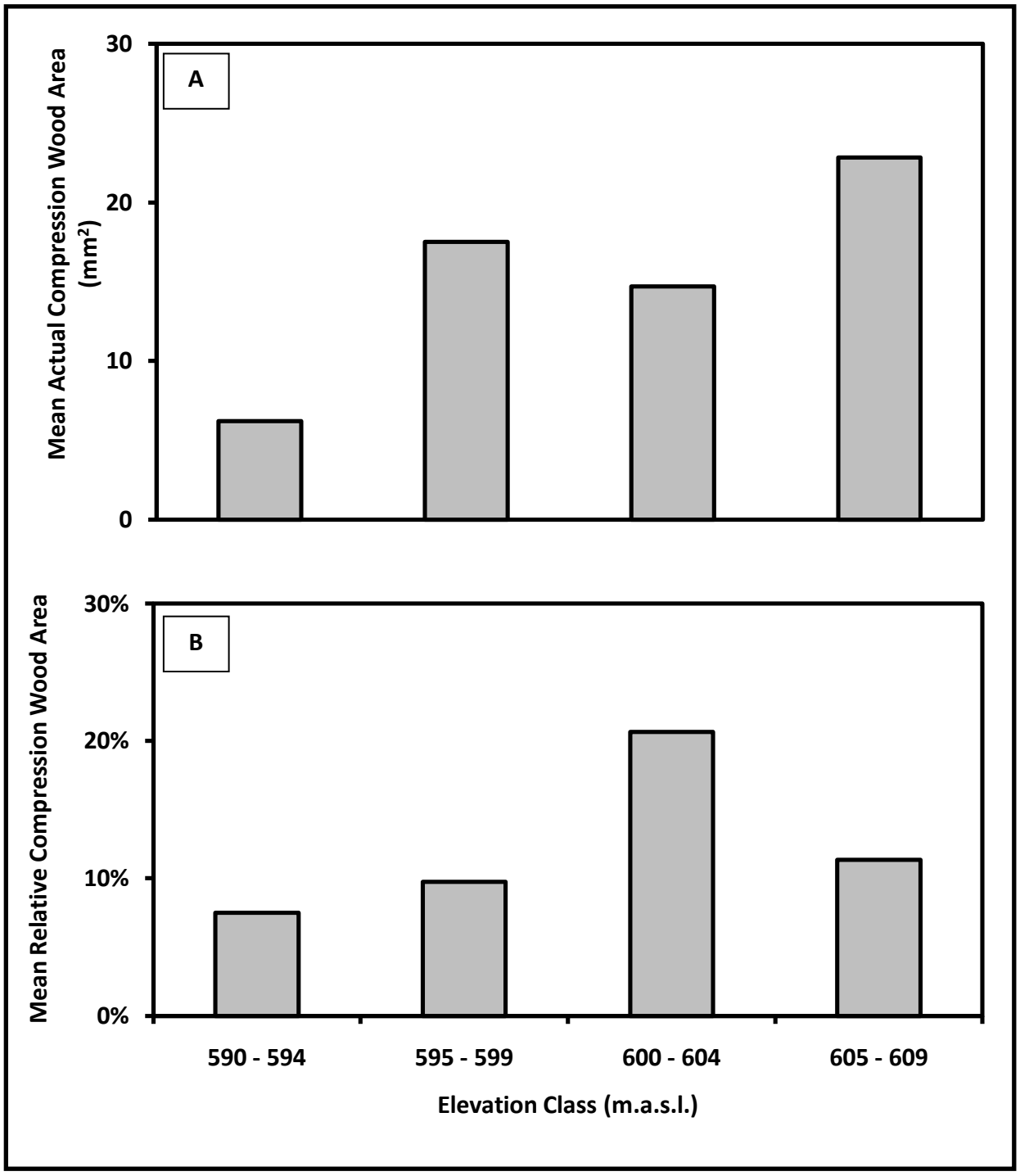

Figure 17. *Actual compression wood **(A)** and relative compression wood **(B)** cross-sectional area by elevation class. Different lowercase letters indicate classes that were significantly different.*

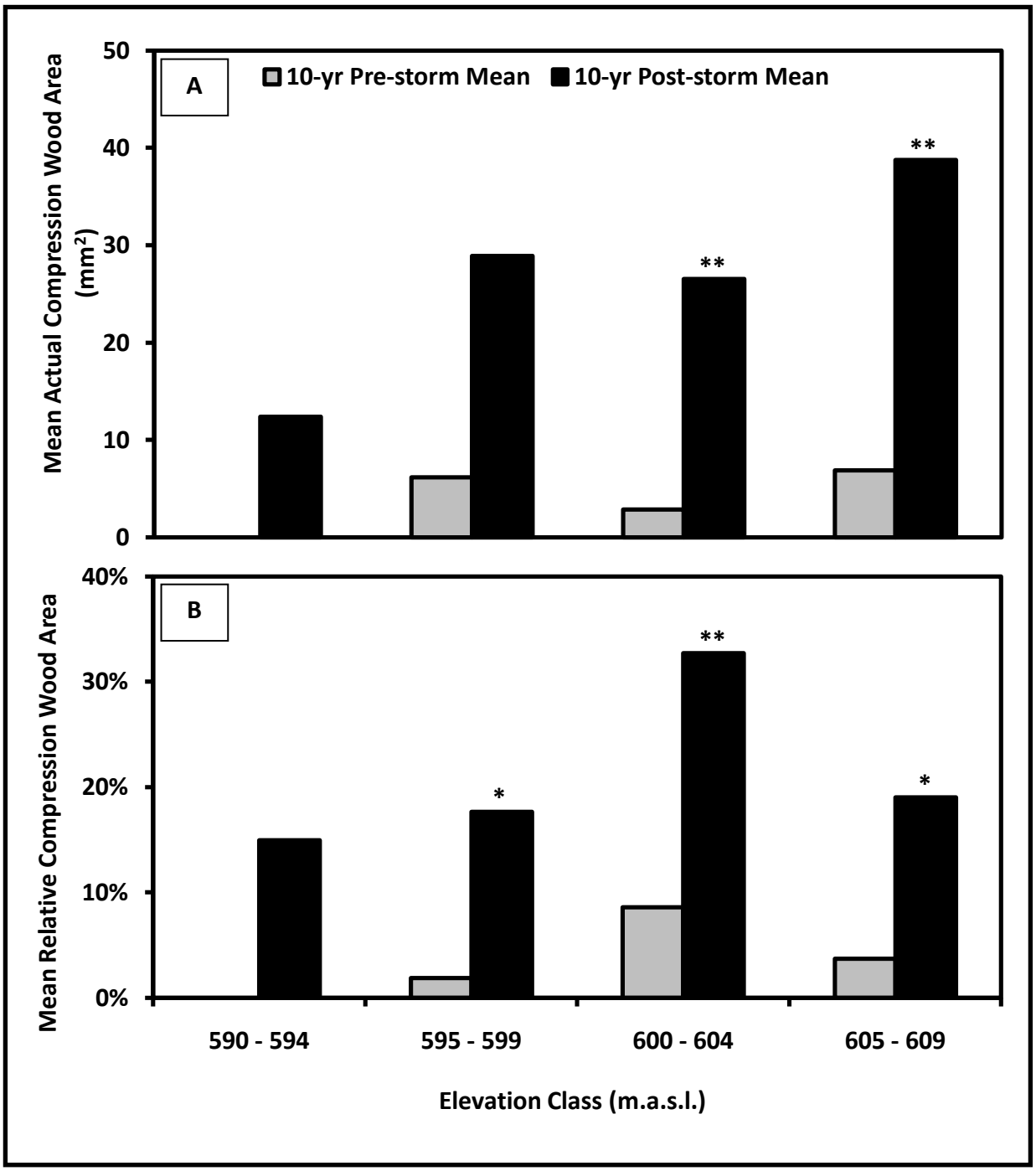

Figure 18. *Pre- and post-storm actual **(A)** and relative **(B)** compression wood by elevation class. Asterisks indicate elevation classes that formed significantly more compression wood after the ice storm (** = P < 0.01, * = P < 0.05).*

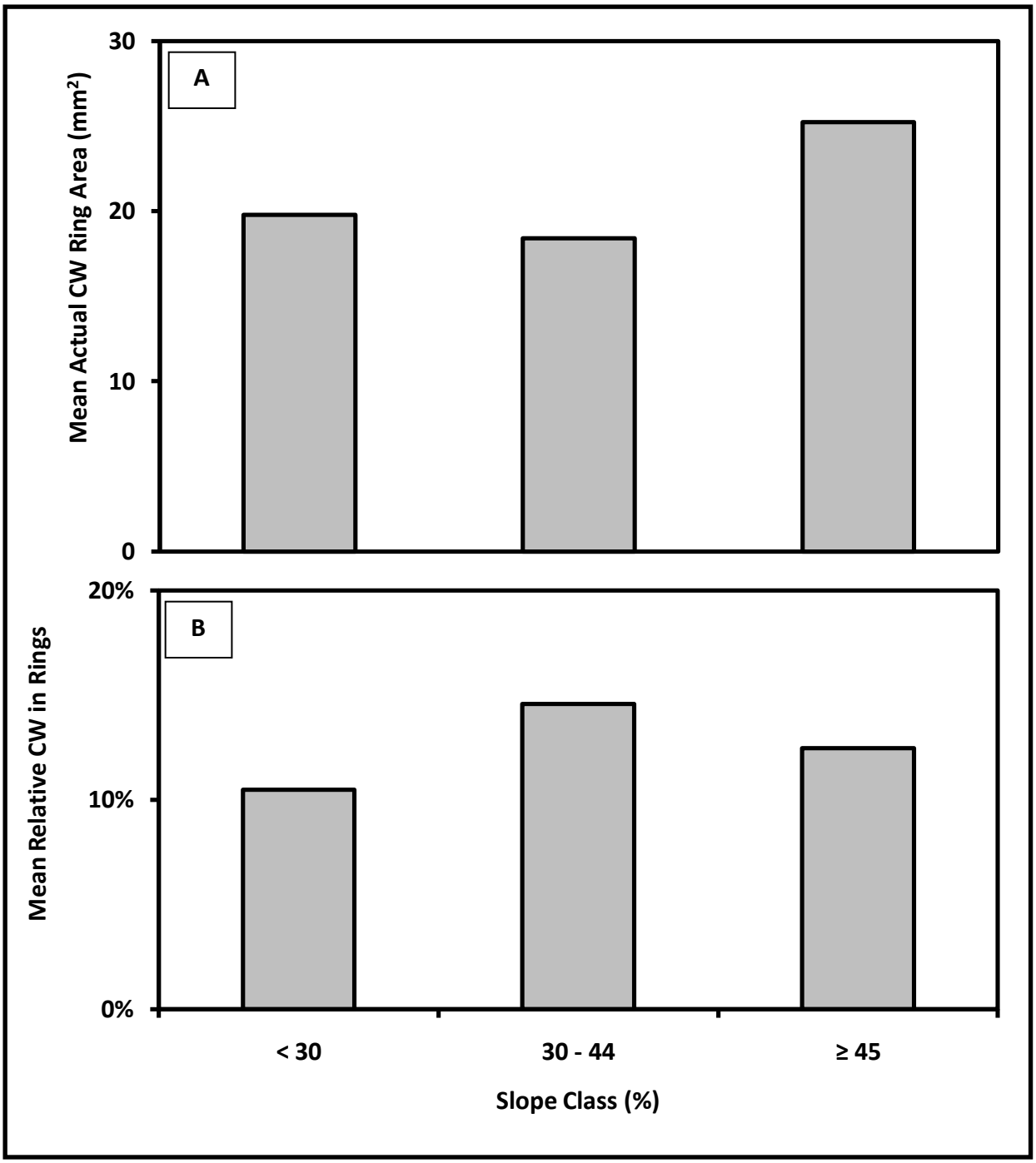

Figure 19. *Actual compression wood **(A)** and relative compression wood **(B)** cross-sectional area by slope class.*

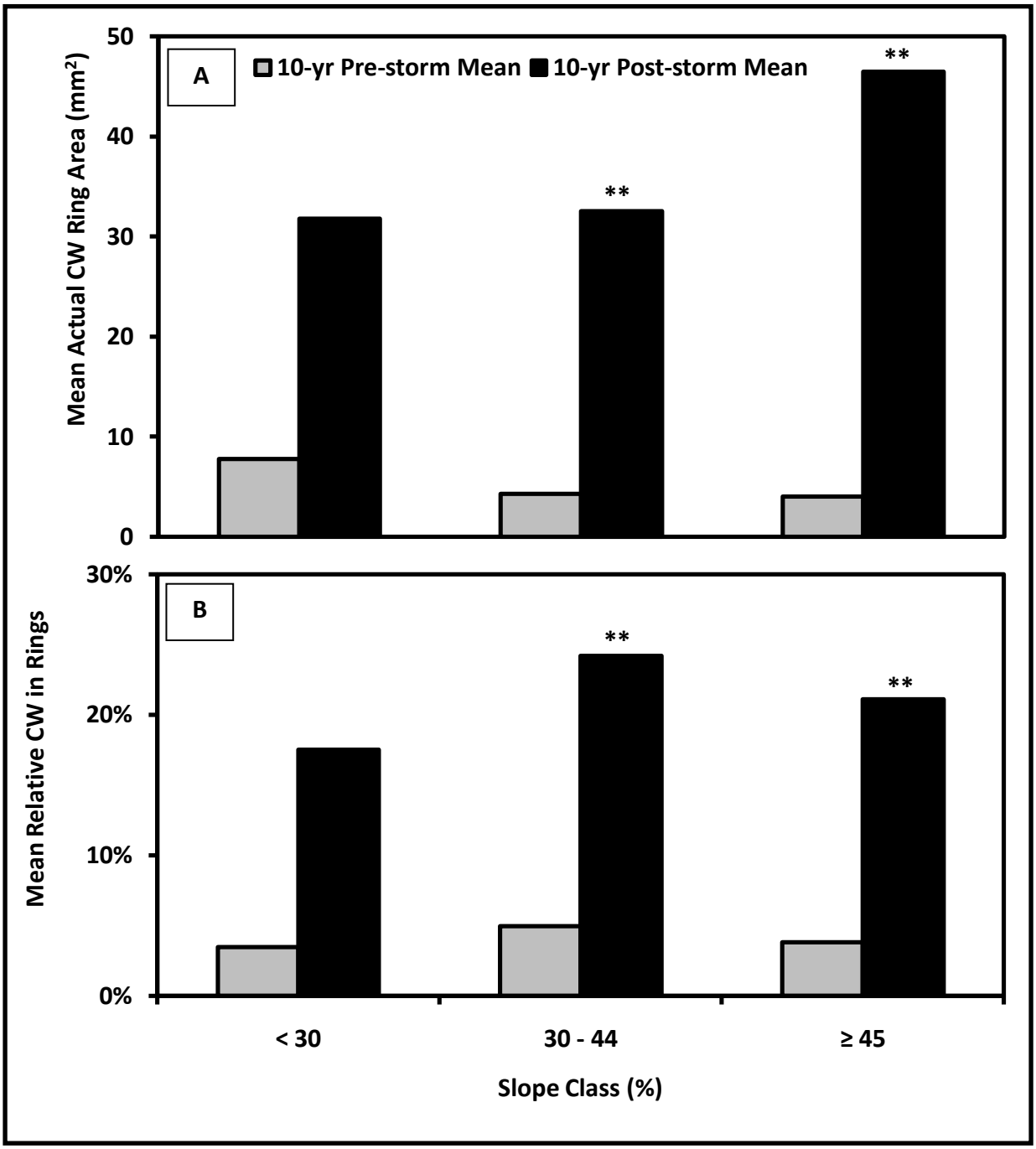

Figure 20. *Pre- and post-storm actual **(A)** and relative **(B)** compression wood by slope class. Asterisks indicate slope classes that formed significantly more compression wood after the ice storm (** = P < 0.01, * = P < 0.05).*

Aspect highly influenced *P. strobus* establishment, creating conditions that did not allow a fair test between hillsides. Due to the small sample size of *P. strobus* trees on the southwest aspect that were mature at the time of the ice storm (n = 4), no statistical difference could be detected between the two aspects (actual: $F = 1.33$, $P = 0.255$; relative: $F = 1.6$, $P = 0.212$) (Figure 21). Significant increases in compression wood area after the ice storm were found on the northeast aspect (actual: $t = -4.83$, $P < 0.001$; relative: $t = -5.03$, $P < 0.001$), but not on the southwest aspect (actual: $t = -2.67$, $P = 0.116$; relative: $t = -1.23$, $P = 0.342$) (Figure 22).

Frequency of *Pinus strobus* establishment was highly dependent on aspect ($\chi 2 = 35.57$, $df = 1$, $P < 0.001$). On the northeast aspect, year of establishment ranged from 1966 to 1976 and the median year of establishment was 1968 (n = 99). On the southwest aspect (n = 31), median year of establishment was 1994 (Figure 23). Across both aspects, tree diameter ranged (2 – 48 cm) with a negatively skewed frequency distribution (mean = 9.5 cm, median = 7.2 cm) as is commonly seen in many natural populations of biological organisms. On the southwest aspect, diameter classes ranged (2 – 13 cm) with a mode at 4 cm, and on the northeast aspect tree diameter ranged from 3 – 48 cm, with a mode at 7 cm (Figure 24).

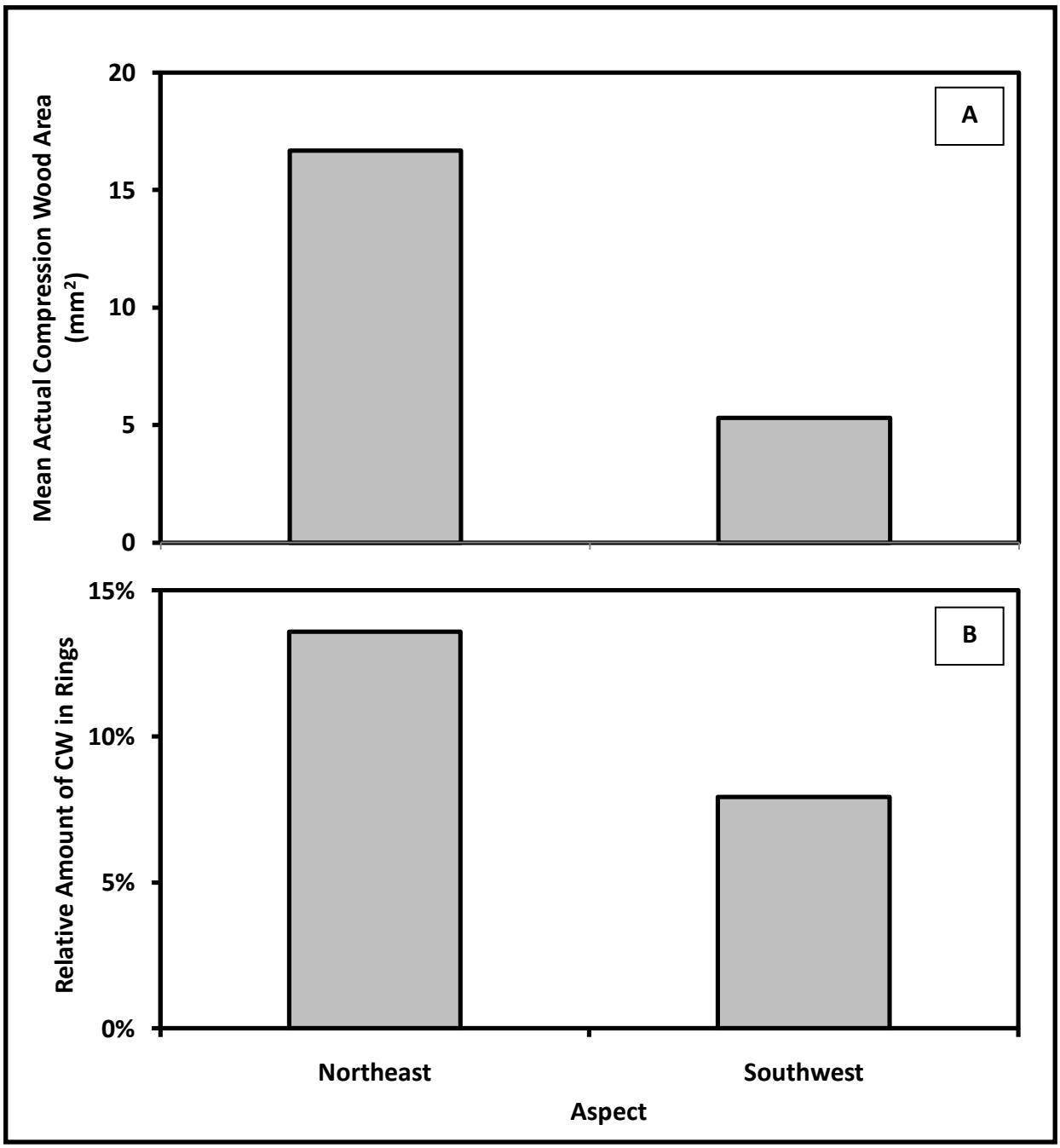

Figure 21. *Actual compression wood **(A)** and relative compression wood **(B)** cross-sectional area by aspect.*

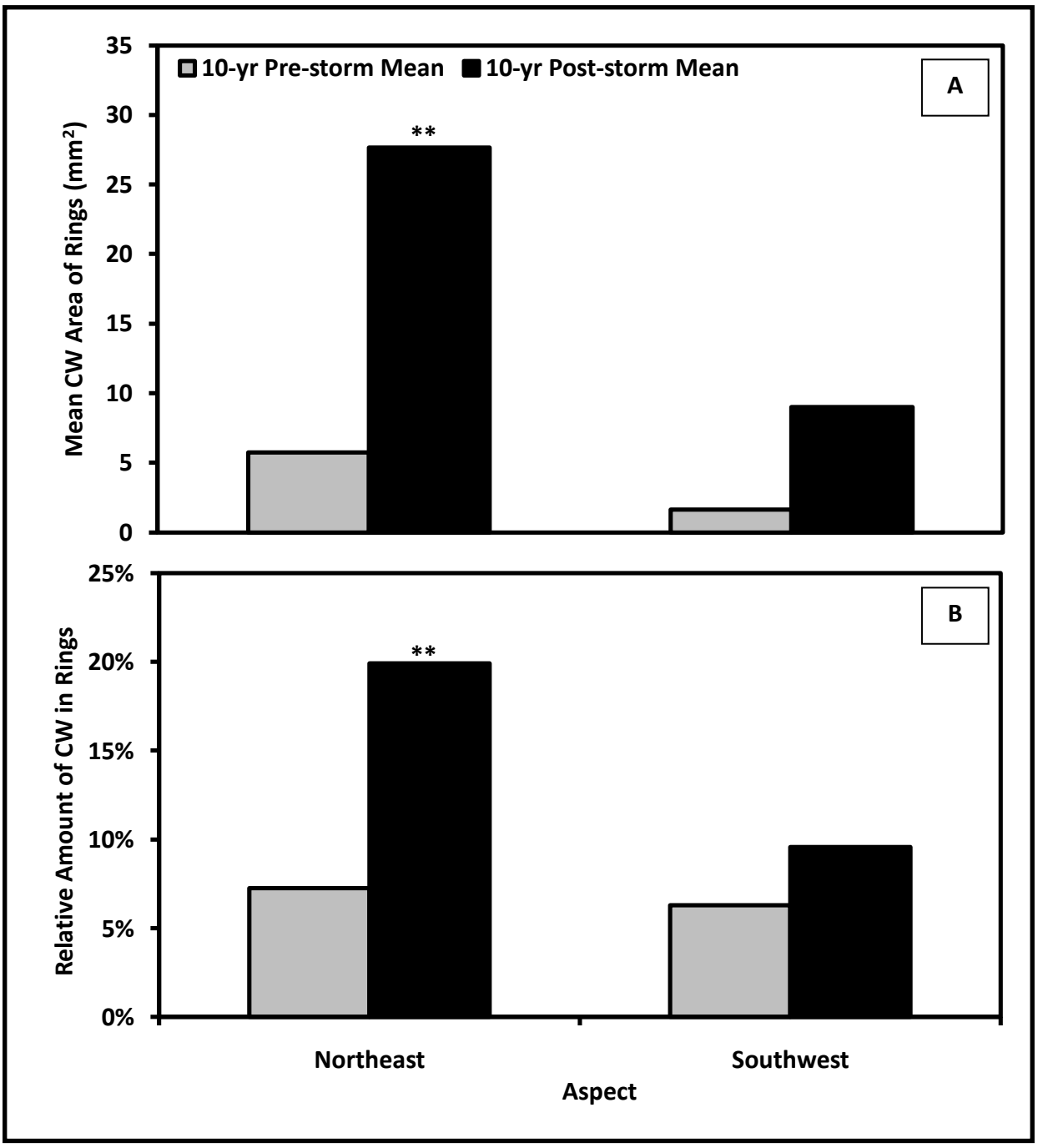

Figure 22. *Pre- and post-storm actual **(A)** and relative **(B)** compression wood by aspect. Asterisks indicate aspects that formed significantly more compression wood after the ice storm (** = P < 0.01, * = P < 0.05).*

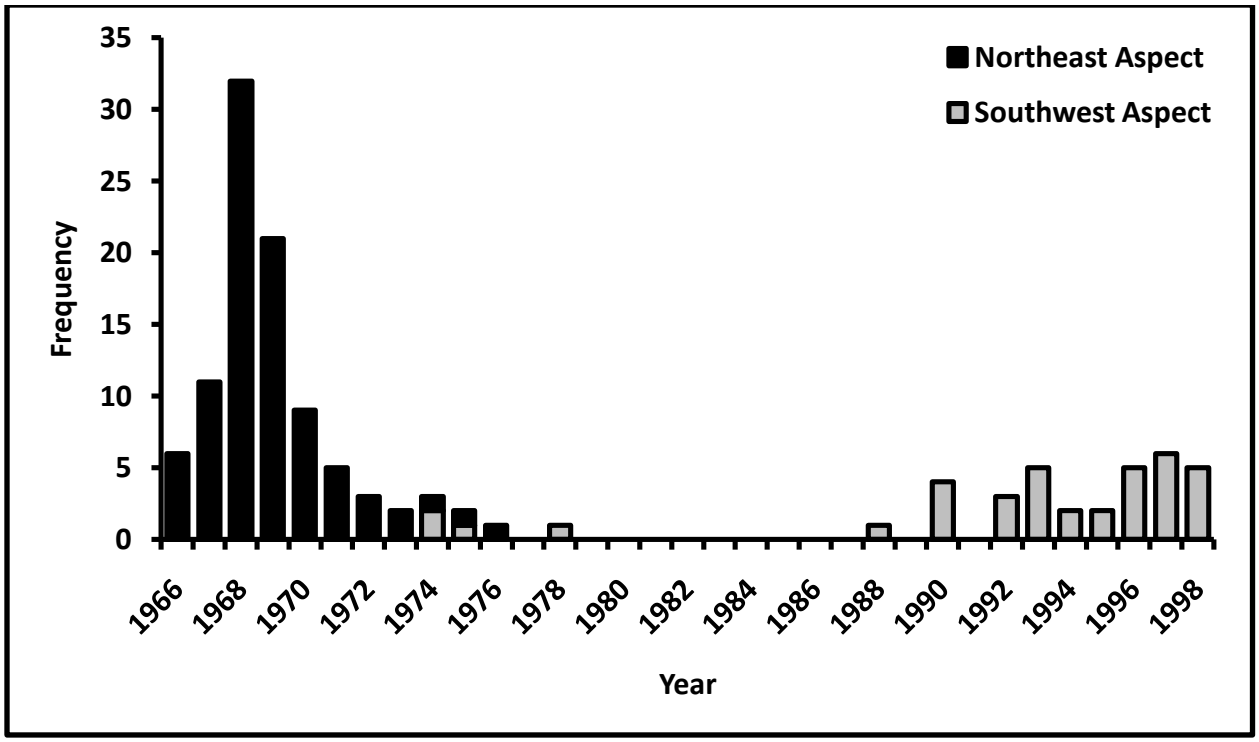

Figure 23. *Histogram of Pinus strobus establishment on northeast and southwest aspects.*

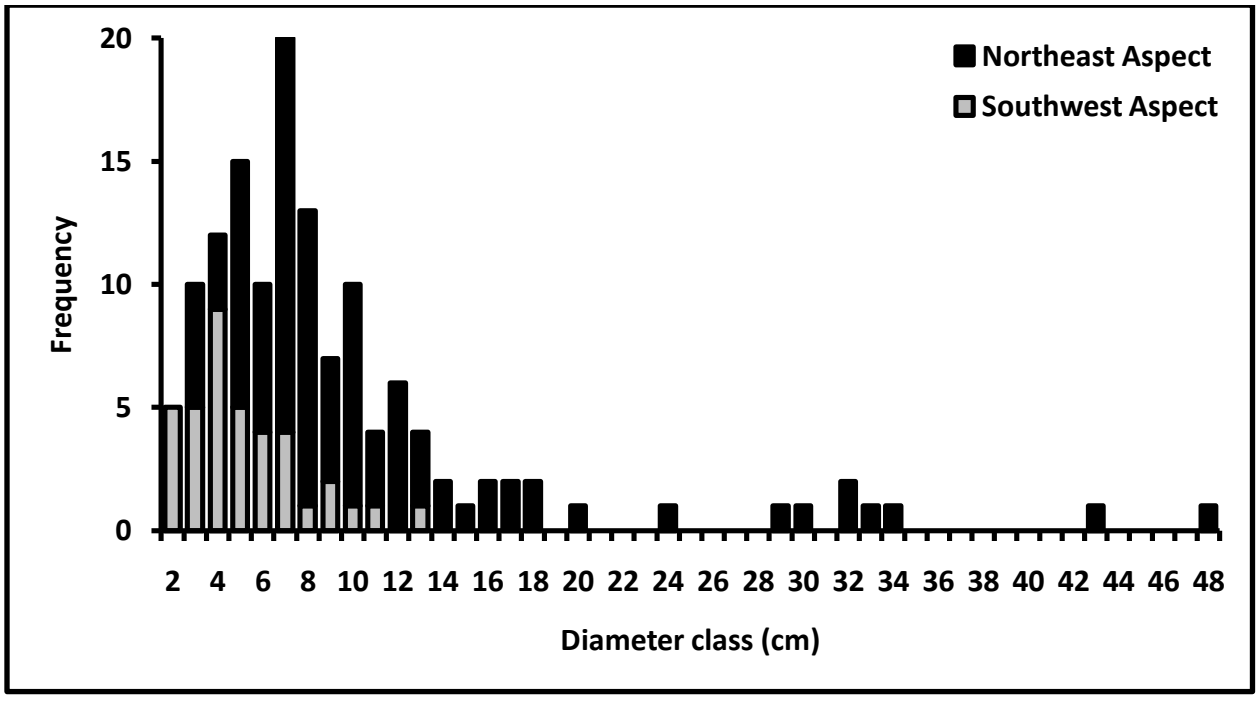

Figure 24. *Histogram of Pinus strobus diameter classes on northeast and southwest aspects.*

Pinus strobus stem locations (x, y, z coordinates) were plotted on the northeast aspect, along with their cross-sectional area (unfilled black circles) and compression wood area (filled red circles) in each year of the cohort's lifetime. Reproducing this graph for each year (1969 – 2006) revealed spatial and temporal patterns in normal and compression wood growth (Appendix E2). One such graph for the outer tree-ring (2006) is provided here (Figure 25). Thirteen years after the ice storm, highest compression wood formation was found at the upper ridge-top position, which contained moderate soil depths (1 m) and *P. strobus* tree diameters in the 6 – 13 cm range. High relative compression wood was found in trees in the 2 – 5 cm diameter range growing at the steep (>60%) mid-slope position. Trees growing in the valley attained larger sizes due to higher water and nutrient availability, and did not form much compression wood after the ice storm.

One large-diameter tree (16.2 cm diameter at the time of the storm) that grew on a steep slope formed unusually high amounts of compression wood for its size. It was also close to several larger *P. strobus* trees, suggesting that upper canopy branch breakage could have increased the weight load on this tree. This tree was removed from the data analysis due to its high leverage which obscured other relationships among independent variables. The purpose of this study was to investigate the effects of ice deposition, so if this tree was damaged additionally by large broken branches it may not be comparable to trees that only received ice damage (Figure 25).

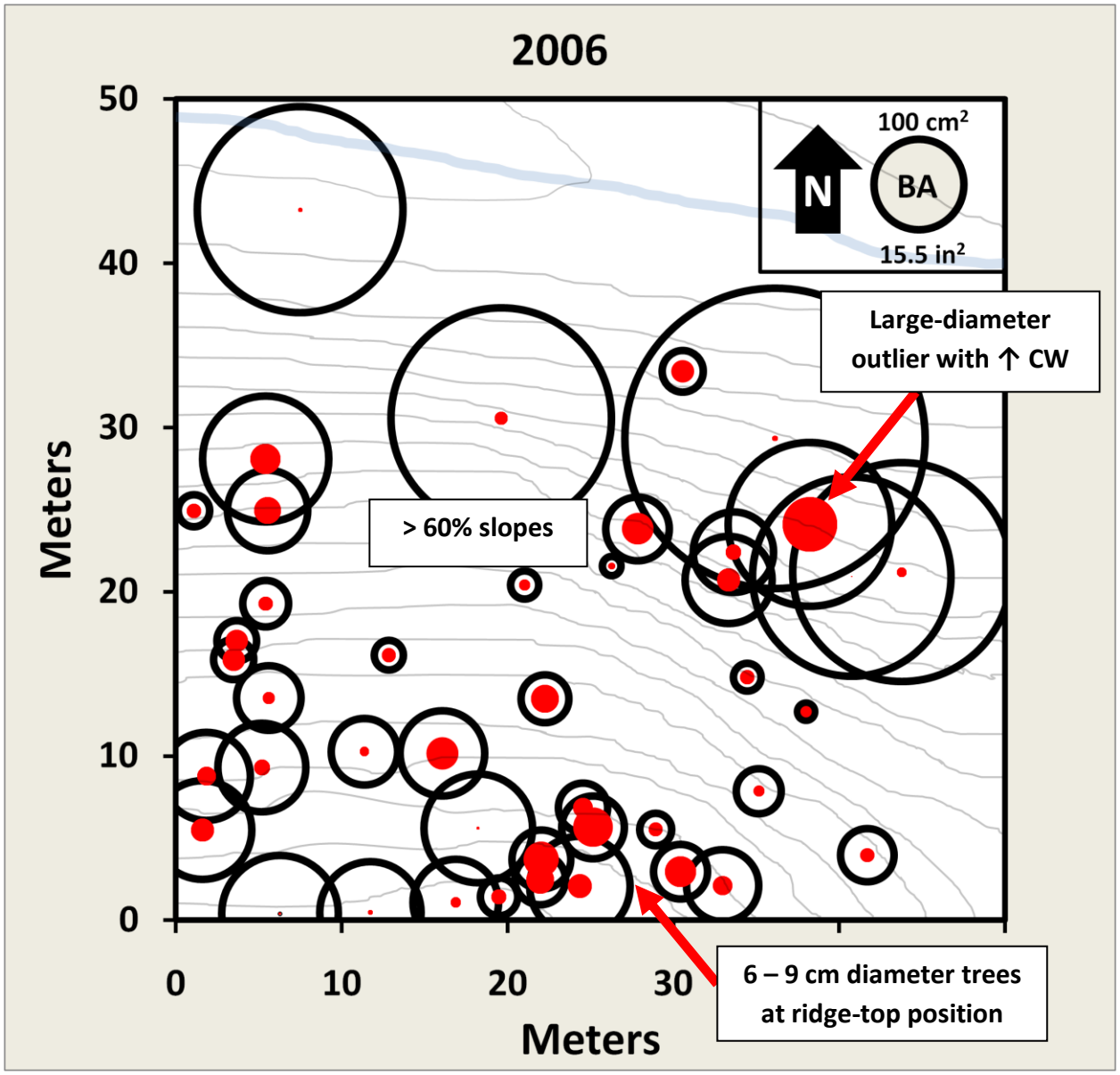

Figure 25. *Total compression wood area by study tree on the northeast aspect of the plot. Unfilled black circles indicate tree cross-sectional area in 2006, while interior red filled circles indicate total compression wood area formed in the tree's lifetime. A 100 cm^2 reference circle is shown in the upper right corner along with a north arrow.*

Another outlier in the dataset provides an example of the possibilities for compression wood as a tool for reconstructing past tree movement events. This tree was an outlier in terms of the mean direction of compression formation; it was not leaning downhill. When examined in the field, it was observed that the tree was actually growing on the eastern edge of a small depression in the soil caused by a larger fallen tree. It turned out that the tree *was* leaning downhill, but on a microtopographical scale. Looking at that tree's rings, we can see a shift in compression wood direction starting in 1977, and then significantly from 1979 onward. It is possible that a larger tree could have died a few years before the 1979 ice storm, and its bole was uprooted under the weight of ice, creating the pit-and-mound topography that caused this small *P. strobus* nearby to deviate from the norm (Figure 26).

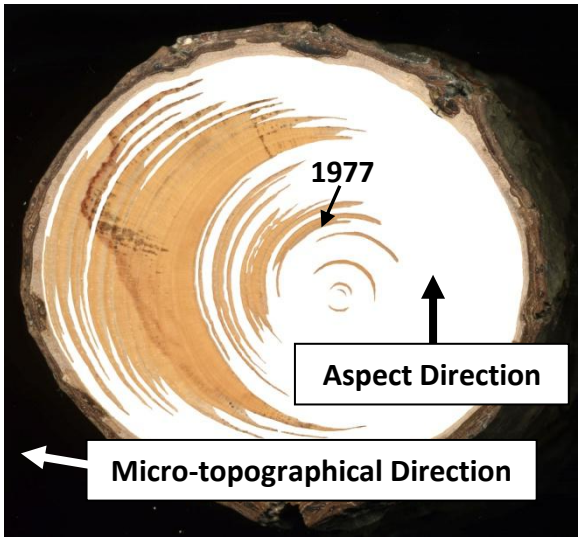

Figure 26. *Pinus strobus sample after image processing. All normal wood area (white area) has been removed in Photoshop, leaving only the compression wood area (dark wood remaining) in each tree-ring.*

Competition Index

No direct relationship existed between the modified competition index and compression wood ($F = 1.43$, $P = 0.245$) (Figure 27-A), but a significant difference existed when the percentage of compression wood in cross-sections was examined ($F = 3.73$, $P = 0.012$) (Figure 27). The lowest competition index class (< 0.5) contained significantly less compression wood than other classes, and no other differences existed. However, the lowest competition class contained the largest diameter trees with low compression wood formation.

Competition index class was significantly negatively correlated with tree diameter ($r = -0.5$), which is a mathematical artifact because focal tree diameter is the numerator in the competition index equation. It is uncertain whether a true relationship exists between competition index class and compression wood, or if the negative relationship with tree diameter is driving this relationship. Both variables explain a similar portion of the variance in compression wood distribution (Appendix D1).

After the ice storm, trees in the second and third competition index classes formed the most actual and relative compression wood (class 2 actual $t = -2.91$, $P = 0.016$; relative $t = -2.99$, $P = 0.014$) and the largest departure from the ten year pre-storm mean was in the third class (class 3: actual $t = -2.93$, $t = 0.019$; relative $t = -3.66$, $P = 0.006$) (Figure 28). In addition, the highest competition index class formed significant relative compression wood after the storm (class 5: actual $t = -1.91$, $P = 0.105$; relative $t = -2.5$, $P = 0.046$). No significant differences were found in the first or fourth classes (class 1: actual $t = -1.1$, $P = 0.301$; relative $t = -1.05$, $P = 0.319$; class 4: actual $t = -1.86$, $P = 0.137$; relative $t = -1.76$, $P = 0.153$).

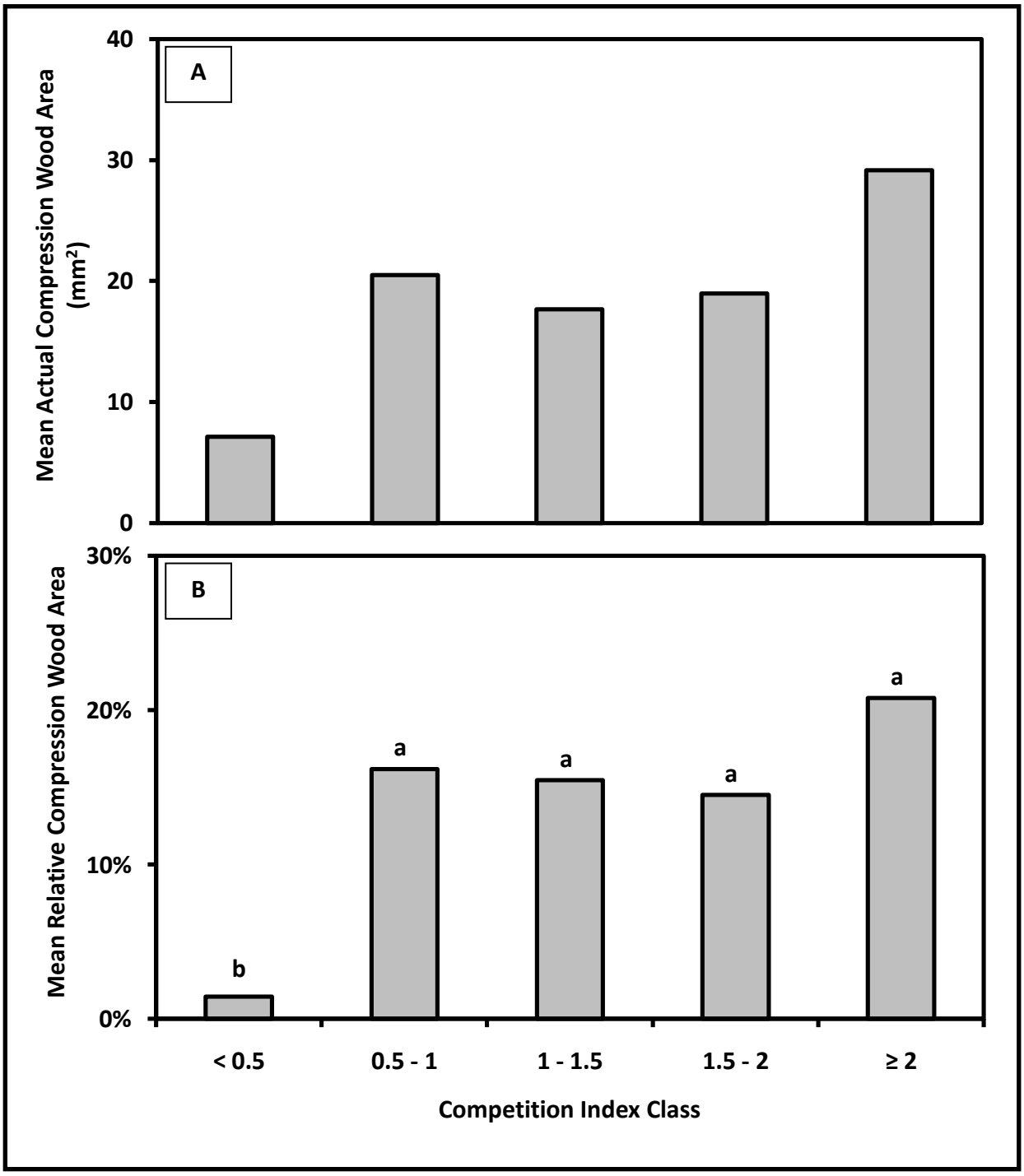

Figure 27. *Actual compression wood **(A)** and relative compression wood **(B)** cross-sectional area by competition index class. Different lowercase letters indicate classes that were significantly different.*

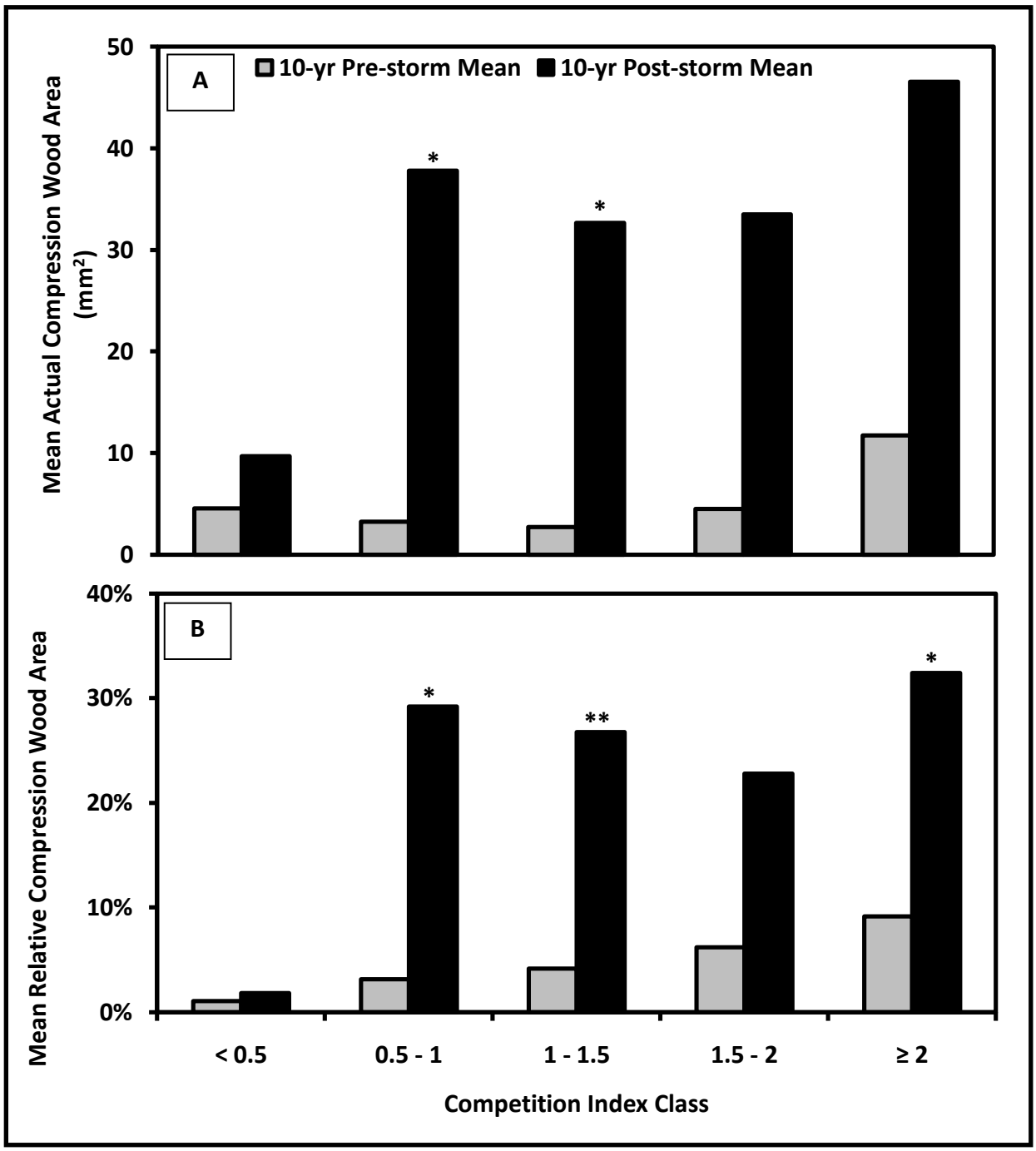

Figure 28. *Pre- and post-storm actual **(A)** and relative **(B)** compression wood by competition index class. Asterisks indicate competition index classes that formed significantly more compression wood after the ice storm (** = P < 0.01, * = P < 0.05).*

Cellular Features Before and After the Ice Storm across a Tree Diameter Gradient

Comparisons of Features among Compression, Opposite, and Normal Wood Cells

Tree-rings containing compression wood were significantly wider on the downhill stem side than the uphill side containing opposite wood, but were not significantly different than normal wood ring widths ($F = 7.29$, $P < 0.001$) (Figure 29). Compression wood contained significantly more cells in a radial file than opposite ($\chi^2 = 18.107$, $df = 1$, $P < 0.001$), or normal wood cells ($\chi^2 = 13.719$, $df = 1$, $P < 0.001$). No significant differences were found between compression and normal wood cell counts ($\chi^2 = 0.173$, $df = 1$, $P = 0.677$), or between normal wood rings on different sides of the stem ($\chi^2 = 0.999$, $df = 1$, $P = 0.317$). Compression wood contained significantly more cells per mm than normal wood, but was not significantly different than opposite wood ($F = 8.56$, $P < 0.001$) (Table 6).

Table 6. *Mean number of cells per mm in a radial file of compression, opposite, and normal wood measured on the downhill and uphill sides of Pinus strobus stems. Different lowercase letters indicate classes that were not significantly different.*

Type of Cell (Stem Side)	Mean Number of Cells mm^{-1} in a Radial File
Compression Wood (Downhill)	33.2 [a]
Opposite Wood (Uphill)	31.4 [a]
Normal Wood (Downhill)	26.5 [b]
Normal Wood (Uphill)	26.6 [b]

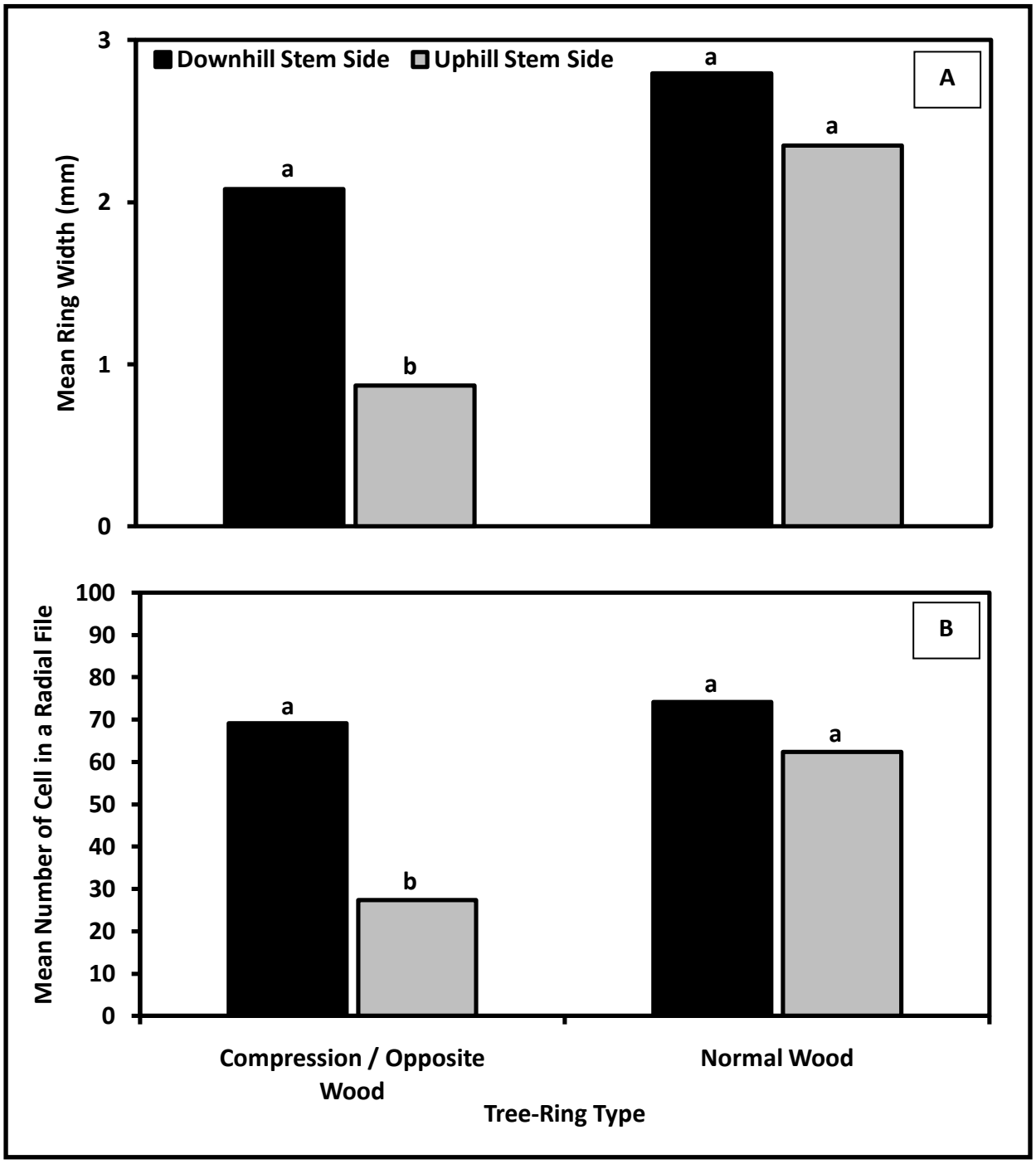

Figure 29. *Mean tree-ring width* ***(A)*** *and mean number of cells in a radial file* ***(B)*** *by tree-ring type (compression/opposite wood vs. normal wood). Different lowercase letters indicate classes that were significantly different.*

Mean tracheid diameter was smaller in compression wood than normal wood cells, but was not significantly different than that of opposite wood ($F = 7.41$, $P < 0.001$) (Figure 30). Compression wood had significantly smaller-mean lumen diameter than opposite wood, both of which were smaller than normal wood ($F = 17.32$, $P < 0.001$). Compression wood cell wall thickness was significantly higher than other cell types ($F = 13.23$, $P < 0.001$).

Outer tracheid area of normal wood was significantly larger than compression or opposite wood cells ($F = 7.53$, $P < 0.001$) (Figure 31). Lumen area mirrored this pattern ($F = 14.36$, $P < 0.001$). However, cell wall area was statistically similar among normal, compression, and opposite wood cell types ($F = 1.73$, $P = 0.164$). Overall, compression wood cells filled a greater percentage of the wood cross-section (47%) with cellular material than any other cell type ($F = 12.32$, $P < 0.001$) (Table 7). Compression wood cell circularity was significantly higher than in normal or opposite wood cells ($F = 22.61$, $P < 0.001$) (Figure 32).

Table 7. *Mean cross-sectional percentage of wood filled with cell wall tissue by cell type. Different lowercase letters indicate classes that were not significantly different.*

Type of Cell (Stem Side)	Cross-sectional area filled with cell wall (%)
Compression Wood (Downhill)	47 [a]
Opposite Wood (Uphill)	36 [a]
Normal Wood (Downhill)	32 [b]
Normal Wood (Uphill)	30 [b]

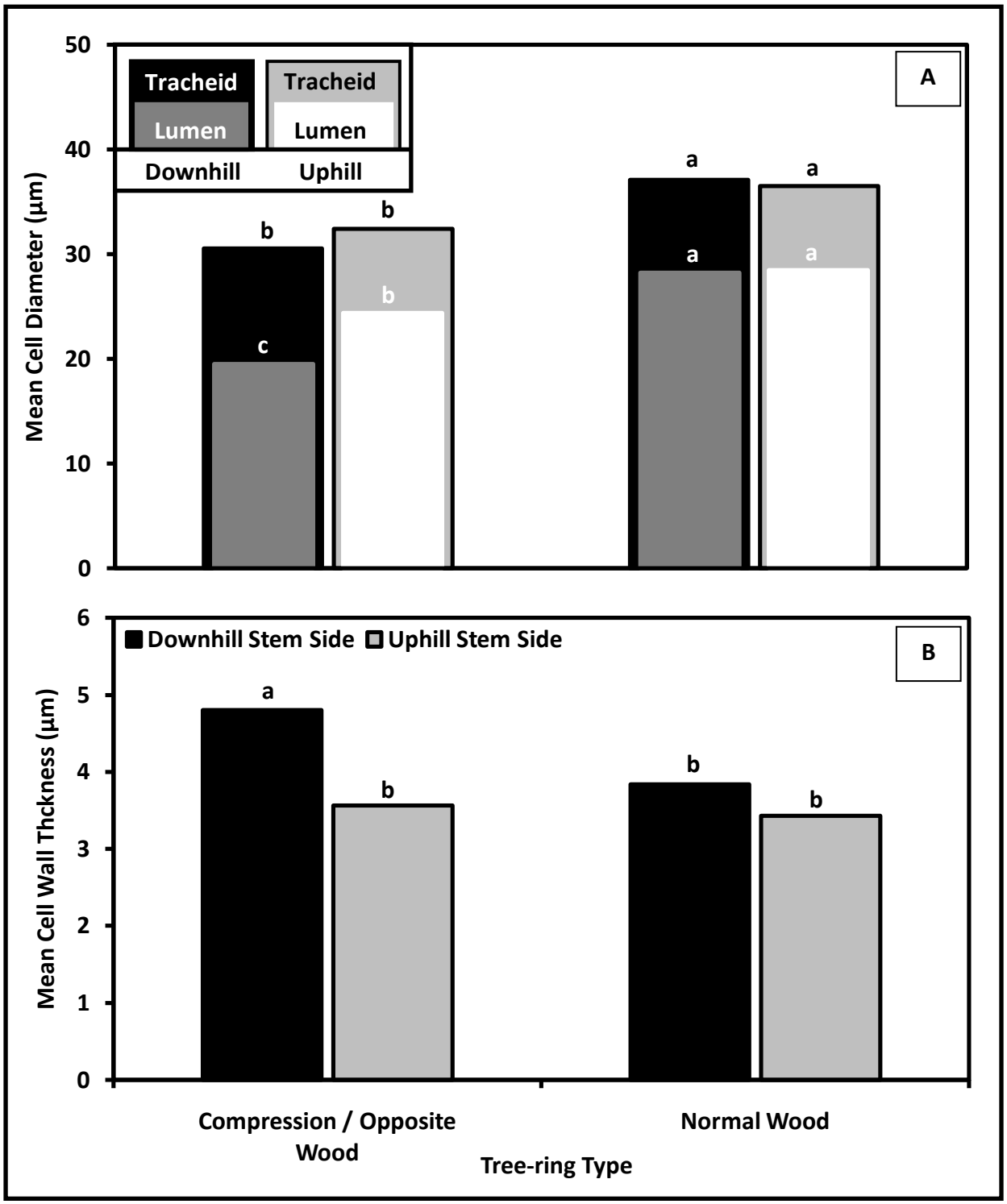

Figure 30. *Mean cell diameter* ***(A)*** *and cell wall thickness* ***(B)*** *by tree-ring type (compression/opposite wood vs. normal wood). Different lowercase letters indicate classes that were significantly different.*

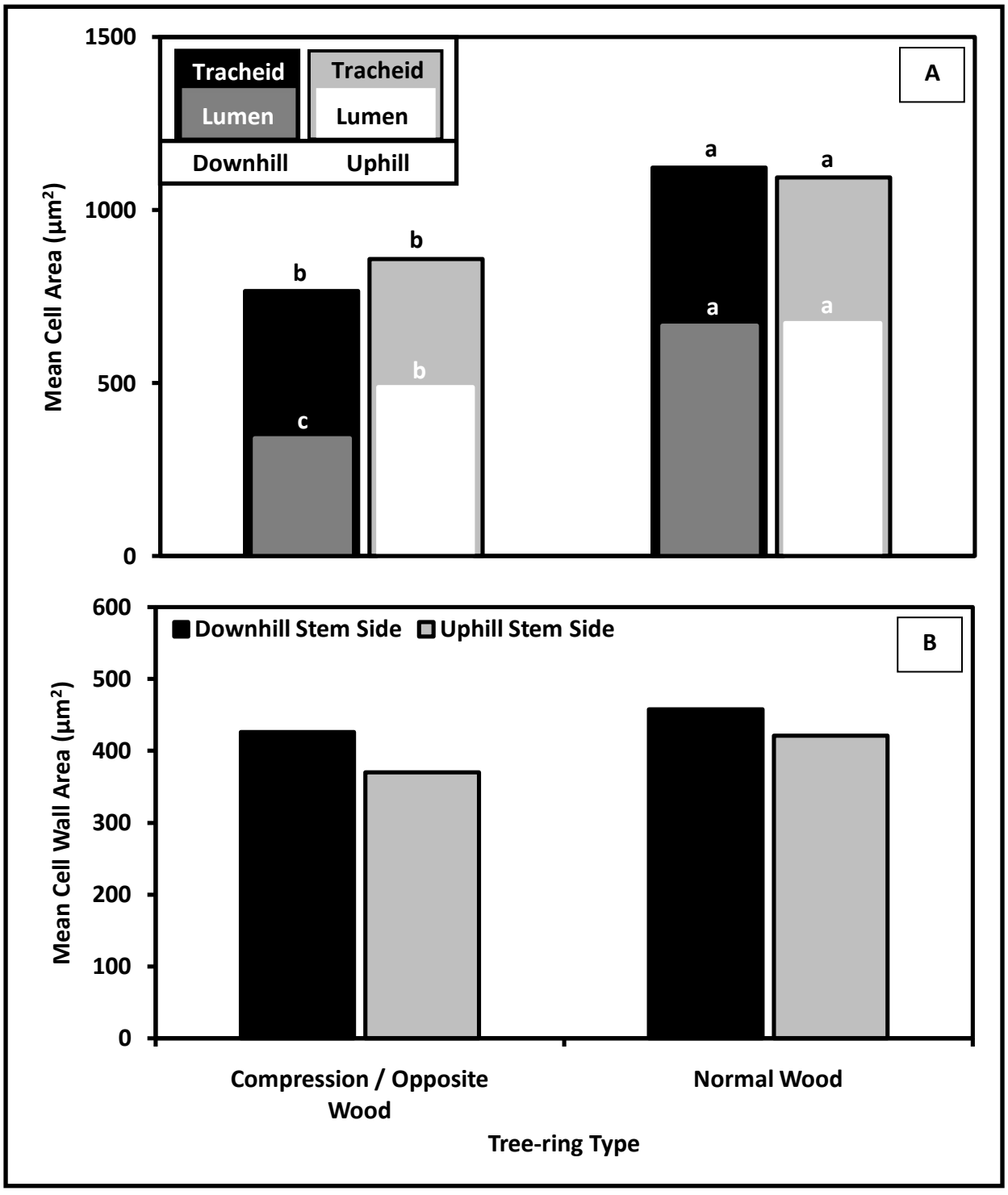

Figure 31. *Mean cell area* ***(A)*** *and cell wall area* ***(B)*** *by tree-ring type (compression/opposite wood vs. normal wood). Different lowercase letters indicate classes that were significantly different.*

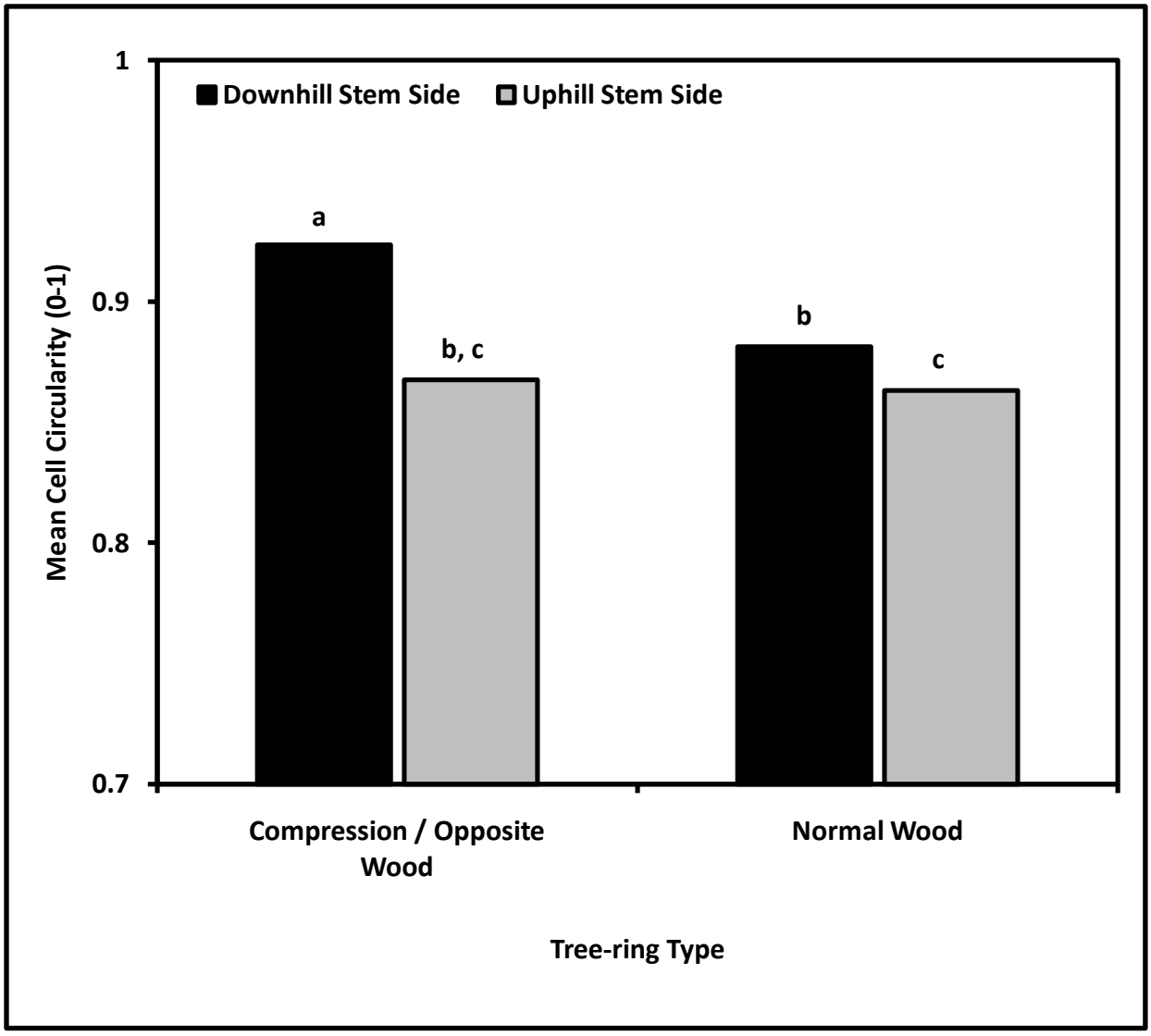

Figure 32. *Mean cell circularity by tree-ring type (compression/opposite wood vs. normal wood). Different lowercase letters indicate classes that were significantly different.*

Comparisons of Features by Year of Wood Formation

There were no significant differences in ring width among the six years examined on the downhill ($F = 0.41$, $P = 0.840$) or uphill side of the stem ($F = 0.11$, $P = 0.989$) (Figure 33). However, tree-rings were significantly wider on the downhill side of the stem than the uphill side in every year except 1993, which was a year of drought and a consistently small-width ring in the stand (1991: $t = 3.54$, $P = 0.005$; 1992: $t = 2.39$, $P = 0.036$; 1993: $t = 0.85$, $P = 0.414$; 1994: $t = 3.75$, $P = 0.003$; 1995: $t = 2.92$, $P = 0.014$; 1996: $t = 3.04$, $P = 0.011$).

On the downhill stem side significantly more compression wood cells were created after the 1994 ice storm than before ($\chi^2 = 14.745$, $df = 5$, $P = 0.012$), but on the uphill side there were no differences among years ($\chi^2 = 1.831$, $df = 5$, $P = 0.872$) (Figure 33). In the three years before the ice storm cell counts were similar on different sides of the stem (1991: $\chi^2 = 1.725$, $df = 1$, $P = 0.189$; 1992: $\chi^2 = 1.141$, $df = 1$, $P = 0.285$; 1993: $\chi^2 = 0.205$, $df = 1$, $P = 0.651$), but in the three years after, the downhill stem side contained significantly more cells (1994: $\chi^2 = 14.842$, $df = 1$, $P < 0.001$; 1995: $\chi^2 = 11.006$, $df = 1$, $P = 0.001$; 1996: $\chi^2 = 12.022$, $df = 1$, $P = 0.001$).

Mean tracheid diameter remained constant from 1991 – 1996 ($F = 0.39$, $P = 0.851$) (Figure 34). However, cell wall thickness increased significantly on the downhill stem side after the 1994 ice storm ($F = 3.14$, $P = 0.015$). Opposite wood cell wall thickness was similar before and after the ice storm ($F = 0.17$, $P = 0.972$). No differences were found in other measurements of cell size among different years (lumen diameter: $F = 1.18$, $P = 0.310$; tracheid area: $F = 0.28$, $P = 0.989$; lumen area: $F = 0.79$, $P = 0.651$; cell wall area: $F = 0.46$, $P = 0.925$).

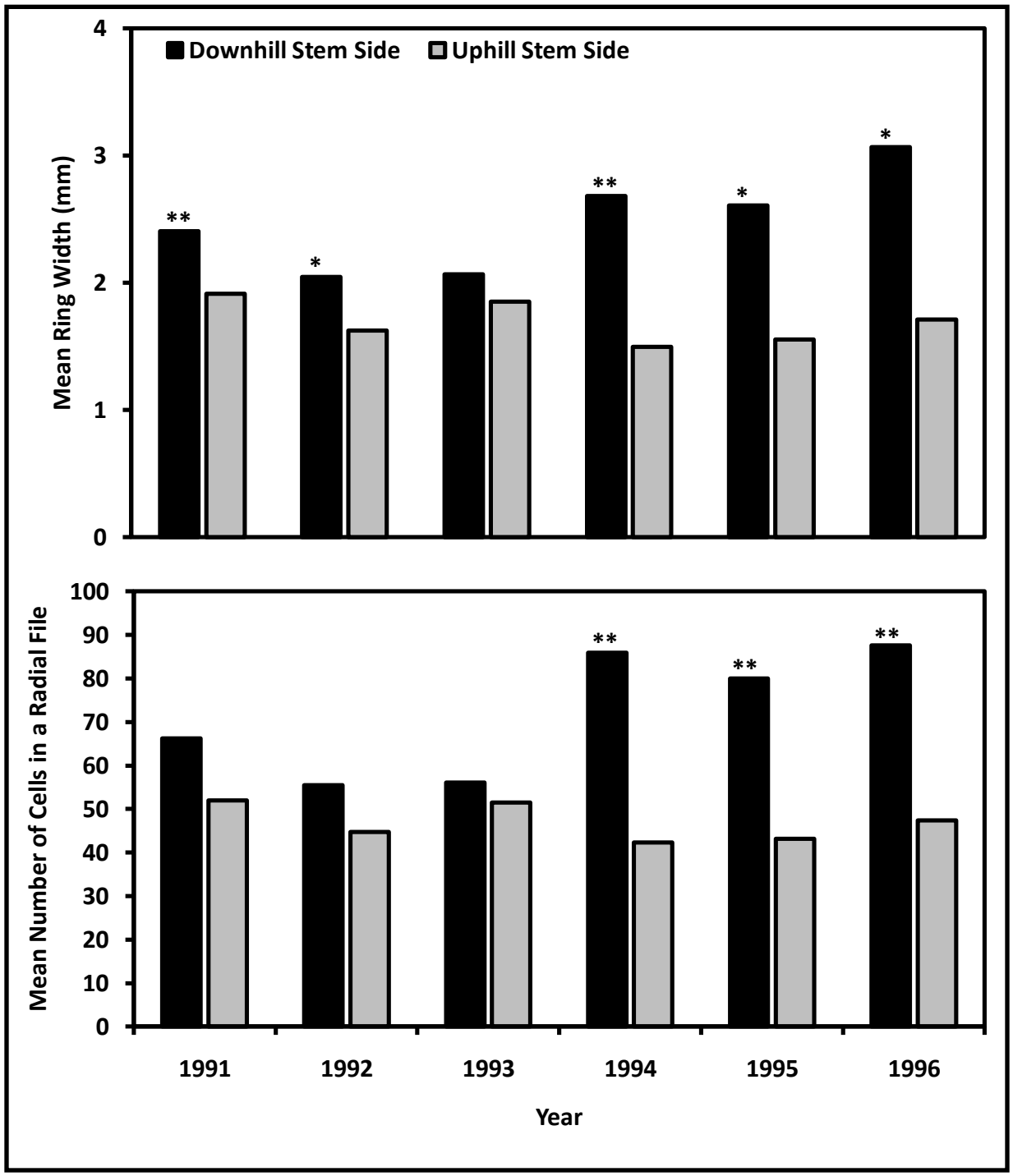

Figure 33. *Mean tree-ring width* ***(A)*** *and mean number of cells in a radial file* ***(B)*** *by year. Asterisks indicate years in which significantly more cells formed on the downhill stem side (** = P < 0.01, * = P < 0.05).*

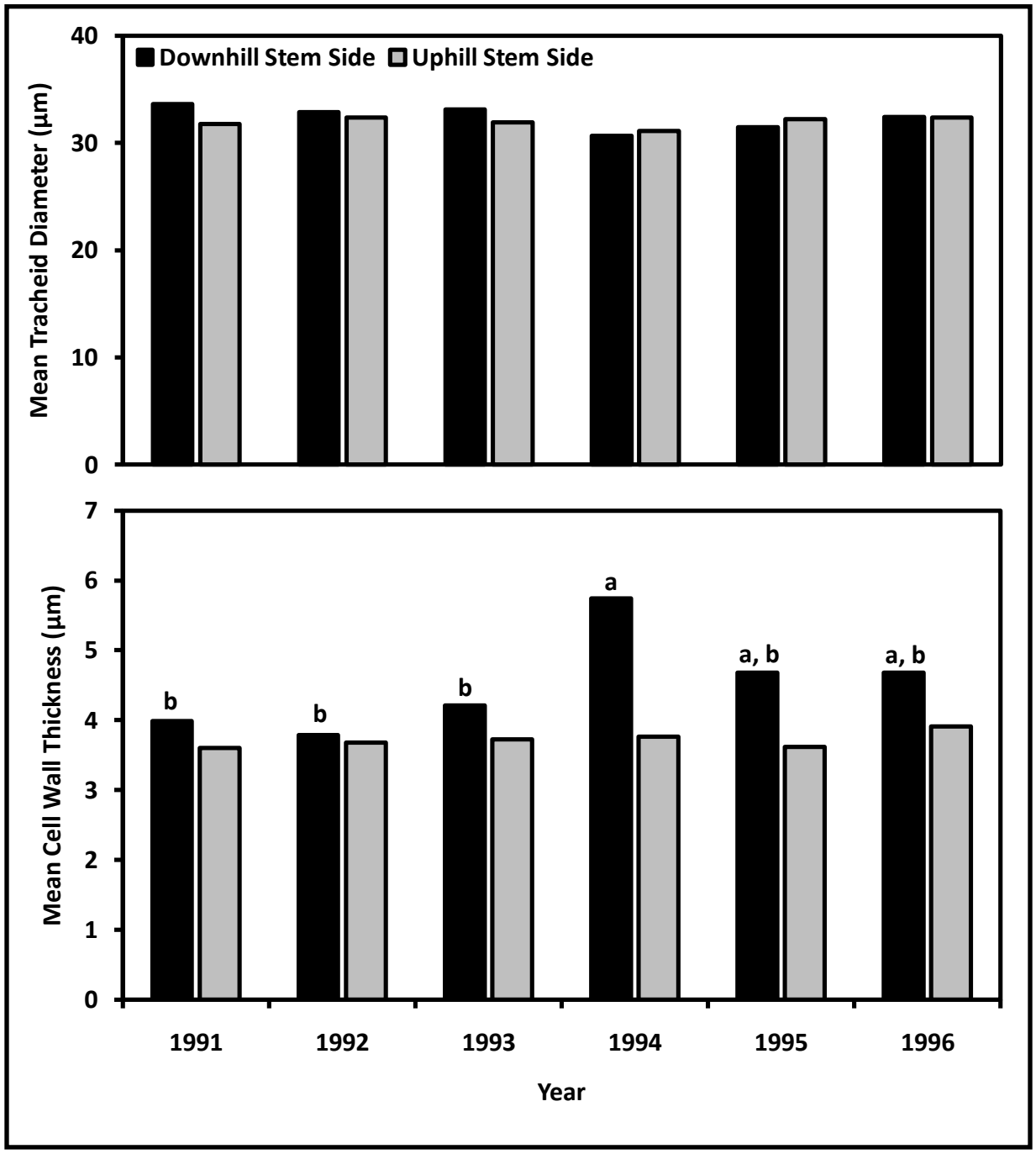

Figure 34. *Mean tracheid diameter **(A)** and mean cell wall thickness **(B)** by year. Different lowercase letters indicate classes that were significantly different.*

Year of cell formation significantly affected mean circularity ($F = 5.32$, $P < 0.001$) (Figure 35). In 1994, compression wood cells were significantly more circular than cells in other years examined, except 1995. Likewise, 1995 cells were not different from 1996 cells, but were more circular than pre-storm cells. There were no significant differences in opposite wood circularity in the six years examined.

Limited investigations of ultraviolet fluorescence revealed that in a sample containing severe compression wood, the first formed earlywood cells were classified as severe compression wood cells (Figure 36). Normal latewood tracheids formed in 1993 of similar cell wall thickness (Figure 36-B) did not fluoresce (Figure 36-A), because their lignin content was less than that of compression wood formed at cambial reactivation in the spring of 1994.

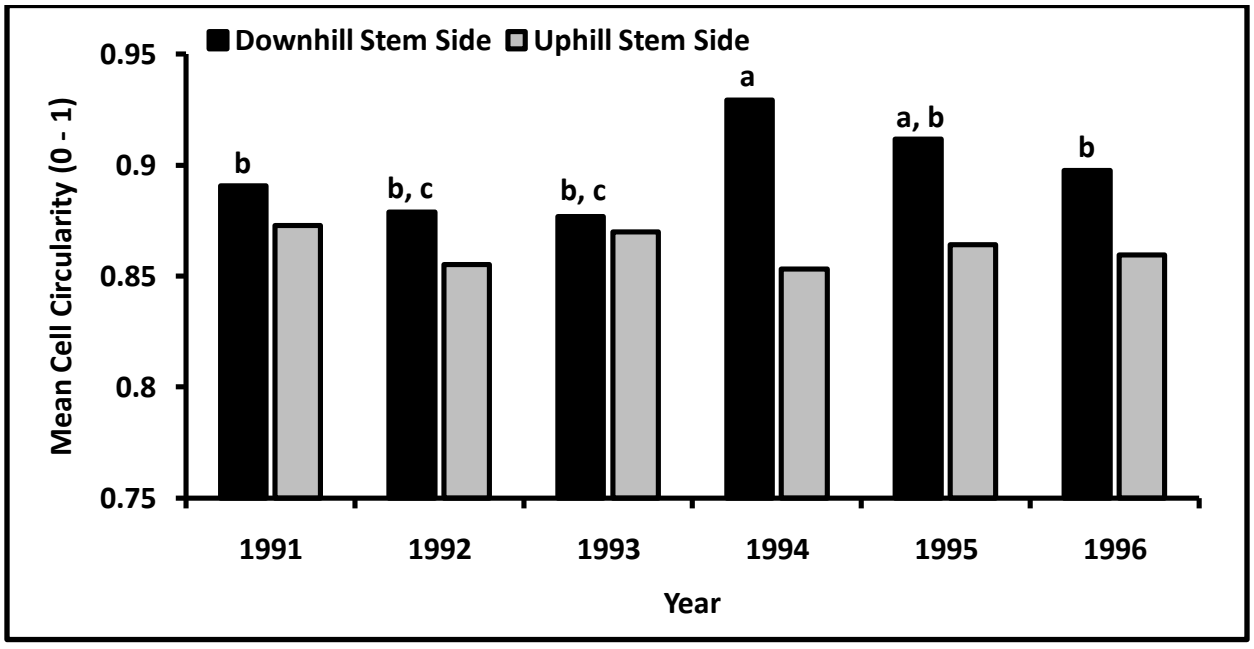

Figure 35. *Mean cell circularity by year. Different lowercase letters indicate classes that were significantly different.*

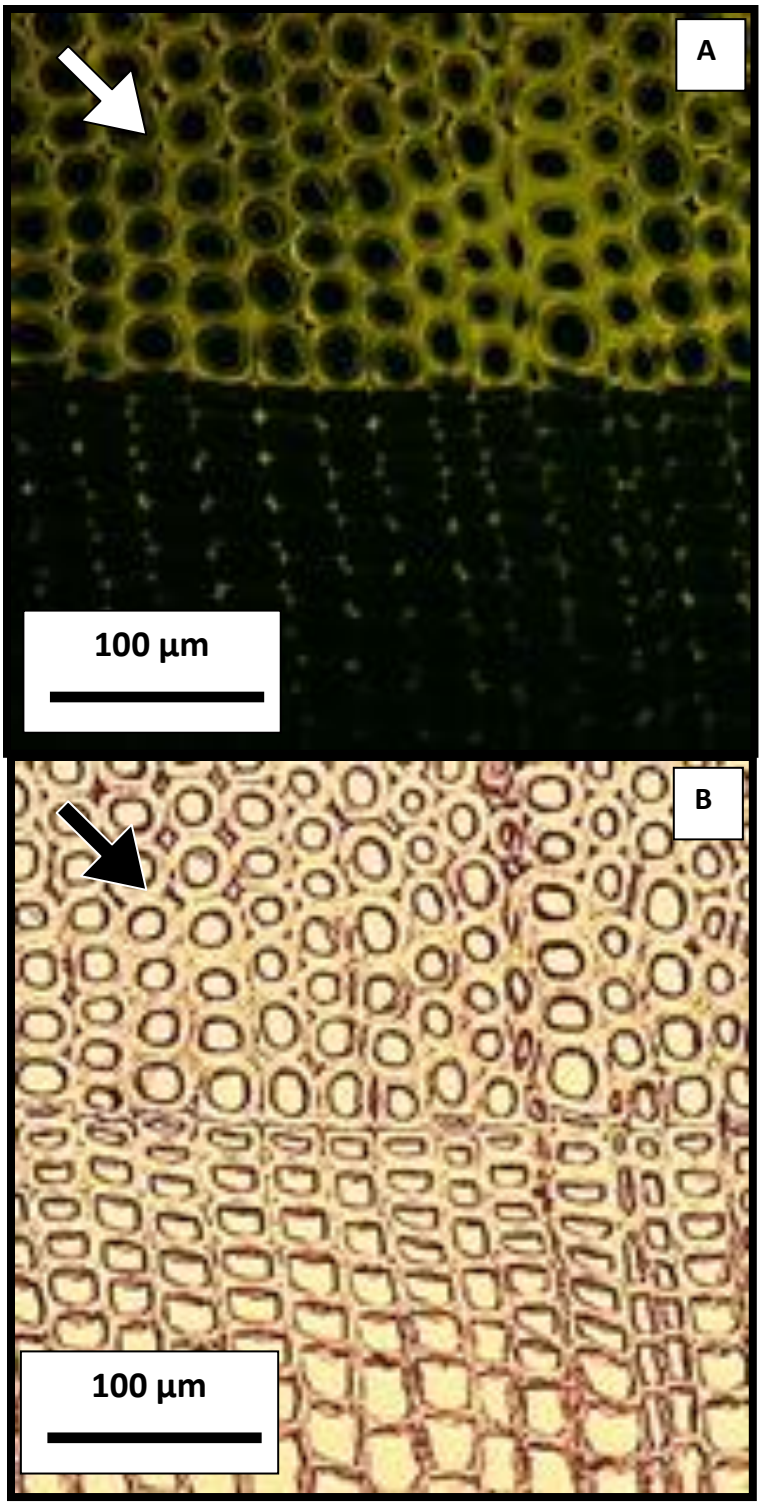

Figure 36. *The 1993/1994 growth ring boundary, viewed in an unstained 30-µm section of Pinus strobus wood in* ***(A)*** *ultraviolet (UV) light and* ***(B)*** *transmitted light under 100-x magnification. Compression wood cells (arrows) formed in 1994 fluoresced in UV light while normal latewood in 1993 did not.*

Comparisons of Features among Tree Diameter Classes

Tree diameter growth was influenced by both ring width ($r = 0.749$, $P < 0.001$) and the number of tracheids produced by the cambium ($r = 0.631$, $P < 0.001$). Tree rings were widest in the largest diameter class, and no significant differences in ring width existed on the downhill stem side among the smallest three classes ($F = 24.19$, $P < 0.001$); the uphill stem side followed a similar pattern ($F = 48.64$, $P < 0.001$) (Figure 37). Cell counts were related to tree diameter class (downhill side: $\chi^2 = 102.0$, df = 4, $P < 0.001$; uphill side: $\chi^2 = 146.462$, df = 4, $P < 0.001$). Only the largest diameter class did not show a significant difference in cell counts on opposite sides of the stem (2 – 5 cm: $\chi^2 = 13.569$, df = 1, $P < 0.001$; 6 – 9 cm: $\chi^2 = 11.361$, df = 1, $P = 0.001$; 10 – 13 cm: $\chi^2 = 4.52$, df = 1, $P = 0.033$; 14 – 30 cm: $\chi^2 = 4.609$, df = 1, $P = 0.032$; 30+ cm: $\chi^2 = 3.214$, df = 1, $P = 0.073$).

Tracheid diameter was correlated with tree diameter ($r = 0.856$, $P < 0.001$). Each successively larger diameter class had a significantly larger mean tracheid diameter than the preceding smaller class ($F = 107.23$, $P < 0.001$); all but the smallest two classes had a different mean lumen diameter ($F = 45.33$, $P < 0.001$) (Figure 38). Cell walls were significantly thinner in the 2 – 5 cm diameter class, but no differences in cell wall thickness existed among other classes ($F = 4.7$, $P = 0.001$).

Individual cell area was significantly correlated with tree diameter classes ($r = 0.776$, $P < 0.001$); cells with larger area produced larger diameter trees (tracheid area: $F = 95.81$, $P < 0.001$; lumen area: $F = 45.33$, $P < 0.001$; cell wall area: $F = 57.3$, $P < 0.001$) (Figure 39). However, cell circularity did not differ among tree diameter classes ($F = 0.73$, $P = 0.572$).

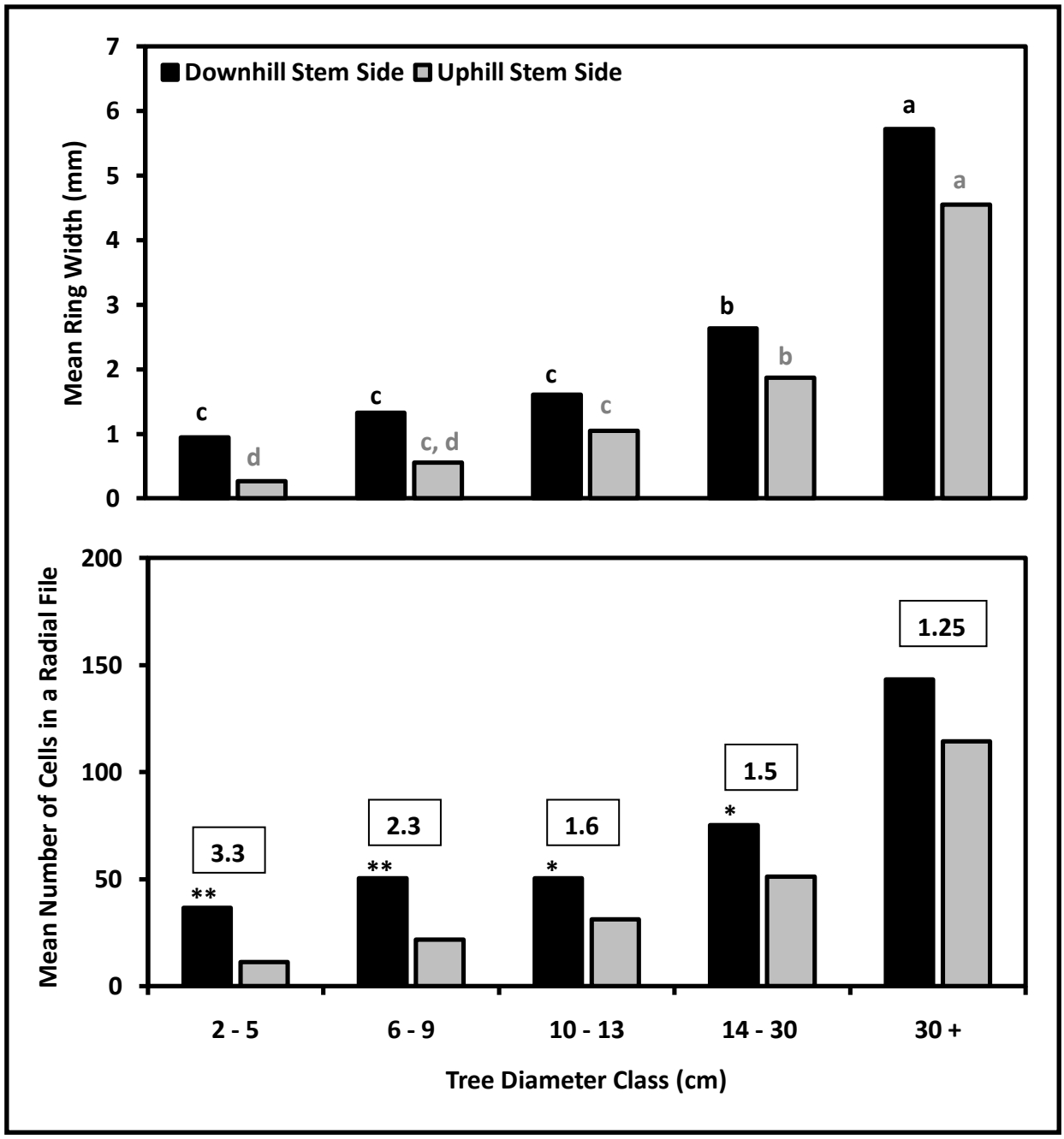

Figure 37. *Mean tree-ring width* ***(A)*** *and mean number of cells in a radial file* ***(B)*** *by diameter class. Different lowercase letters indicate classes that were significantly different. Asterisks indicate classes in which significantly more cells formed on the downhill stem side (** = P < 0.01, * = P < 0.05).*

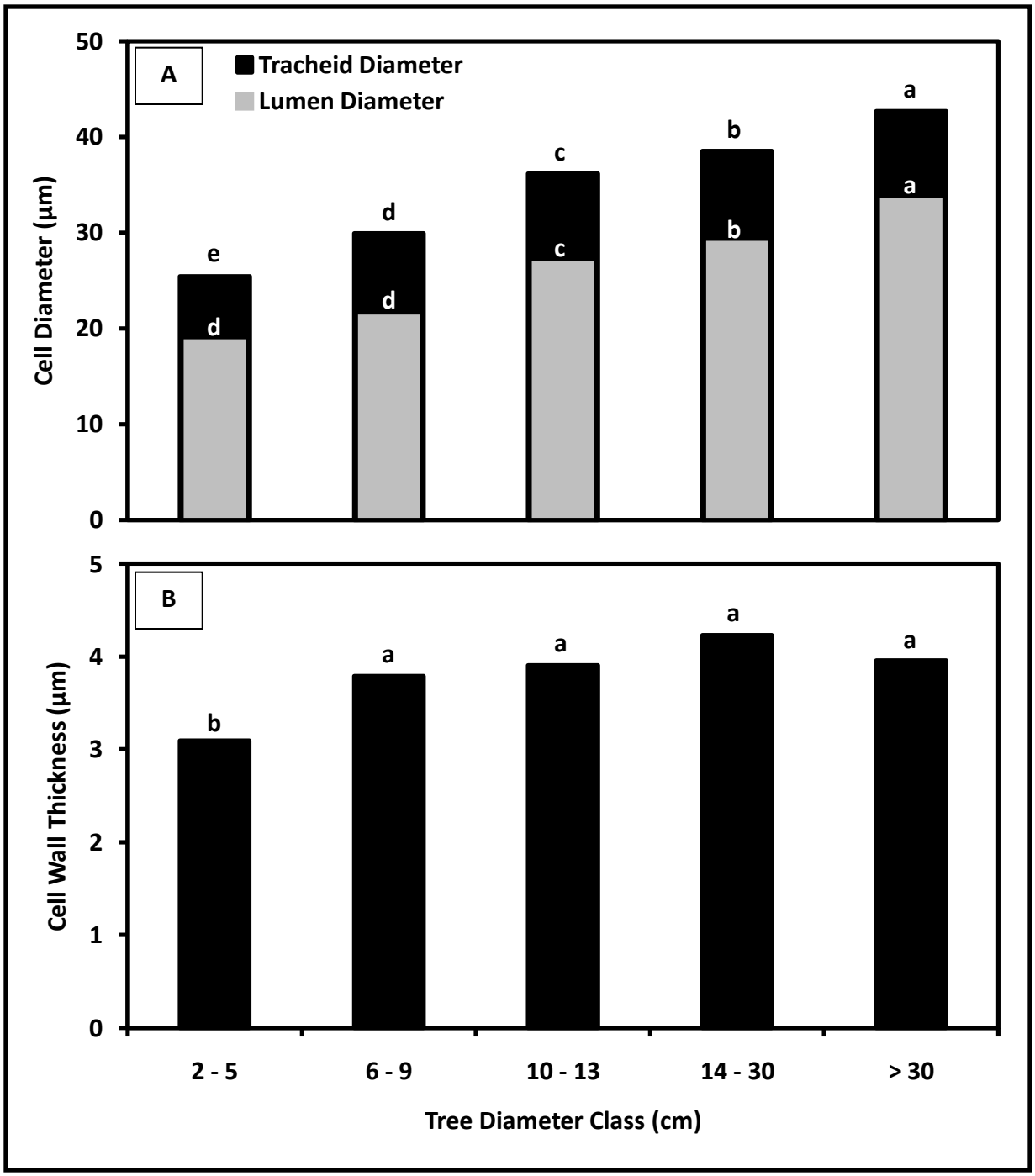

Figure 38. *Mean cell diameter* ***(A)*** *and mean cell wall thickness* ***(B)*** *by diameter class. Different lowercase letters indicate classes that were significantly different.*

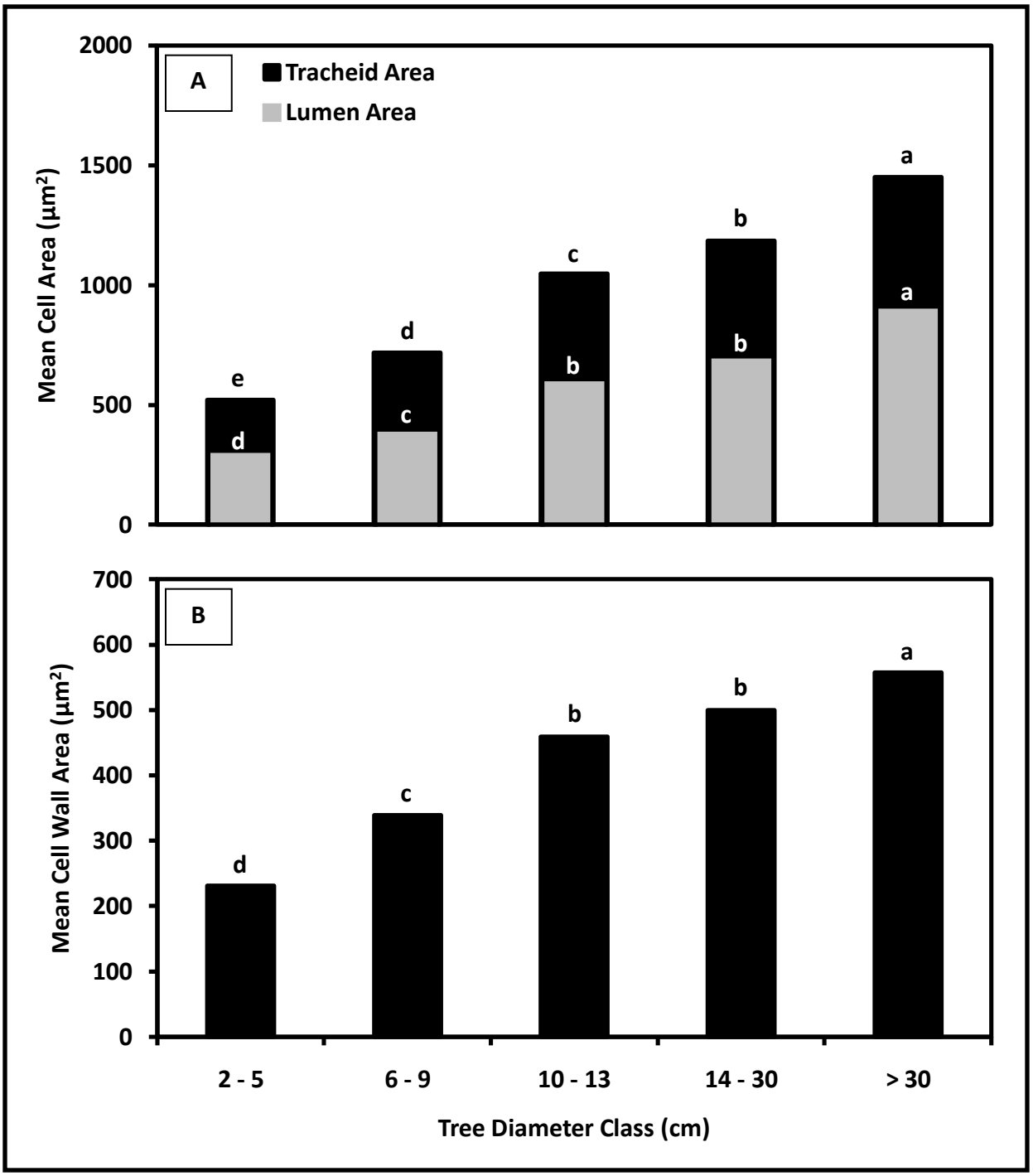

Figure 39. *Mean cell area* ***(A)*** *and mean cell wall area* ***(B)*** *by diameter class. Different lowercase letters indicate classes that were significantly different.*

V. Discussion

Linking Wood Anatomy and Forest Ecology

During wood cell differentiation tracheids respond to chemical signals to adapt to endogenous and exogenous influences. After tracheid cells are formed by the cambial initial cells the primary wall expands, a secondary wall is deposited on the inside, its walls are lignified, and within a few days the cell dies (Plomion et al. 2001). The function of a tracheid is to provide structural support and water transport to the tree (Panshin and deZeeuw 1980). However, when a tree is bent by an exterior force, such as ice deposition, compression wood cells form below the bend and expand longitudinally to push it back into an optimal position to compete for light (Du and Yamamoto 2007).

The primary cell wall establishes the general shape of a tracheid (Zhang et al. 2000). It expands along with neighboring cells adhering to existing wood cells in a radial file, with the occasional periclinal division to compensate for expanding tree diameter (Panshin and deZeeuw 1980). In compression wood cells, circularity is therefore determined by the primary wall, and the secondary wall is responsible for thickening (Timell 1986). Individual *Pinus strobus* compression wood cells are significantly more circular in cross-section, and smaller in diameter than normal wood cells (Figures 30, 32). Their form contributes to their function: to provide additional structural support to the lower stem side.

On the upper stem side, opposite wood cells are intermediate in size between compression and normal wood cells. Compression, opposite and normal wood mean tracheid diameter is 30.5, 32.4, and 36.8 µm, respectively, and mean lumen diameter is 19.5, 24.4, and

28.4 µm, respectively (Figure 30). These findings differ from those of Tarmian and Azadfallah (2009) who found that opposite wood cells had larger mean tracheid and lumen diameters than normal and compression wood cells in Norway spruce (*Picea abies* L.). However, it is unclear whether they sampled true opposite wood (the uphill stem side within the same growth ring as compression wood), or merely normal wood from the upper stem side that formed before the tree was bent. Mean cell wall thickness of *P. strobus* compression wood cells was 4.8 µm (Figure 30), which was comparable to results obtained from *P. abies* compression wood (4.6 µm) (Tarmian and Azadfallah 2009).

A gymnosperm tracheid normally contains three layers in its secondary cell wall (S_1, S_2 and S_3), each layer alternating the direction of its cellulose microfibrils imbedded within the lignin matrix (Panshin and deZeeuw 1980). In compression wood tracheids, however, there are only two layers (S_1 and S_2), and the S_2 layer is modified by a higher percentage of lignin, an increased microfibril angle, and the presence of helical checks, all of which lend to its physical properties (Timell 1986). Despite having a different cell wall structure than normal, this study found no significant differences in mean cell wall area among compression, normal, or opposite wood cells (Figure 31). This suggests that trees allocate a similar amount of glucose to each cell for cellulose thickening, and the thicker wall and reduced lumen size of compression wood are consequences of being constrained by the smaller shape of the primary cell wall.

The small size of compression wood cells allow them to pack more tightly together, leading to more average cells per mm in a radial file (33) than in normal wood (27) (Table 6). However, because no significant differences exist in mean cell wall area among cell types, a

higher cumulative cell wall area exists in compression wood tissue (47%) than in normal wood (31%) (Table 7). Opposite wood cell counts are extremely low in tree-rings with severe compression wood growth, sometimes as few as 3 – 4 cells per radial file. This is especially true of compression wood rings in smaller diameter trees; there are over three times as many cells on the downhill stem side as the uphill side in trees in the smallest diameter class, but in the largest diameter class there were only 1.25 times as many on the downhill side (Figure 37). Normal wood cell counts were not significantly different on opposite sides of the stem, suggesting that normal wood growth is relatively evenly distributed around the tree stem.

In 1994, heavy ice deposition (8.5 cm) caused compression wood formation in severely bent small-diameter *P. strobus* trees (< 10 cm) (Figure 11). *Pinus strobus* wood has poor bending strength compared to other species (Warrillow and Mou 1999). When wood is bent in a wet condition, its cells undergo a plastic deformation process in which a Velcro-like stick-slip mechanism may occur at the molecular level (Keckes et al. 2003). The wood material bends fluidly, and molecular bonds are broken and then formed in the bent position (Kretchmann 2003). It follows that larger trees bent by an exterior force would form more molecular bonds in the bent position than smaller trees, thus requiring more compression wood formation.

After the 1994 ice storm, many smaller trees began forming compression wood cells immediately after cambial reactivation in the spring (Figure 36). Due their high content of GH-lignin, a natural fluorophore, compression wood cells fluoresce in the S2 layer of the cell wall, while normal wood cells fluoresce only in the compound middle lamella, indicating higher lignification at this location (Donaldson et al. 2010). Some researchers have suggested that a

few normal wood cells are usually formed first before compression wood cells (Timell 1986). However, in this study trees with the most severe bending (6 – 9 cm 2007 diameter class) started forming compression wood immediately upon cambial re-activation in the spring, suggesting that compounds that induce compression wood formation are transported rapidly or may already present in the cambium, or that the mechanical stress may be a factor in compression wood cell differentiation (Kwon et al. 2001, Thibeault-Martel et al. 2008).

In addition to causing thin sections to fluoresce under ultraviolet light, compression wood lignification leads to some interestingly abnormal wood properties. While soaking the wood in water to cut them with a microtome, samples of compression wood sink to the bottom of the water faster than normal wood, and samples containing both compression and normal wood float with the compression wood side down. This is due to the fact that compression wood is denser than normal wood (Bowyer et al. 2007). When cutting the wood on a microtome, thin sections of severe compression wood commonly curl, making it difficult to mount them on glass slides. With curled thin-sections it is necessary to carefully pry them open in a moist condition with forceps and a soft brush, and then place them concave side down onto a drop of mounting medium (e.g. glycerin) when making glass slides. In tree-rings that did contain a few thin-walled earlywood cells between larger sections of compression wood tracheids, this was point of least resistance that often split when dried.

Compression wood sacrifices lumen area for cell wall area, which may impact hydraulic conductivity locally in the stem (Spicer and Gartner 2002). Opposite wood cell lumina are slightly larger, but their numbers are so low a significant impact in increased water permeability is doubtful. If functional sapwood area is reduced by severe compression wood and internal

heartwood formation, increased water stress could reduce photosynthetic ability leading to growth declines (Stokes and Berthier 2000). However, growth declines could also be due to the fact that compression wood uses more glucose to build thicker cell walls contained in a smaller cross-sectional area (Figure 31). Several trees 6 – 9 cm in diameter had severe compression wood and heartwood formation, and had begun to decline in ring width in outer tree-rings (Appendix E1). However, it is uncertain whether these growth declines were solely due to water stress, or some other limiting factor such as decreased light levels in the understory following canopy closure (Beaudet et al. 2007). It is also possible that growth in these trees was limited by local soil conditions.

Access to water, light, and soil nutrients are highly influential on tracheid and tree size (Plomion 2000, Mou and Warrillow 2000). In this study, trees located in the valley were able to attain greater mean tracheid diameter than those in thinner soil on steep slopes (Figure 38). This increase in cellular growth led to larger trees which were able to withstand greater loads of ice without bending. However, their inflexibility risks upper canopy branch breakage instead (Timell 1986). Branch breakage occurs when the stress on a stem (bending force) becomes greater than its maximum bending moment, which is based on a tree species' modulus of rupture and diameter (Petty and Worrell 1981, Peltola et al. 1999). The breaking point is exponentially related to tree diameter, so increasingly higher amounts of ice loading are required to break larger stems (Bragg et al. 2003). Trees that lose many limbs during an ice storm experience a sudden ring-width reduction, while those unaffected may experience a growth release (Lafon and Speer 2002, Smolnik 2004).

Advances in Disturbance Ecology

Most studies of ice storm impacts on forests focus on branch breakage that occurs immediately following the storm and the tree-ring width suppression or release that follows (Whitney and Johnson 1984, Lafon 1999, Warrillow and Mou 1999, Mou and Warrillow 2000, Lafon and Speer 2002, Millward and Kraft 2003, Smolnik 2004, Stueve et al. 2007). Few have examined the indirect effects to wood quality that occur years after ice deposition through compression wood formation in severely bent trees (Rhoads 2002). On mountainous slopes, even-aged cohorts of *P. strobus* can achieve variable growth depending on micro-site edaphic conditions, resulting in a spatially and temporally complex heterogeneous compression wood growth response after ice storm damage within a small plot (Appendix E).

While *Pinus strobus* tree size varied tremendously depending on slope position, age on the northeast aspect was relatively constant in this stand (Figure 23). Due to the dearth of tree age classes the true relationship between cambial age and compression wood formation could not be tested; the 21 -27 cambial age class formed the most compression wood because the stand was that old during the ice storm of 1994 (Figure 9). Other studies have found that on pine plantations younger trees (< 10 years old) are more susceptible to bending than older trees, but in such cases age can be reliably predicted by tree size due to edaphic uniformity on the site (Cayford and Haig 1961).

On the northeast aspect, a cohort of *P. strobus* germinated from 1966 – 1976; median year of establishment was 1968 (Figure 23). This date coincides with Virginia Tech's purchase of Fishburn Forest a few years earlier, and the large pulse in *P. strobus* establishment could

indicate a timber harvest by the previous landowner (Copenheaver et al. 2006). A younger cohort of *P. strobus* germinated on the southwest aspect in the 1990s; median year of establishment on the southwest aspect was 1994 (Figure 23). This surge in post-storm *P. strobus* seedling growth supports the theory that heavy ice damage can increase populations of species that require more light; thus reversing forest succession (Smolnik et al. 2006). The northeast aspect did not experience a post-storm surge in *P. strobus* establishment, but many suppressed trees formed significant compression wood after the storm (Figures 10, 23).

Nutrient, light, and water availability are the driving factors in tree size (Kozlowski and Pallardy 1997). The most dramatic differences were found between trees growing in the valley that were > 30 cm in diameter and trees nearly the same age growing in shallow soil that were just 2 cm in diameter in 2007 (Appendix E2). According to these results, tree age is not a factor in tree size and studies that assume tree age based on size could be in error, especially if edaphic conditions are variable on the site. This highlights the need for a dendrochronological component in studies of forest dynamics.

The most important variable governing compression wood formation was tree size. Tree size depended on nutrient and water availability and compression wood formation after heavy ice deposition depended on tree size. Most trees 2 – 13 cm in diameter form significant post-storm compression wood due to severe bending (Figure 11). However, the critical diameter range for *Pinus strobus* bending and subsequent compression wood formation is 4 – 8 cm (Appendix E1). These findings agree with findings that southern pines 5 – 15 cm DBH tend to be bent by ice deposition, while 15 – 25 cm trees are more likely to be broken (Timell 1986).

In the understory if pine trees are bent they will form compression wood, but the amount will vary depending on their size. In this study, *Pinus strobus* trees 4 – 8 cm in diameter at the time of the storm (1994) formed by far the most compression wood in the thirteen years after the event. Smaller saplings (< 4 cm) and slightly larger trees (9 – 12 cm) only formed a minor amount of compression wood before resuming normal growth, while larger trees (> 12 cm) formed very little amounts at the base after 8.5 cm of ice loading in 1994. The largest trees (> 18 cm) formed no compression wood after the ice storm, but observations in the field found that many large trees had forked tops, indicating previous breakage (Appendix E1).

The smallest trees (2 – 5 cm in 2007) were lightweight and had less surface area on which glaze could adhere so they formed less compression wood to return upright after the storm. Trees that were an average 2.6 (±0.2) cm in diameter during the storm had high relative compression wood formation but low actual area due to smaller total stem area (Figure 10, Appendix E1). Many trees of this size were located in shallow soils at the steep mid-slope position; it is likely that their growth was limited by low nutrient and water availability.

The 6 – 9 cm (2007) diameter class formed the most compression wood area after the storm (Figure 11). During the storm, the mean diameter of this class was 4.6 (±0.2) cm (Appendix E1). The peak in actual compression wood area in this diameter class suggests that the trees were the optimal size for compression wood formation. From this data it is inferred that 8.5 cm of ice deposition was enough to severely bend these trees but not break them, and more compressive force was needed to return them to an upright position than in other tree diameter classes. Field observations revealed that many trees in this size class had developed

sinuous stems as they regained a vertical position. Trees that are more sinuous earlier in life are more likely to develop compression wood, but once the upper portion of the tree is vertical, normal wood growth resumes (Spicer et al. 2000).

The next largest diameter class (10 – 13 cm) was second in actual compression wood formation (Figure 10). Intermediate trees in this diameter class formed more actual compression wood than the 2 – 5 cm class, but this was a relatively small amount compared to their normal wood area. This suggests that this size class was moderately bent at the base by 8.5 cm of ice deposition. At the time of the storm the mean diameter in this class was 8.6 (±0.3) cm (Appendix E1). If lumber were to be made from trees in this class in the future, any boards made from the lower stem wood would likely be subject to a large amount of warp, as sections would contain both normal and compression wood tissues (Xu et al. 2009).

Most trees > 13 cm in diameter did not form much compression wood after the storm, so it is assumed that their average stem size at the time of the storm (10.8 (±0.4) cm) was not severely bent by 8.5 cm of glaze (Appendix E1). Trees this size occupy intermediate crown classes, and could have been supported by other neighboring trees, thus reducing their bend (Bragg et al. 2003). The ice storm did not induce trees in the 14 – 17 cm class to form significant compression wood after the storm (Figure 11). However, this size class was within the critical diameter range (4.5 cm) for *P. strobus* during the 1979 ice storm (2.5 cm ice), and formed the most compression wood of any diameter class during the following growing season (Appendix E1).

Unlike snow, which tends to accumulate in piles on upper branches, freezing rain easily penetrates the leafless branches in winter to freeze on contact with all forest strata in temperate forests. Therefore, shelterwood systems would most likely offer no shelter to the seedlings below (Timell 1986). Larger trees in the canopy would have offered little protection from ice deposition to the understory. There are no leaves on deciduous trees in February or March in Virginia, and drops of freezing rain can easily penetrate through the canopy branches and adhere to sub-canopy trees. While snow precipitation is already frozen before falling on trees and may accumulate in piles on upper branches, glaze is more evenly distributed throughout the vertical profile of the forest. This is evident when considering 1993, a year in which more than 30 inches of snow fell on Montgomery County during the "Superstorm of '93". However, the 1993 tree-ring contains little to no compression wood in most samples, instead showing low growth due to low rainfall in that year (Appendix E1).

The > 18 cm diameter class formed very little post-storm compression wood at the base (Figure 11). This size class had a mean diameter of 18.7 (±1.0) cm during the ice storm and overall this class experienced a minor growth release after the storm (Appendix E1). They did, however, experience upper canopy branch breakage, as evidenced by a forked branch pattern in the upper canopy (20 – 30 m high on the tree stem). After the leader stem is broken, the branches in the tier below the break begin to form large amounts of compression wood in late July and compete for canopy dominance (Wilson and Archer 1981). In time, this leads to the characteristic forked pattern of trees damaged by ice or heavy winds aloft. Post-storm ring widths were not reduced, but actually increased in the largest diameter class, suggesting that

although *P. strobus* trees do not resprout (i.e. epicormic branching), they do respond quickly to increases in the light environment with increased growth (Appendix E1).

Although limited topography was sampled in this study, we found that topographic factors did not influence compression wood formation directly, but did influence tree size, so they had an indirect effect on compression wood distribution (Figure 25). A recent study of ice storm damage in nearby Wythe and Bland counties found that south and east aspects of mountains experienced the most direct breakage due to the 1994 storm (Stueve et al. 2007). It is possible that the same was true at the Fishburn plot, and more ice was deposited on the southwest aspect. If more limb breakage and tree uprooting occurred on that hill side than the northeast aspect, the evidence would have long since disappeared, leaving us only the more indirect form of evidence on the northeast aspect; the compression wood formed in trees of a certain size.

Elevation and slope were correlated with each other, but neither was linearly related to compression wood formation (Figures 17, 19). This could be a consequence of the limited geographic area studied. Relative area of post-storm compression wood was highest in the 600 – 604 m elevation class, at the mid-slope position (Figure 18). This section of the plot had the shallowest soils (due to soil creep downhill) and the smallest-diameter trees, explaining why less actual compression wood area but the highest relative compression wood was formed (Table 5). The shallow soils stunted tree growth leading to more severe bending by the ice, and consequently tree stems contained > 20% compression wood on average (Figure 17).

The positive relationship found between competition index and compression wood formation is likely a mathematical artifact reflecting the negative relationship between tree diameter and competition index; a relationship that is strengthened in indices that sum all trees within larger search radii around the focal tree (Appendix D1). The modified competition index we used in this study did not show a strong trend with respect to actual compression wood area, but did show a positive relationship with relative compression wood area. This pattern most likely reflects the strong relationship found between tree diameter and competition index, due to the fact that diameter is part of the equation for competition index.

Conclusions

Although age was relatively constant in this *Pinus strobus* cohort, tree size was highly dependent on slope location; larger trees grew in valleys with thicker soils while smaller trees grew on steep slopes with shallower soils. All *P. strobus* formed minor amounts of compression wood as juvenile trees (< 10 years old) to attain stability. In 1994, 8.5 cm of freezing rain deposition caused a highly heterogeneous compression wood response within a small geographic area due to differences in tree diameter. The critical tree diameter range for compression wood formation in *P. strobus* trees was 4 – 8 cm after 8.5 cm of ice. No significant relationships were found between compression wood formation and topographic variables (slope, aspect, and elevation) or the modified competition index. The negative relationship between competition index and focal tree diameter is a mathematical artifact of the equation

for the index; this relationship is strengthened in indices that sum the influence of all neighboring trees within a radius of the focal tree.

Microscopic examinations of the three tree-rings formed before and after the 1994 ice storm found that freezing rain deposition significantly increases cell circularity and cell wall thickness, common characteristics of compression wood cells. Compression wood cells are significantly smaller than normal wood cells, and had significantly smaller lumina than normal or opposite wood cells. Secondary cell wall thickening is constrained by the smaller size and more circular shape of compression wood cells, resulting in a thicker cell wall. The cumulative cell wall area in compression wood was significantly higher than in other wood types, thus distributing the weight of the tree over a larger wood surface area on the underside of the stem.

Advances in computer technology have enhanced researchers' ability to quantify a wide range of features in dendrochronology. Image analysis software will allow increased precision and accuracy in studies of compression wood and other tree-ring studies. Future work in quantifying reaction wood should focus on a wider range of species and geographical areas to add a new dimension to the micro-scale detail provided by this study of compression wood formation in *Pinus strobus*.

Literature Cited

Agafonov, L., H. Strunk, and T. Miber. 2004. Thermokarst dynamics in Western Siberia: insights from dendrochronological research. Palaeogeography, Palaeoclimatology, Palaeoecology **209**(1-4): 183 – 196.

Amateis, R. L. and H. E. Burkhart. 1996. Impact of heavy glaze in a loblolly pine spacing trial. Southern Journal of Applied Forestry **20**:151-155.

Archer, R. R. 1987. On the Origin of Growth Stresses in Trees .1. Micro Mechanics of the Developing Cambial Cell-Wall. Wood Science and Technology **21**:139-154.

Archer, R. R. and B. F. Wilson. 1982. Apical Control of Branch Movements in White-Pine - Compression Wood Action. Wood Science and Technology **16**:181-191.

Beaudet, M., J. Brisson, C. Messier, and D. Gravel. 2007. Effect of a major ice storm on understory light conditions in an old-growth Acer-Fagus forest: Pattern of recovery over seven years. Forest Ecology and Management **242**:553-557.

Belanger, R. P., J. F. Godbee, R. L. Anderson, and J. T. Paul. 1996. Ice damage in thinned and nonthinned loblolly pine plantations infected with fusiform rust. Southern Journal of Applied Forestry **20**:136 - 142.

Boerner, R. E. J., S. D. Runge, D. S. Cho, and J. G. Kooser. 1988. Localized Ice Storm Damage in an Appalachian Plateau Watershed. American Midland Naturalist **119**:199-208.

Bowyer, J.L., R. Shmulsky, and J.G. Haygreen; drawings by K. Lilley. 2007. Forest Products and Wood Science: An Introduction. 5th ed. Blackwell Publishing. Ames, Iowa.

Boyd, J. D. 1972. Tree growth stresses - Part V: Evidence of an origin in differentiation and lignification. Wood Science and Technology **6**:251-262.

Bragg, D. C., M. G. Shelton, and B. Zeide. 2003. Impacts and management implications of ice storms on forests in the southern United States. Forest Ecology and Management **186**:99-123.

Brommit, A. G., N. Charbonneau, T. A. Contreras, and L. Fahrig. 2004. Crown loss and subsequent branch sprouting of forest trees in response to a major ice storm. Journal of the Torrey Botanical Society **131**:169-176.

Cayford, J.H, and Haig, R.A. 1961a. Glaze damage in red and Scots pine plantations in southeastern Manitoba. Forestry Chronicle **37**: 16 - 21.

Cayford, J.H, and Haig, R.A. 1961b. Glaze damage in forest stands in southeastern Manitoba. Canadian Department of Forestry Technical Note 102, 16 pp.

Cave, I. D. 1972. A theory of the shrinkage of wood. Wood Science and Technology **6**:284-292.

Copenheaver, C. A., J. M. Matthews, J. M. Showalter, and W. E. Auch. 2006. Forest stand development patterns in the southern Appalachians. Northeastern Naturalist **13**:477-494.

Cosgrove, D. J. 2005. Growth of the plant cell wall. Nature Reviews Molecular Cell Biology **6**:850-861.

Cown, D. J. and B. C. Clement. 1983. A Wood Densitometer Using Direct Scanning with X-Rays. Wood Science and Technology **17**:91-99.

Creggar, W.H., and H.C. Hudson. 1985. Soil Survey of Montgomery County, Virginia. United States Department of Agriculture Soil Conservation Service. In cooperation with Virginia Polytechnic Institute and State University.

Darwin, A. T., D. Ladd, R. Galdins, T. A. Contreras, and L. Fahrig. 2004. Response of forest understory vegetation to a major ice storm. Journal of the Torrey Botanical Society **131**:45-52.

De Micco, V. and G. Aronne. 2007. Combined histochemistry and autofluorescence for identifying lignin distribution in cell walls. Biotechnic & Histochemistry **82**: 209-216.

Dietze, M. C. and J. S. Clark. 2008. Changing the gap dynamics paradigm: Vegetative regeneration control on forest response to disturbance. Ecological Monographs **78**: 331-347.

Donaldson, L.A., Turner, J.C.P. 2001. The influence of compression wood and microfibril angle on the occurrence of distortion in window frames made from radiata pine (Pinus radiata). Holz Roh Werkst **59**: 163 - 168.

Donaldson, L., K. Radotic, A. Dalauzi, D.Djikanovic, and M. Jeremic. 2010. Quantification of compression wood severity in tracheids of Pinus radiata D. Don using confocal fluorescence imaging and spectral deconvolution. Journal of Structural Biology **169**: 106 - 115.

Douglass, A.E. 1940. Examples of spiral compression wood. Tree-ring Bulletin **6**(3): 21-22.

Du, S., M. Sugan, M. Tsushima, T. Nakamura, and F. Yamamoto. 2004. Endogenous indole-3-acetic acid and ethylene evolution in tilted Metasequoia glyptostroboides stems in relation to compression wood formation. Journal of Plant Research **117**: 171-174.

Du, S. and F. Yamamoto. 2007. An overview of the biology of reaction wood. Journal of Integrative Biology **49**(2): 131-142.

Duguay, S. M., K. Arii, M. Hooper, and M. J. Lechowicz. 2001. Ice storm damage and early recovery in an old-growth forest. Environmental Monitoring and Assessment **67**: 97-108.

Duncker, P. and H. Spiecker. 2008. Cross-sectional compression wood distribution and its relation to eccentric radial growth in *Picea abies* [L.] Karst. Dendrochronologia **26**: 195-202.

Duncker, P. and H. Spiecker. 2009. Detection and classification of norway spruce compression wood in reflected light by means of hyperspectral image analysis. International Association of Wood Anatomists (IAWA) Journal **30**: 59-70.

Forbes, G. S., R. A. Anthes, and D. W. Thomson. 1987. Synoptic and Mesoscale Aspects of an Appalachian Ice Storm Associated with Cold-Air Damming. Monthly Weather Review **115**: 564-591.

Fromm, J., B. Rockel, S. Lautner, E. Windeisen, and G. Wanner. 2003. Lignin distribution in wood cell walls determined by TEM and backscattered SEM technologies. Journal of Structural Biology **143**: 77-84.

Gärtner, H. and I. Heinrich. 2009. The formation of traumatic rows of resin ducts in *Larix decidua* and *Picea abies* (Pinaceae) as a result of wounding experiments in the dormant season. International Association of Wood Anatomists (IAWA) Journal **30**:199-215.

Gärtner, H. and D. Nievergelt. 2010. The core-microtome: A new tool for surface preparation on cores and time series analysis of varying cell parameters. Dendrochronologia. **28**: 85 - 92.

Harris, J. M. 1977. Shrinkage and density of radiata pine compression wood in relation to its anatomy and mode of formation. New Zealand Journal of Forest Science **7**:91-106.

Hatfield, R. and R. S. Fukushima. 2005. Can lignin be accurately measured? Crop Science **45**:832-839.

Hsu, L. C. Y., J. C. F. Walker, B. G. Butterfield, and S. L. Jackson. 2006. Compression wood does not form in the roots of *Pinus radiata*. International Association of Wood Anatomists (IAWA) Journal **27**:45-54.

Husch, B., T.W. Beers, and J.A. Kershaw Jr. 2003. Forest Mensuration. 4th ed. John Wiley & Sons, Inc. Hoboken, New Jersey.

Irland, L. C. 1998. Ice storm 1998 and the forests of the Northeast - A preliminary assessment. Journal of Forestry **96**:32-40.

Irland, L. C. 2000. Ice storms and forest impacts. Science of the Total Environment **262**:231-242.

Jain, K. K. and M. K. Seth. 1980. Effect of bole inclination on ring width, tracheid length and specific gravity of wood at breast height in blue pine. Holzforschung **34**:52-60.

Johnston, D.R. 1962. Growing conifers in South Africa

Kagawa, A., A. Sugimoto, and T. C. Maximov. 2006. Seasonal course of translocation, storage and remobilization of 13C pulse-labeled photoassimilate in naturally growing Larix gmelinii saplings. New Phytologist **171**:793-804.

Keckes, J., I. Burgert, K. Fruhmann, M. Muller, K. Kolln, M. Hamilton, M. Burghammer, S. V. Roth, S. Stanzl-Tschegg, and P. Fratzl. 2003. Cell-wall recovery after irreversible deformation of wood. Nature Materials **2**:810-814.

Kozlowski, T.T., and S.G. Pallardy. 1997. Physiology of Woody Plants. 2nd ed. Academic Press, Inc. San Diego, California.

Kretschmann, D. 2003. Natural materials - Velcro mechanics in wood. Nature Materials **2**:775-776.

Kwon, M., D.L. Bedgar, W. Piastuch, L.B. Davin, and N.G. Lewis. 2001. Induced compression wood formation in Douglas-fir (Psuedotsuga menziesii) in microgravity. Phytochemistry **57**: 847 - 857.

Lachenbruch, B., F. Droppelmann, C. Balocchi, M. Peredo, and E. Perez. 2010. Stem form and compression wood formation in young Pinus radiata trees. Canadian Journal of Forest Research **40**: 26 - 36.

Lafon, C. W. 2004. Ice storm disturbance and long-term forest dynamics in the Adirondack Mountains. Journal of Vegetation Science **15**:267-276.

Lafon, C. W. 2006. Forest disturbance by ice storms in Quercus forests of the southern Appalachian Mountains, USA. Ecoscience **13**:30-43.

Lafon, C.W., and J. Speer. 2002. Using dendrochronology to identify major ice storm events in oak forests of southwest Virginia. Climate Research **20**: 41 - 54.

Lafon, C. W., D. Y. Graybeal, and K. H. Orvis. 1999. Patterns of ice accumulation and forest disturbance during two ice storms in southwestern Virginia. Physical Geography **20**:97-115.

Lautenschlager, R. A., J. H. Pedlar, and C. M. Nielsen. 2003a. Ice storm damage: Effects of competition and fertilization on near-ground vegetation. Forestry Chronicle **79**:54-62.

Lautenschlager, R. A., J. H. Pedlar, J. A. Winters, and C. M. Nielsen. 2003b. Ice storm damage: Effects of competition and fertilization on the growth of sugar maple trees. Forestry Chronicle **79**:63-69.

Lemon, P. C. 1961. Forest ecology of ice storms. Bulletin of the Torrey Botanical Club **88**:21-29.

Lorimer, C. G. 1983. Tests of age-independant competition indices for individual trees in natural hardwood stands. Forest Ecology and Management **6**:343-360.
Lott, N. and T. Ross. 1994. TR 94-03, 1994 Weather in the Southeast: February Ice Storm and July Flooding
Mandelbrot, B.B. 1967. How long is the coast of Britain? Statistical self-similarity and fractional dimension. Science **156**: 636 - 638.
Meylan, B. A. 1972. The influence of microfibril angle on the longitudinal shrinkage-moisture content relationship. Wood Science and Technology **6**:293-301.
Millward, A. A. and C. E. Kraft. 2004. Physical influences of landscape on a large-extent ecological disturbance: the northeastern North American ice storm of 1998. Landscape Ecology **19**:99-111.
Moore, J. R., J. D. Tombleson, J. A. Turner, and M. Van der Colff. 2008. Wind effects on juvenile trees: a review with special reference to toppling of radiata pine growing in New Zealand. Forestry **81**:377-387.
Mou, P. and M. P. Warrillow. 2000. Ice storm damage to a mixed hardwood forest and its impacts on forest regeneration in the ridge and valley region of southwestern Virginia. Journal of the Torrey Botanical Society **127**:66-82.
Mugasha, A. G. 1989. Evaluation of simple competition indices for the prediction of volume increment of young jack pine and trembling aspen trees. Forest Ecology and Management **26**:227-235.
Mukoyoshi, S.-i., J.-i. Azuma, and T. Koshijima. 1981. Lignin-carbohydrate complexes from compression wood of *Pinus densiflora* Sieb et. Zucc. Holzforschung **35**:233-240.
Nelson, T.C., and W.M. Zillgitt. 1969. A Forest Atlas of the South. Southeast Forest Experiment Station, Ashville, NC. USDA Forest Service. 27 p.
Nicholas, N. S., T. G. Gregoire, and S. M. Zedaker. 1991. The reliability of tree crown position classification. Canadian Journal of Forest Research-Revue Canadienne De Recherche Forestiere **21**:698-701.
Nimz, H. H., D. Robert, and M. Nemr. 1981. Carbon-13 NMR spectra of lignins, 8: Structural differences between lignins of hardwoods, softwoods, grasses, and compression wood. Holzforschung **35**:16-26.
Onaka, F. 1949. (Studies on compression and tension wood.) Mokuzai Kenkyo Wood Res Inst Kyoto Univ 1, 88 pp. Trans For Prod Lab Can 93 (1956), 99 pp.
Panshin, A. J. and C. de Zeeuw. 1980. Textbook of Wood Technology. 4th edition. McGraw-Hill.
Peltola, H., Kellomäki, S., Väisänen, H., Ikonen, V.-P. 1999. A mechanistic model for assessing the risk of wind and snow damage to single trees and stands of Scots pine, Norway spruce, and birch. Canadian Journal of Forest Research **29**, 647 - 705.
Petty, J.A. and Worrell, R. 1981. Stability of coniferous tree stems in relation to damage by snow. Forestry **54**: 155 - 128.
Pillow, M.Y. 1931. Compression wood records hurricane. Journal of Forestry **29**: 575 - 578.
Pisaric, M. F. J., D. J. King, A. J. M. MacIntosh, and R. Bemrose. 2008. Impact of the 1998 ice storm on the health and growth of sugar maple (Acer saccharum Marsh.) dominated forests in Gatineau Park, Quebec. Journal of the Torrey Botanical Society **135**:530-539.
Plomion, C., G. Leprovost, and A. Stokes. 2001. Wood formation in trees. Plant Physiology **127**:1513-1523.

Plomion, C., C. Pionneau, J. Brach, P. Costa, and H. Bailleres. 2000. Compression wood-responsive proteins in developing wood of maritime pine (Pinus pinaster Ait.). Plant Physiology **123**:959-969.

Pont, D., R.K. Brownlie, and J.C. Grace. 2007. Disc image-processing software for three-dimensional mapping of stem ring width and compression wood. New Zealand Journal of Forest Science **37** (2): 168-185.

Rebertus, A. J., S. R. Shifley, R. H. Richards, and L. M. Roovers. 1997. Ice storm damage to an old-growth oak-hickory forest in Missouri. American Midland Naturalist **137**:48-61.

Rhoades, R. W. and R. J. Stipes. 2007. Ice damage to trees on the Virginia Tech campus from ice storms. Northeastern Naturalist **14**:51-60.

Rhoads, A. G., S. P. Hamburg, T. J. Fahey, T. G. Siccama, E. N. Hane, J. Battles, C. Cogbill, J. Randall, and G. Wilson. 2002. Effects of an intense ice storm on the structure of a northern hardwood forest. Canadian Journal of Forest Research-Revue Canadienne De Recherche Forestiere **32**:1763-1775.

Shepard, R. K. 1975. Ice storm damage to loblolly pine in northern Louisiana. Journal of Forestry. **73**: 420 - 423.

Shepard, R.K. 1978. Ice storm damage to thinned loblolly pine plantations in northern Louisiana. Southern Journal of Applied Forestry **2**: 83 - 85.

Smolnik, M.J. 2004. Using dendrochronology to identify species-specific ice storm damage in Delaware. MS Thesis. Eberly College of Arts & Sciences. West Virginia University.

Smolnik, M., A. Hessl, and J. J. Colbert. 2006. Species-specific effects of a 1994 ice storm on radial tree growth in Delaware. Journal of the Torrey Botanical Society **133**: 577-584.

Spicer, R. and B.L. Gartner. 2000. Sinuous stem growth in a Douglas-fir (Pseudotsuga menziesii) plantation: growth patterns and wood-quality effects. Canadian Journal of Forest Research **30**: 761 - 768.

Spicer, R. and B. L. Gartner. 2002. Compression wood has little impact on the water relations of Douglas-fir (Pseudotsuga menziesii) seedlings despite a large effect on shoot hydraulic properties. New Phytologist **154**: 633-640.

Spicer, R., B.L. Gartner, and R.L. Darbyshire. 2000. Sinuous stem growth in a Douglas-fir (Pseudotsuga menziesii) plantation: growth patterns and wood-quality effects. Canadian Journal of Forest Research **30**: 761 - 768.

Stokes, A. and S. Berthier. 2000. Irregular heartwood formation in Pinus pinaster Ait. is related to eccentric, radial, stem growth. Forest Ecology and Management **135**: 115-121.

Stueve, K. M., C. W. Lafon, and R. E. Isaacs. 2007. Spatial patterns of ice storm disturbance on a forested landscape in the Appalachian Mountains, Virginia. Area **39**: 20-30.

Terashima, N. 1979. Gravitational stimuli and wood lignin formation. Kagaku te Seibutsu (Chem and Biol) **17**: 124-127.

Thibeault-Martel, M., C. Krause, H. Morin, and S. Rossi. 2008. Cambial Activity and Intra-annual Wood Formation in Roots and Stems of Abies balsamea and Picea mariana. Annals of Botany **102**: 667-674.

Timell, T. E. 1982. Recent Progress in the Chemistry and Topochemistry of Compression Wood. Wood Science and Technology **16**: 83-122.

Timell, T. E. 1986. Compression Wood in Gymnosperms. (V. 1 - 3). Springer-Verlag, Berlin, Heidelberg, New York, Tokyo.

Urban, S. T., V. J. Lieggers, and S. E. MacDonald. 1994. Release in radial growth in the trunk and structural roots of white spruce as measured by dendrochronology. Canadian Journal of Forest Research-Revue Canadienne De Recherche Forestiere **24**: 1550-1556.

Warrillow, M. and P. Mou. 1999. Ice storm damage to forest tree species in the ridge and valley region of southwestern Virginia. Journal of the Torrey Botanical Society **126**: 147-158.

Watson, A.J., and H.R. Dadswell. 1957. Paper making properties of compression wood from Pinus radiata. Appita **11**: 56 - 70.

Watson, B. M. 1999. Virginia Winters: Snow, wind, ice and cold. NOAA National Weather Service Report. Accessed through website: http://www.erh.noaa.gov/lwx/Historic_Events/va-winters.htm on April 1, 2009.

Wendel, G. W. and H. C. Smith. 1990. Eastern white pine. Pages 476 - 488 *in* R. M. Burns and B. H. Honkala, editors. Silvics of North America. USDA Forest Service Agricultural Handbook 654.

Wernsdörfer, H., P. Reck, U. Seeling, G. Becker, and T. Seifert. 2004. Erkennung und messung des reakionsholzes bei fichte (Picea abies (L.) Karst) mittels verfahren der digitalen bildanalyse. Holz als Roh-und Werkstoff **62**: 243-252.

Whitney, H. E. and W. C. Johnson. 1984. Ice Storms and Forest Succession in Southwestern Virginia. Bulletin of the Torrey Botanical Club **111**: 429-437.

Wiley, S. and Zeide, B. 1991. Investigation of growth 14 years agter glaze damage in a loblolly pine plantation. In: Coleman, S.S., Neary D.G. (comps.) Proceedings of the Sixth Biennial Southern Silvicultural Research Conference. General Technical Report SE - 70. USDA Forest Service pp. 272 - 281.

Williams, C.B. 1966. Snow damage to coniferous seedlings and saplings. USDA Forestry Service Research Note PNW - 40.

Wilson, B. F. 1986. Apical Control of Compression Wood Action in White-Pine Branches. Wood Science and Technology **20**: 111-117.

Wilson, B. F. and R. R. Archer. 1981. Apical Control of Branch Movements in White-Pine - Biological Aspects. Plant Physiology **68**: 1285-1288.

Xu, P., H. Liu, R. Evans, L.A. Donaldson. 2009. Longitudinal shrinkage behavior of compression wood in radiata pine. Wood Science and Technology **43**: 428 - 439.

Yamaguchi, D. K. 1991. A simple method for cross-dating increment cores from living trees. Canadian Journal of Forest Research-Revue Canadienne De Recherche Forestiere **21**: 414-416.

Yamaguchi, K., K. Shimaji, and T. Itoh. 1983. Simultaneous Inhibition and Induction of Compression Wood Formation by Morphactin in Artificially Inclined Stems of Japanese Larch (*Larix leptolepis* Gordon). Wood Science and Technology **17**: 81-89.

Yasuda, T. and A. Sakakibara. 1981. Hydrogenolysis of protolignin in compression wood. Holzforschung **35**: 183-187.

Yumoto, M., S. Ishida, and K. Fukazawa. 1983. Studies on the formation and structure of the compression wood cells induced by artificial inclination in young trees of Picea glauca. IV. Gradation of the severity of compression wood tracheids. Research Bulletin College Experimental Forestry, Hokkaido University **40**: 409-454

Zedaker, S.M., H.E. Burkhart, and A.R. Stage. 1987. General principles and patterns of conifer growth and yield. In: Forest Vegetation Management for Conifer Production. J.D. Walstad and P.J. Kuch, eds. John Wiley & Sons, New York. pp. 203 - 241.

Zeide, B. and Sharer, D. 2000. Good Forestry at a Glance: A guide for managing even-aged loblolly pine stands. University of Arkansas Agricultural Experiment Station. Forest Resources Center Series No. 3.

Zeide, B. and Sharer, D. 2002. Sustainable and profitable management of even-aged loblolly pine stands. Journal of Sustainable Forestry **14**: 93 - 106.

Zhang, Y., R.R. Sederoff, and I. Allona. 2000. Differential expression of genes encoding cell wall proteins in vascular tissues from vertical and bent loblolly pine trees. Tree Physiology **20**: 457 – 466.

APPENDIX A: MACROSCOPIC IMAGE ANALYSIS

Appendix A1: Randomization Procedure for Selection of Samples for Macro-Image Analysis

Time limitations required that we choose a representative subsample for image analysis (Table 8). Samples were stratified by diameter class and hill side, and then a random number was assigned to each sample in MS Excel, and those with values > 0.5 were selected from each class. On the southwest aspect, natural limitations prevented a large sample of mature trees at the time of the ice storm (n = 4) so randomization was not possible on this aspect; all four samples were used in image analysis. Site limitations also reduced the number of large-diameter samples available. Samples within the 18+ cm diameter class were randomly selected by choosing all random values > 0.25, so they represent 7/11 (64%) of the total possible large trees. Similarly, 5/7 (71%) of the trees in the 14 – 17 cm class were selected by choosing all random values > 0.25.

Table 8. *Image analysis sample frequency by diameter class and aspect. Physiographic limitations resulted in lower P. strobus sample sizes on the southwest aspect (n = 4) than on the northeast (n = 43).*

	Number of samples used in image analysis	
Diameter Class (cm)	Northeast Aspect	Southwest Aspect
2 – 5	0	9
6 – 9	2	13
10 – 13	2	9
14 – 17	0	5
18+	0	7

Appendix A2: Comparisons of Measurement Methods for Macro-Image Analysis

There was a high correlation (r = 0.999) between both methods of tree-ring diameter measurement in Perimeter-based and Linear-based formats. However, a systematic error occurred with increasing tree-ring diameter in the perimeter-based method (Figure 40). When measuring diameter of identical tree-rings using perimeter in the formula ("Perimeter Method" ≈ diameter-tape measurement) with average linear diameter measurements ("Linear Method" ≈ mean of multiple caliper measurements). In addition, digital resolution (ppi) affected the estimation of diameter based on perimeter: coarser images (lower ppi) had more error than finer images (higher ppi). Using 600 ppi, error ranged up to 2.3 cm in samples up to in 40 cm diameter. With 2400 ppi, error was up to 1 cm in samples up to 10 cm (Figure 40).

I was intrigued by this systematic error, and while researching different shape metrics, I came across an article by B. B. Mandelbrot entitled *How Long is the Coast of Britain: Statistical Self-Similarity and Fractional Dimension,* which gave some insight to this problem (Mandelbrot 1967). Basically, this article highlights the phenomenon that perimeter measurements depend on the scale of measurement; as you shorten the scale, you pay attention to finer and finer details around the perimeter, be it a shore-line or a tree-ring, which amplifies your estimate of the distance. This helps explain why we found a strong positive correlation between tree-ring diameter and measurement error (defined as the difference between Perimeter and Linear Methods). By zooming in and precisely measuring the EW/LW boundary using the Perimeter Method, around resin canals and other abnormalities, the perimeter was being extended and the resulting diameter measurement inflated.

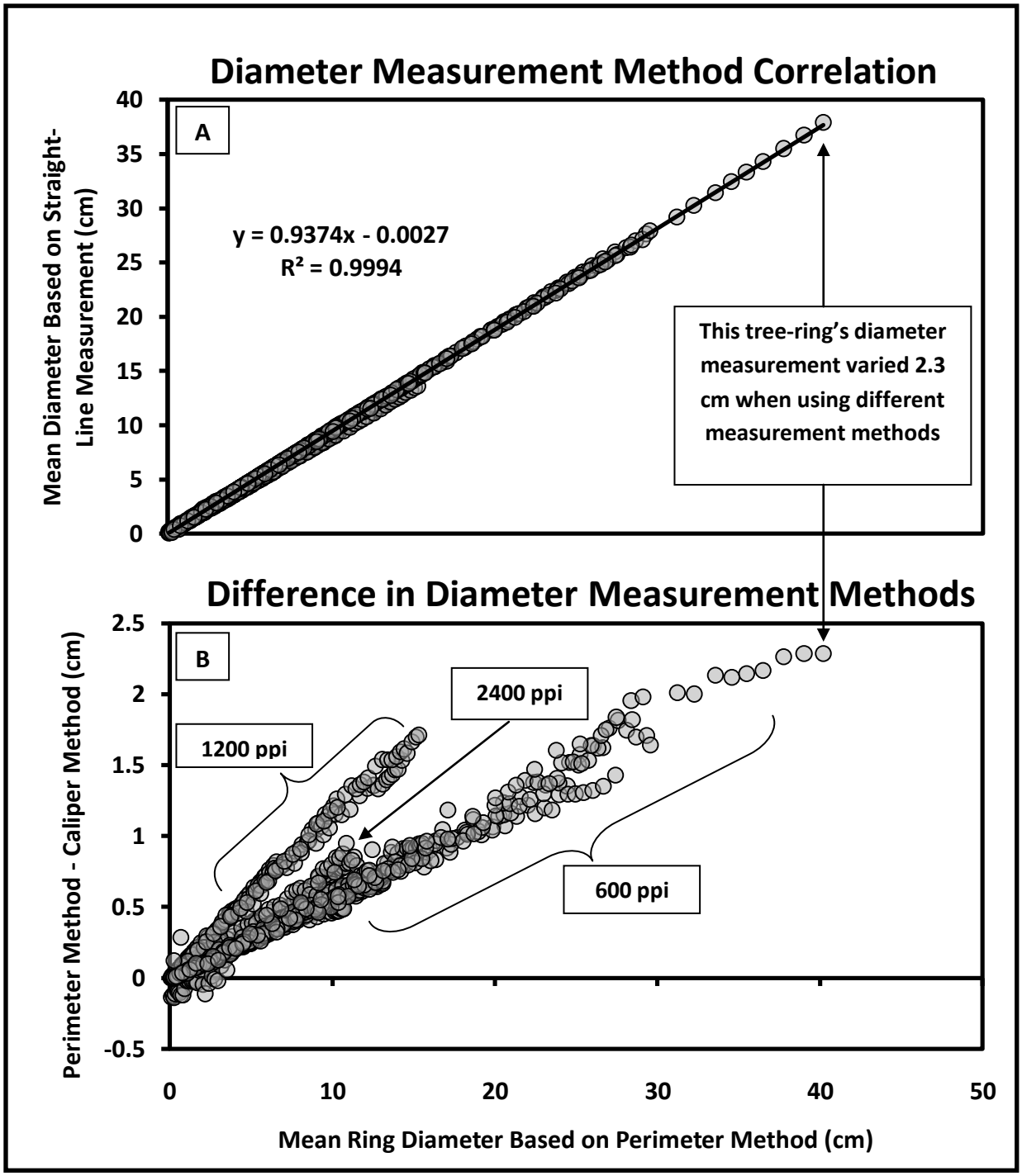

Figure 40. ***(A)*** *While ring diameters measured using the caliper method or perimeter method were highly correlated (r = 0.99),* ***(B)*** *perimeter method error increased with ring diameter due to cellular irregularities in the ring boundary. Pixel resolution was also a factor in measurement error.*

Appendix A3: Simple Linear Regression for Estimation of Diameter Outside Bark

To estimate the diameter outside bark (DOB) of *P. strobus* based on past tree-rings, simple linear regression was used to predict 2007 DOB using 2007 diameter inside bark (DIB) of different sized samples (Husch, Beers, and Kershaw 2003). Age was relatively constant in this cohort, so in this study was assumed not to influence diameter. It is assumed that bark thickness is therefore more closely related to tree growth than age. From microscopic analyses of on-site *P. strobus* trees, it was determined that most of the variation in cell productivity was not due to age, but micro-site characteristics such as soil thickness or proximity to water.

Thirty random selections (Excel random number generator > 0.5) from a sample of *P. strobus* trees (n = 38) were used in separate simple linear regressions, resulting in 30 equations for a best-fit line for predicting DOB using DOB. The mean values of the 30 random slope and intercept coefficients were used in the final equation for DOB prediction, and 95% confidence intervals found for the 30 permutations (Table 9). Strong correlations were found among all DIB and DOB slopes and intercepts, as well as Pearson's correlation coefficients (95% confidence interval for $r = 0.999 \pm 0.0002$) (Table 9).

Table 9. *Descriptive statistics for 30 random permutations of a simple linear regression predicting 2007 diameter outside bark (DOB) using 2007 diameter inside bark (DIB).*

	DIB slope	DIB intercept	DOB slope	DOB intercept	r^2	r
Mean	0.9358467	-0.28959	1.066947	0.30953	0.99845	0.99923
Standard Error	0.0011	0.0181	0.0013	0.0187	0.00019	9.3E-05
Median	0.9375	-0.2894	1.0651	0.3222	0.9987	0.99935
Standard Deviation	0.006	0.099	0.0069	0.1024	0.00102	0.00051
Sample Variance	3.66E-05	0.0098	4.72E-05	0.0105	1E-06	2.6E-07
Kurtosis	0.1345	1.6512	0.5215	0.9704	11.54	11.55
Skewness	-0.7953	-0.3027	0.8713	-0.4714	-3.1129	-3.1151
Range	0.0223	0.5112	0.0272	0.4821	0.0054	0.0027
Minimum	0.923	-0.551	1.055	0.0552	0.9941	0.99705
Maximum	0.9453	-0.0398	1.0822	0.5373	0.9995	0.99975
Sum	28.0754	-8.6878	32.008	9.285	29.954	29.977
Count	30	30	30	30	30	30
Confidence Level (95.0%)	0.0023	0.037	0.0026	0.038	0.0004	0.0002

To predict DOB in all preceding years for the multiple linear regression for prediction of compression wood area in live trees (see Section 5.3), the following equation based on mean slope and intercept was used:

$$\boldsymbol{DOB(cm) = 1.066947 \times DIB(cm) + 0.30953}$$

APPENDIX B: Compression Wood Index (CWI)

Appendix B1: Results of Validation Study

Due to the time required to measure *P. strobus* compression wood area for the detailed image analysis method using Photoshop, we sought an alternate method for quantifying compression wood. Most people or organizations probably do not have the kind of time or funding needed to collect data on compression wood in logs using image analysis software. A quick and simple method that could produce coarser, but comparable, results with greater efficiency may be preferable depending on the needs of the study. Data from 77 samples (each about 40 years old; ≈ 3080 total tree-rings) were recorded.

I used a modified compression wood grading system created by Harris (1977) for rating compression wood severity. See table 4 in the text for a description of the rating system. The groups are not mutually exclusive; that is, it is possible to have a ring containing compression wood in more than half of a tree ring radially, but not 45° of an arc. In such borderline cases, the judgment of the observer comes into play. In this study, "severe" compression wood rings (grade 3) were more identifiable among observers, and "mild" and "moderate" compression wood rings (grades 1 and 2) were less repeatable.

Working about two hours per day, 77 samples were finished in less than two weeks. The compression wood index (CWI) is simply the average of all compression wood ratings over the lifespan of the tree. It theoretically ranges from (0 – 3), but in my sample set the highest CWI values were less than 2 in the most severe cases.

Each tree-ring was given a compression wood rating based on a modified rating system designed by Harris (1977), and then the values were summed and divided by the age of the tree to find the compression wood index (CWI), or the average compression wood rating per sample.

$$CWI = \frac{\sum CW\ ratings}{age\ of\ tree}$$

A validation study was performed to determine whether the CWI method was repeatable. In addition to myself, a Lab Technician (Mr. John Peterson), a Dendrochronologist (Dr. Carolyn Copenheaver), performed the CWI method on a common sample set (n=14) to see how well compression wood ratings correlated with each other. Measurements from the CWI method were also compared to those obtained through Photoshop image analysis, to see how well they are correlated. Independent variables (diameter, height, crown class, elevation, slope, aspect, competition index) were grouped into categories and CWI values were averaged for each to observe trends in CWI distribution.

To test the repeatability of this method among different observers, three observers completed an identical sample set using the CWI system, and all datasets were correlated. Mr. John Peterson, a technician with the Department of Forestry, Resources and Environmental Conservation (FREC) at Virginia Tech, and Dr. Carolyn Copenheaver, a dendrochronologist at FREC both worked for two hours on a common sample set of 20 trees. Mr. Peterson completed 14 samples in this time, while Dr. Copenheaver completed 18.

The CWI method was repeatable among observers. However, some training may be necessary for individuals to identify compression wood before they use this method. Such training, however, would also be required to complete the Photoshop image analysis data collection. Dr. Copenheaver's and my values were not significantly different (paired t-test: $t = 1.43$, $P = 0.170$), and highly correlated (Pearson's $r = 0.946$, $P < 0.001$). Mr. Peterson's values were significantly different than mine and Dr. Copenheaver's (Peterson v. Hook: $t = -6.84$, $P < 0.001$; Peterson v. Copenheaver: $t = 6.73$, $P < 0.001$), but significantly correlated (Peterson v. Hook: $r = 0.855$, $P < 0.001$; Peterson v. Copenheaver: $r = 0.837$, $P < 0.001$). This difference could be due to the smaller sample size completed by Mr. Peterson; however, his completed values tended to be larger than Dr. Copenheaver and I (Figures 41, 42).

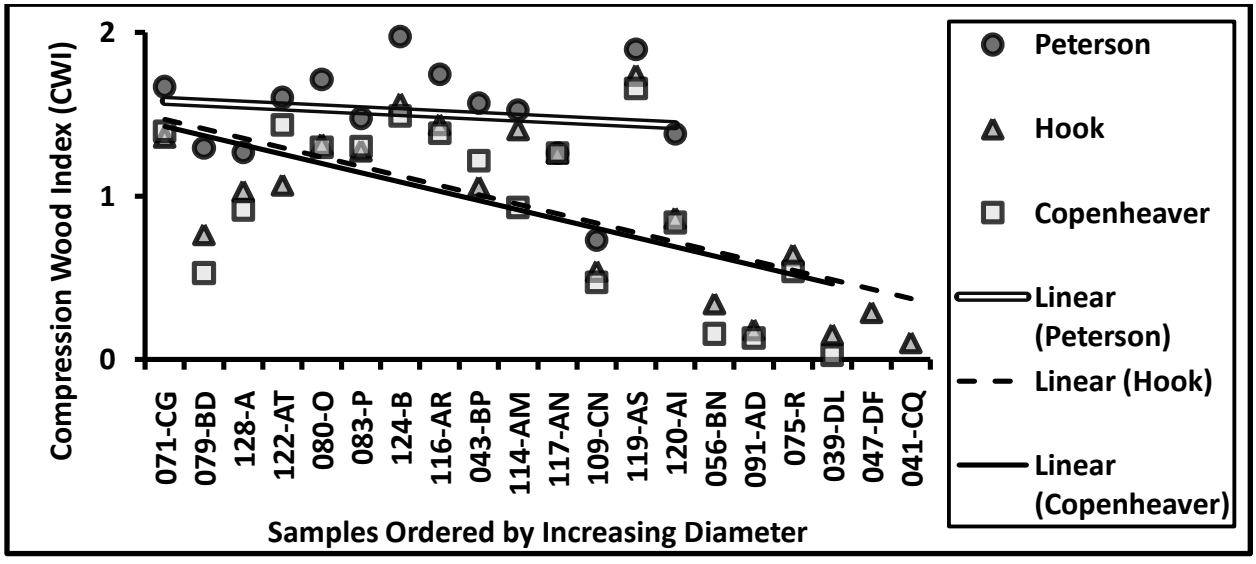

Figure 41. *Scattergraph of compression wood index values for samples ordered by increasing diameter. Trend lines indicated for each observer.*

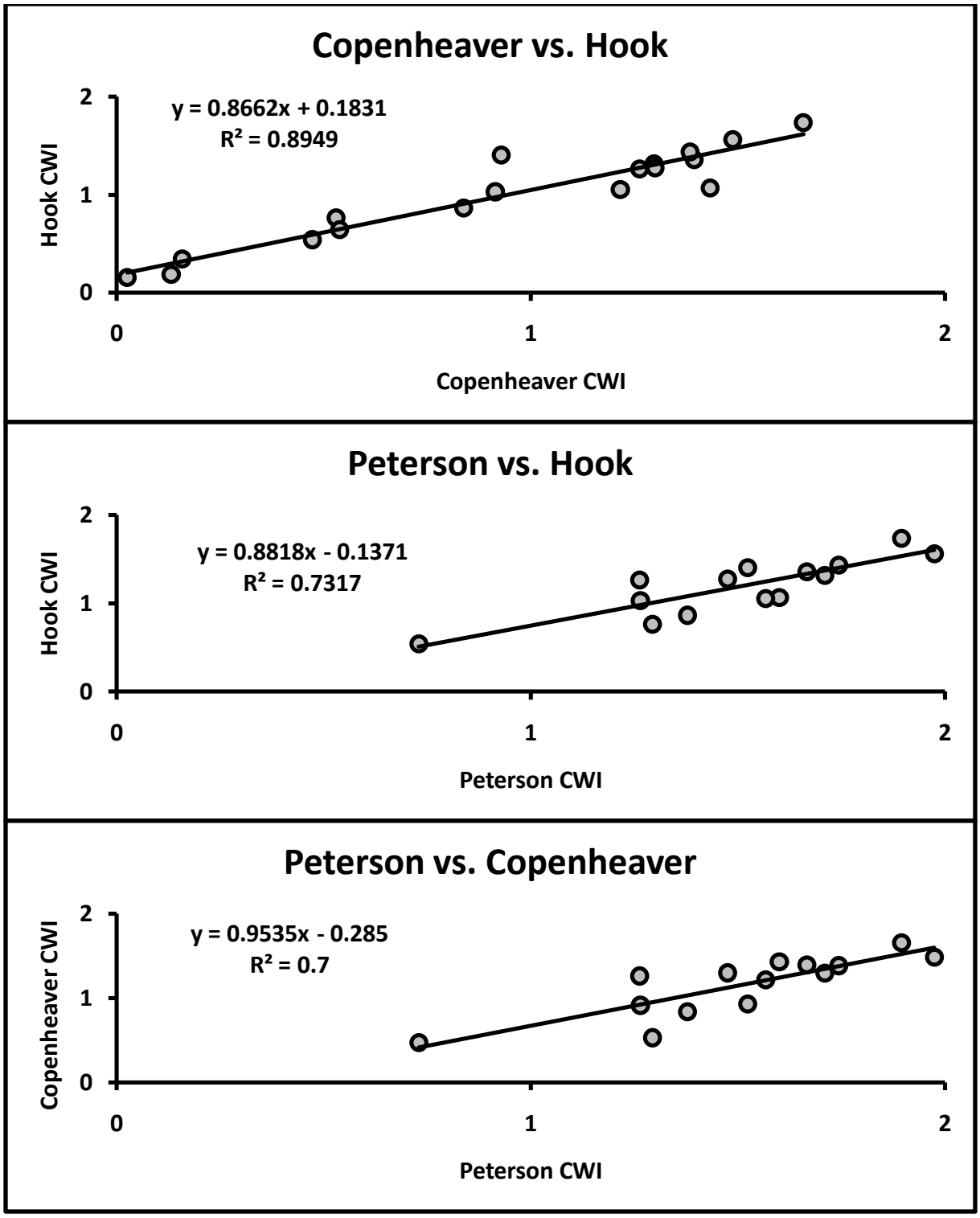

Figure 42. *Correlations of CWI ratings among three observers. Mr. Hook's and Dr. Copenheaver's CWI ratings had high correlation. Lower sample size was the primary reason for low correlations between Mr. Peterson and other observers.*

Appendix B2: Comparison of Compression Wood Index (CWI) and Photoshop Methods

Like the measures of percent compression wood obtained through Photoshop image analysis ($\%CW_R$ and $\%CW_D$), CWI is a relative measure of compression wood area in a sample. Therefore, CWI is better at predicting relative compression wood than actual compression wood in a tree-ring or disk. When comparing CWI individual ring grades with $\%CW_R$ for each tree-ring, a high Pearson's correlation coefficient was found ($r = 0.890$, $P < 0.001$); as well as when comparing total disk CWI with $\%CW_D$ ($r = 0.826$, $P < 0.001$). Correlations were weaker between ring grades and actual compression wood area, but still significant (CW grades v. CW increments: $r = 0.604$, $P < 0.001$; CWI v. CW cumulative: $r = 0.355$, $P < 0.001$) (Figures 43, 44).

Actual compression wood area could be estimated from relative area if a tree's basal area was known. For instance, if the total basal area of a tree was 100 cm^2, and the CWI was 1.5, you could use the trend line in Figure _ to estimate that 20% (± 10%) of the sample's cross-sectional area was compression wood or 20 cm^2 (± 10 cm^2). Granted, this would be a very rough estimate, but would be much more time-efficient than detailed image analysis. Of course, a simpler image analysis that did not focus on every tree-ring but the total compression wood area vs. total basal area would be much quicker to process. Then to find the volume of compression wood within a log, you could take the integral of cross-sectional area measurements of compression wood (Husch, Beers, and Kershaw 2003):

$$V = \int_a^b A(X)dX$$

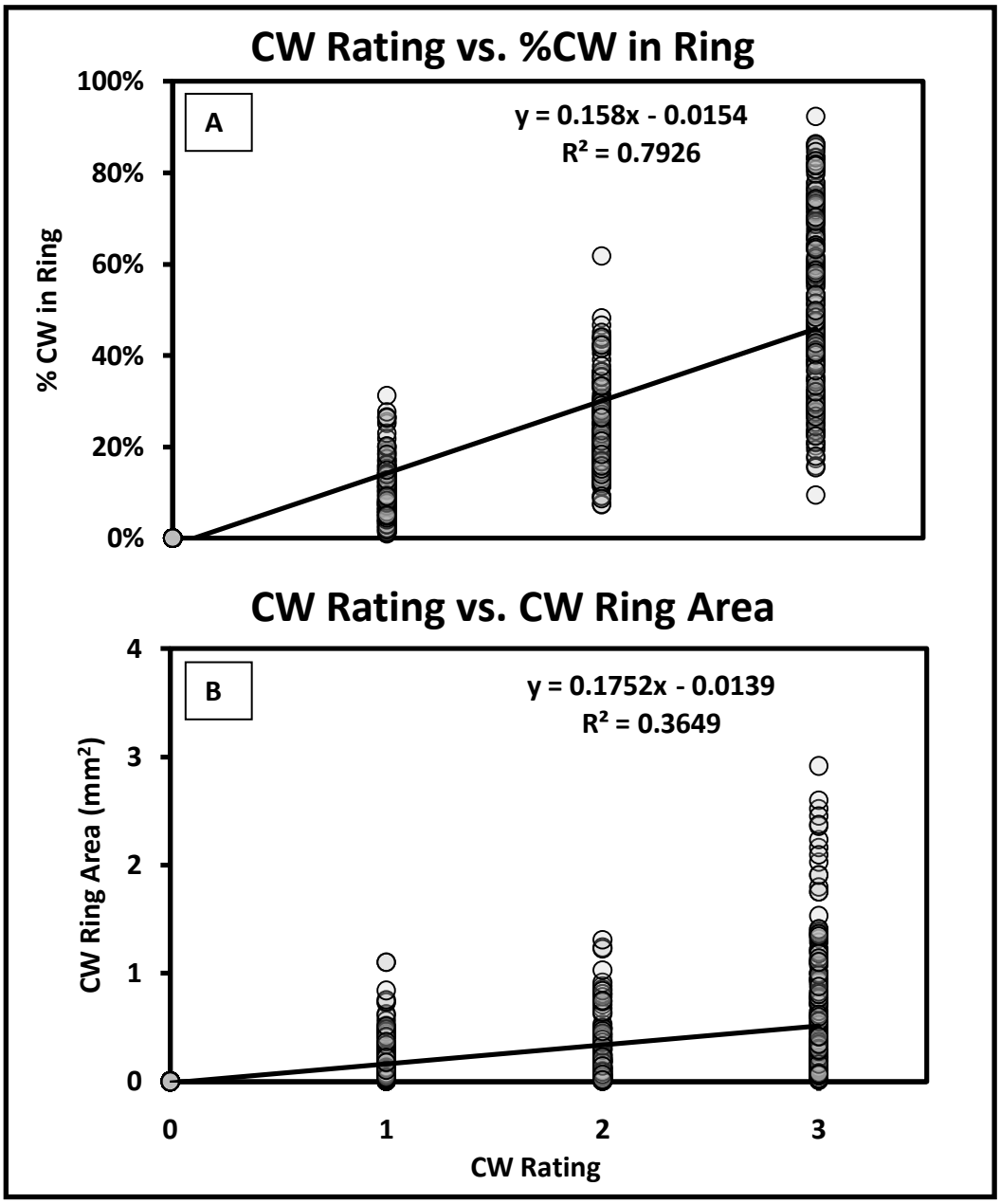

Figure 43. *Compression wood ratings vs. %CW in ring* ***(A)*** *and CW ring area (mm^2)* ***(B)****. Each dot represents a tree-ring (n = 1518) from 42 total trees.*

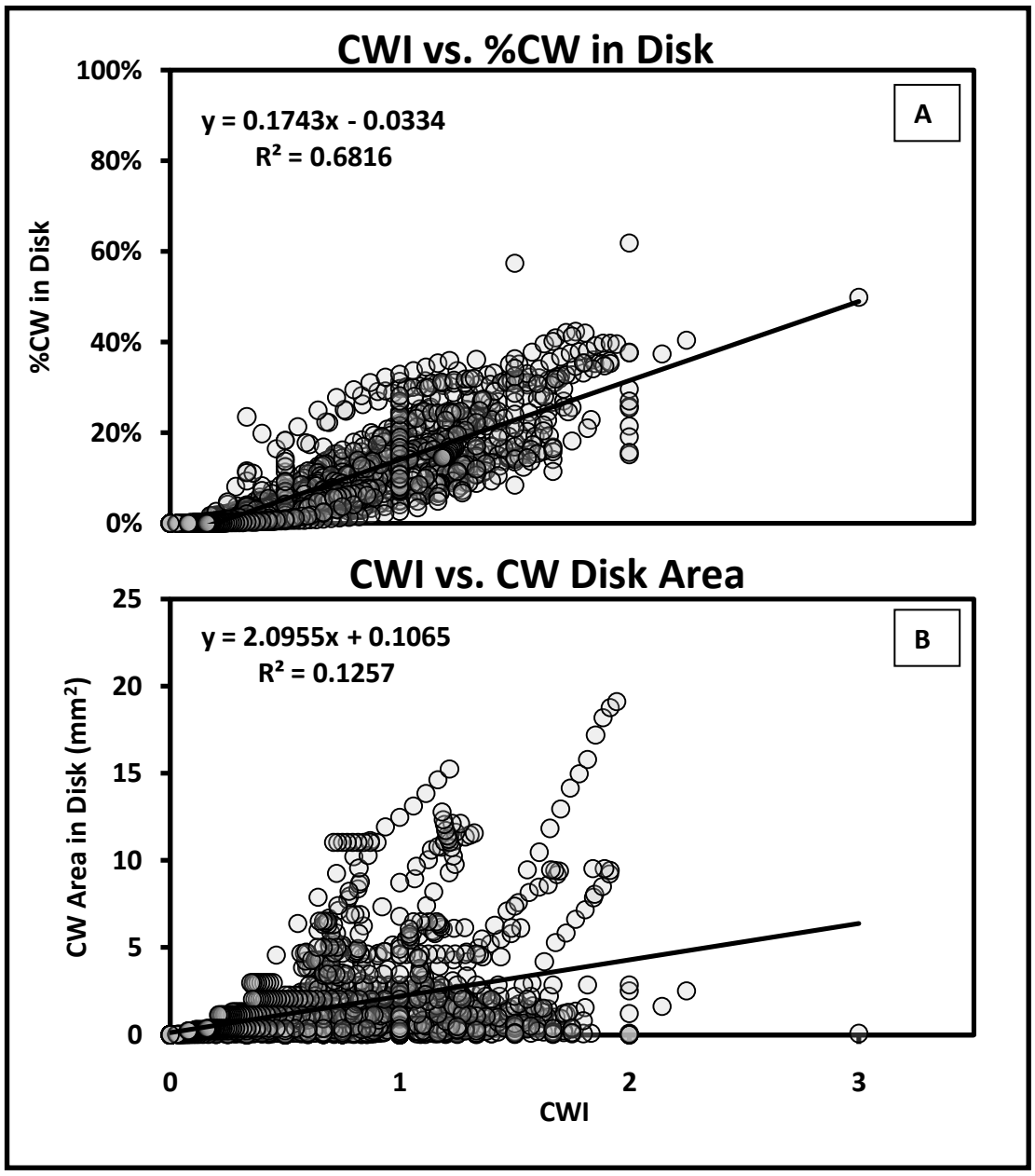

Figure 44. *Compression wood index vs. %CW in disk* ***(A)*** *and CW disk area (mm^2)* ***(B)****. Each dot represents a tree-ring (n = 1518) from 42 total trees.*

Appendix B3: Results of Compression Wood Index

Because the CWI method is a relative measure of compression wood, visually scaled against tree-ring size, graphs of each independent variable vs. mean CWI closely resemble graphs of those same independent variables vs. mean compression wood ring percentage (Figures 45, 46, and 47). Therefore, the CWI method could be applied and then a log volume factor incorporated to estimate the amount of compression wood in a given sample of wood.

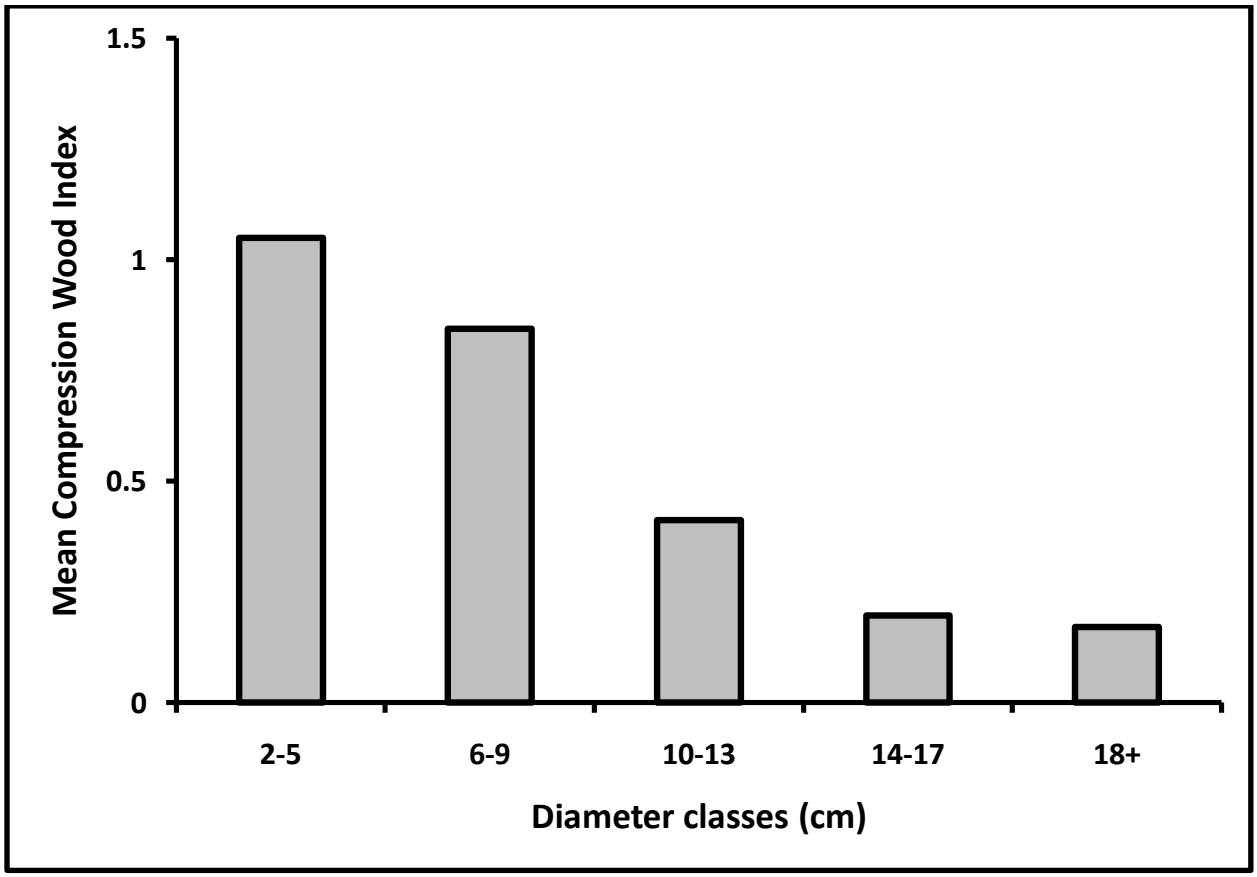

Figure 45. *Mean compression wood index by diameter class.*

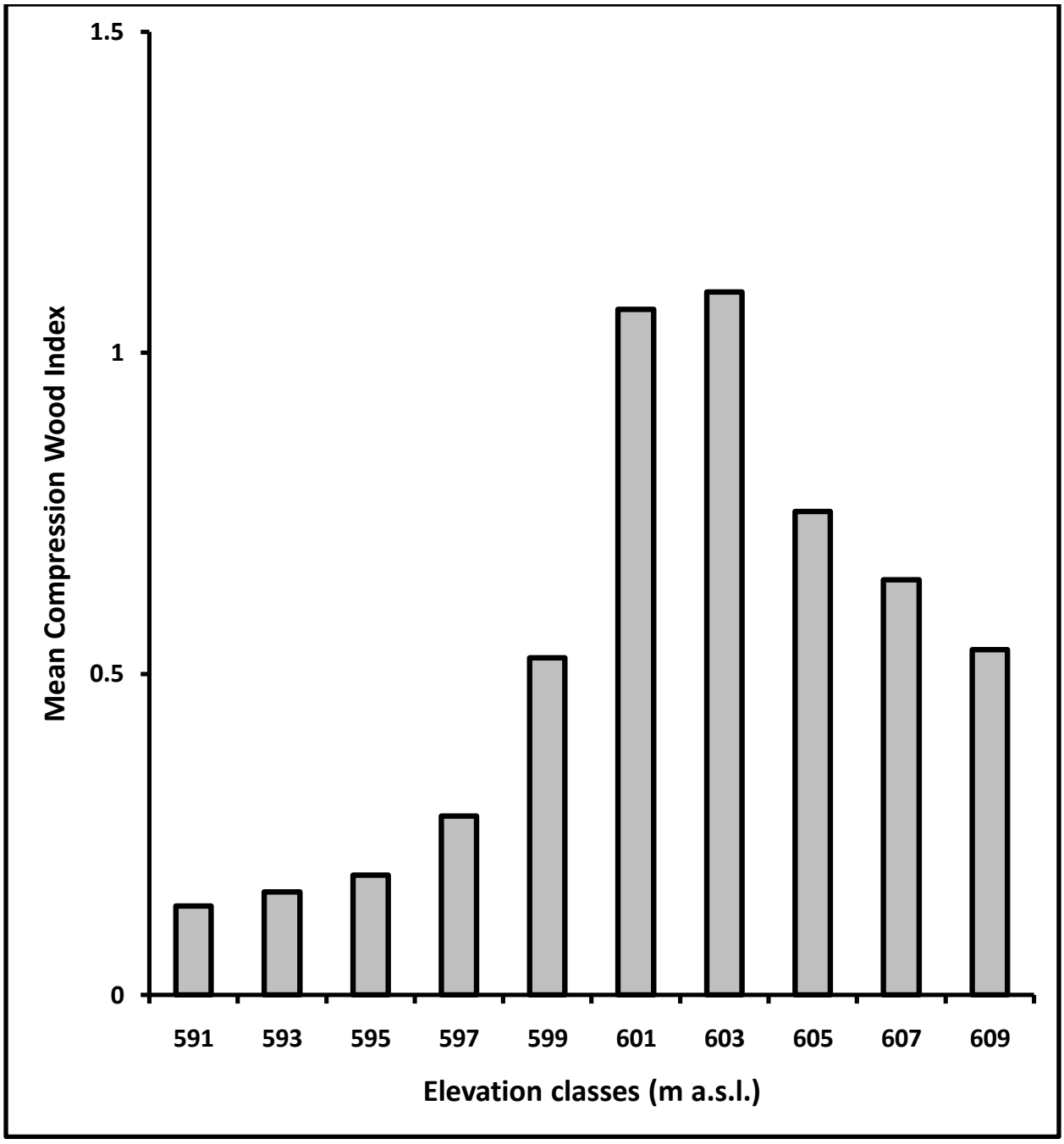

Figure 46. *Mean compression wood index by elevation class.*

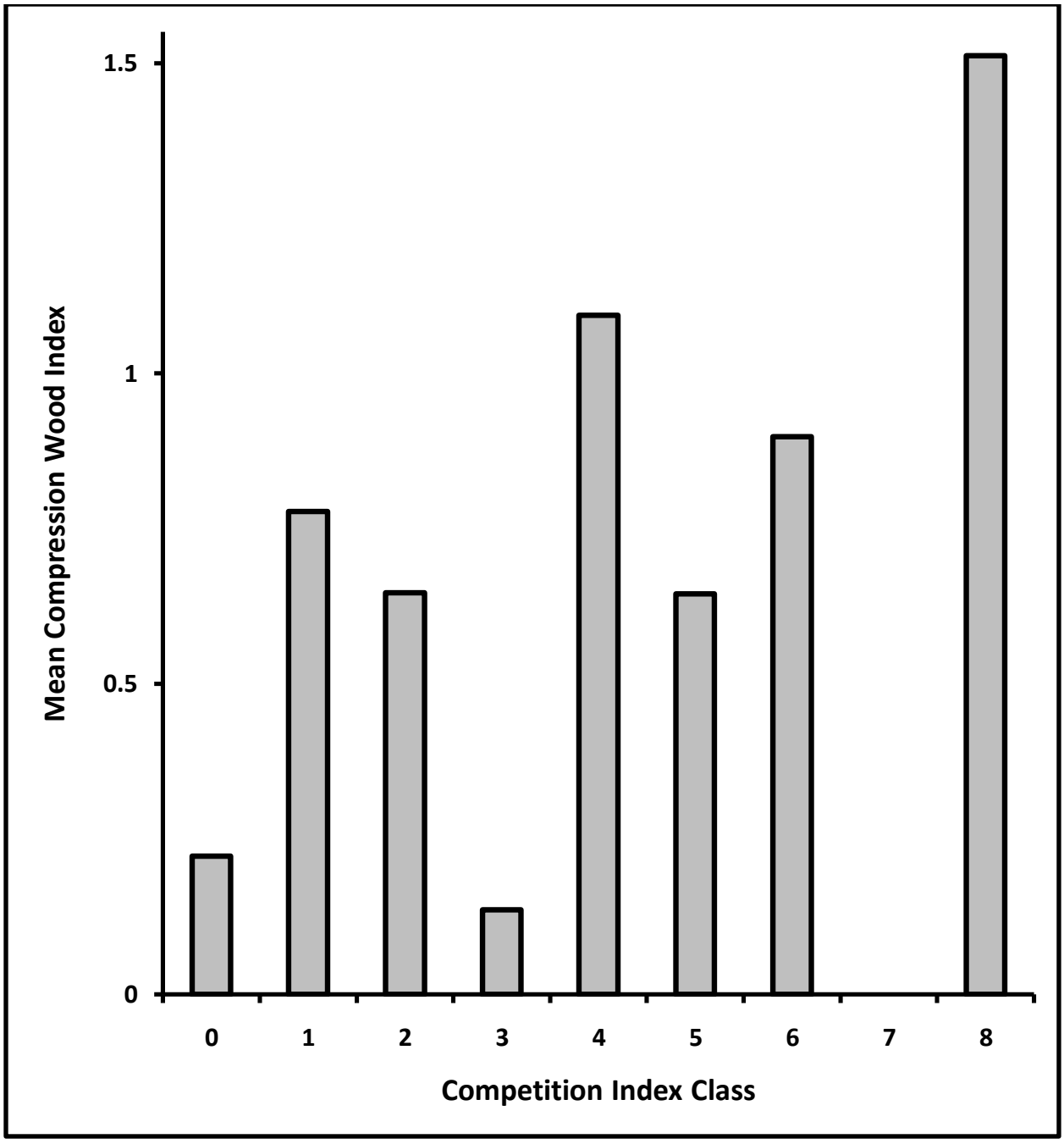

Figure 47. *Mean compression wood index by competition class.*

APPENDIX C: MICROSCOPIC IMAGE ANALYSIS

Appendix C1: Randomization Procedure for Sample Choice

Randomization procedures were used to minimize bias in microscopy work. For images using 25 to 100-x magnification, three ring-width "transects" were randomly established within each tree-ring. First, the image was oriented such that earlywood growth was on the left side of the computer screen, and latewood on the right side. Then the vertical length of the EW/LW boundary on the left side of the screen was measured and multiplied it by three random numbers (0 – 1 random number generator in MS Excel). This produced three random locations from which to start each transect (A, B, and C). A similar method was used to select three random cells on each transect for measurement of tangential cell diameter. In this case, the length of each transect used as the length modifier instead of the EW/LW boundary length. For images of 400-x magnification, a similar randomization procedure was used. In this case two random numbers were generated for 3 cells per image, using image height and width as modifiers for random (x, y) cell coordinates. Three random points were identified for each 400-x image, and the tracheid closest to each random point was measured (A, B, and C).

Appendix C2: Comparison of Cell Measurement Methods

As in the macro-image analysis, different measurement methods of tracheids yielded different results. Perimeter measurements of outer tracheid diameter were significantly different and systematically higher than linear-based measurements for the same reason that perimeter-based measurement inflated tree-ring measurements ($t = 5.559$, $P < 0.001$). In this graph you can see the positive relationship between tree diameter and cell diameter on this site, as well as the systematic measurement inflation in perimeter-based measurements (Figure 48). However, another possible reason for the deviation is that 25-x linear-based measurements are based on mean radial cell diameter, which includes latewood cells which are flattened radially, and latewood cells were avoided in the 400-x measurements.

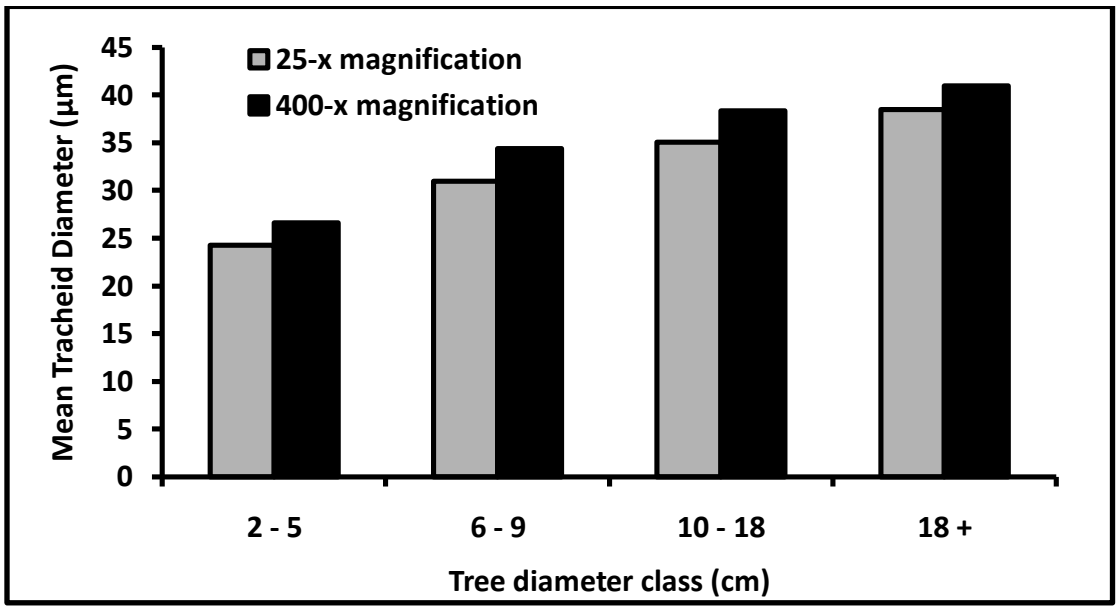

Figure 48. *Mean tracheid diameter by diameter class at 25-x and 400-x magnification.*

Appendix C3: Relationship of Mean Tracheid Diameter and Tree Diameter

Discovering that cell size was related to tree size, tree diameter was plotted against mean cell diameter (μm) within each tree-ring examined. Overall, an increasing logarithmic relationship was found, suggesting that better growing conditions allow greater cellular growth which allows greater tree growth. However, there is an upper limit to cell diameter growth which is why the curve begins to taper off with increasing diameter (Figure 49).

When tree-ring width is used on the x-axis rather than tree diameter, average radial diameter showed a similar pattern, but rings containing compression wood diverged from normal wood rings. The data were grouped by five classes based on sample location within the stem, and the compression wood rating given to each tree-ring: Severe compression wood (grade 3), Moderate compression wood (grade 2), Mild compression wood (grade 1), Normal Wood (grade 0), and Opposite Wood (uphill side of stem). While cell size increased with ring width severe compression wood showed a reduced cell size (Figure 50).

Using these same wood type classes and placing the number of cells in a radial file on the y-axis and ring width on the x-axis also shows a divergence between compression and normal wood, with a bump in cell counts in the 2 – 4 mm ring width range due to severe compression wood formation. Cell counts in moderate compression wood were intermediate between severe compression wood and normal wood (Figure 51).

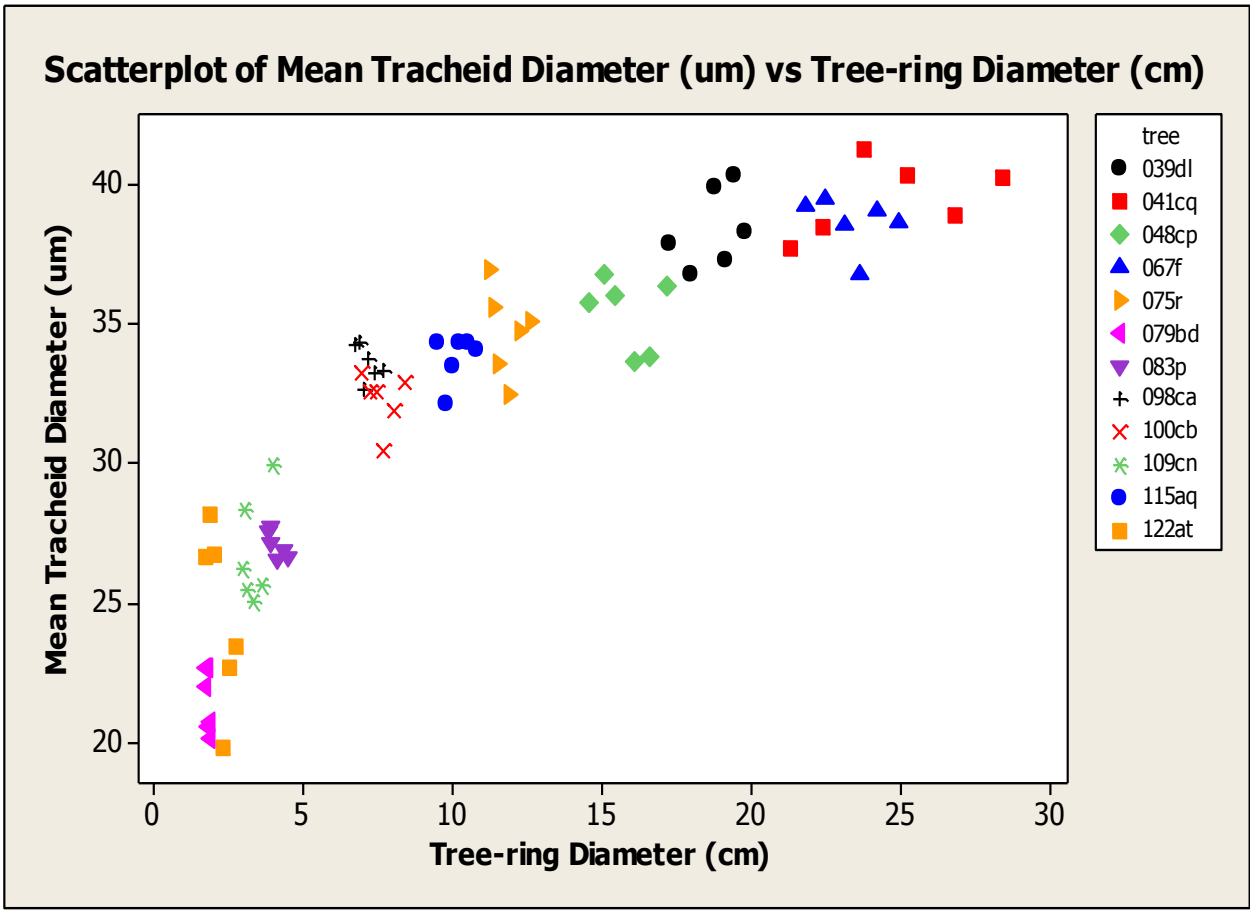

Figure 49. *Mean tracheid diameter by tree-ring diameter. Each point represents the mean radial tracheid diameter in six years (1991 – 1996) examined P. strobus (n = 12) which were relatively equal in cambial age.*

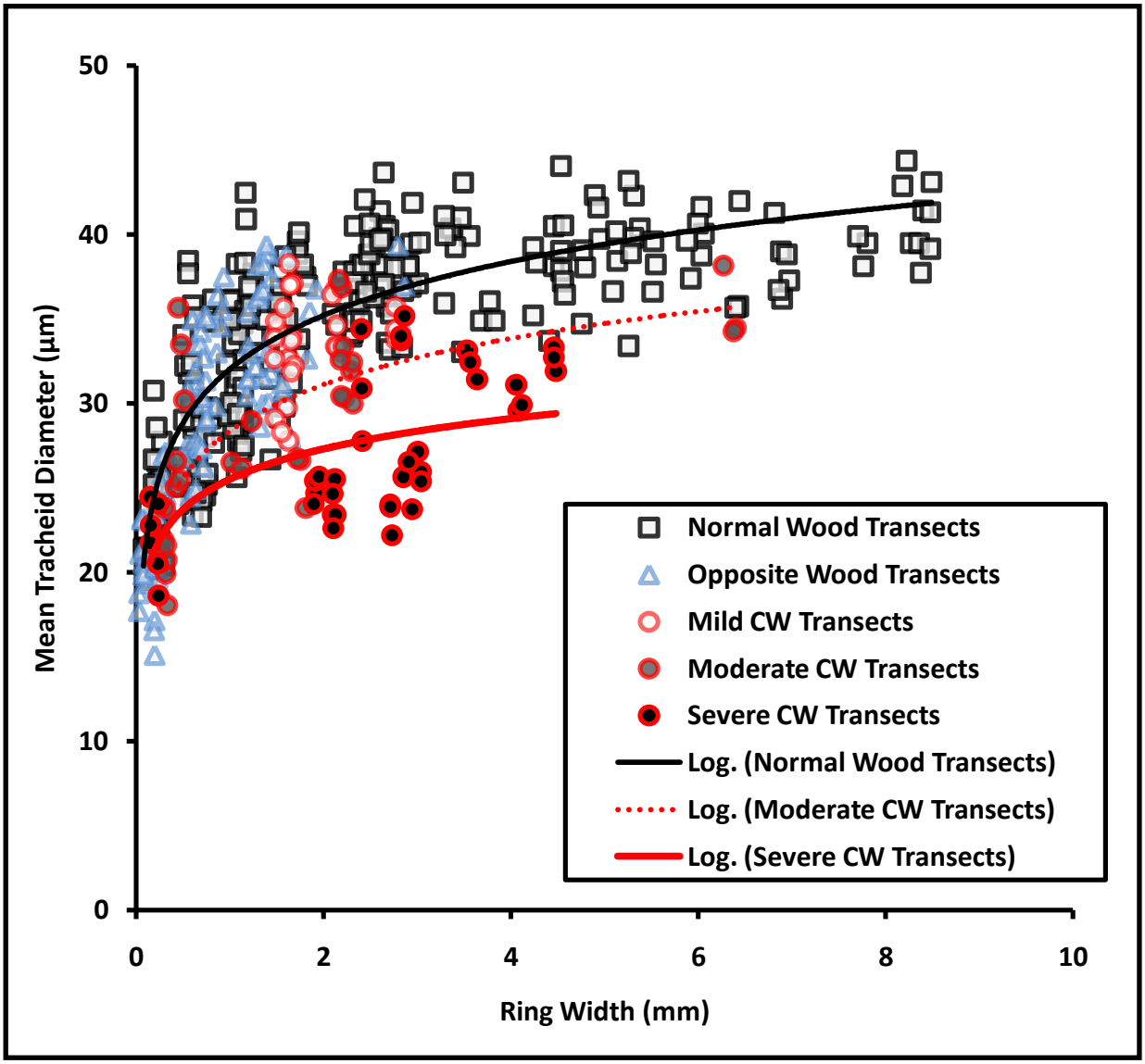

Figure 50. *Mean tracheid diameter by tree-ring width. Each point represents the average cell diameter in all cells in a radial file (ring transect) within each tree ring examined.*

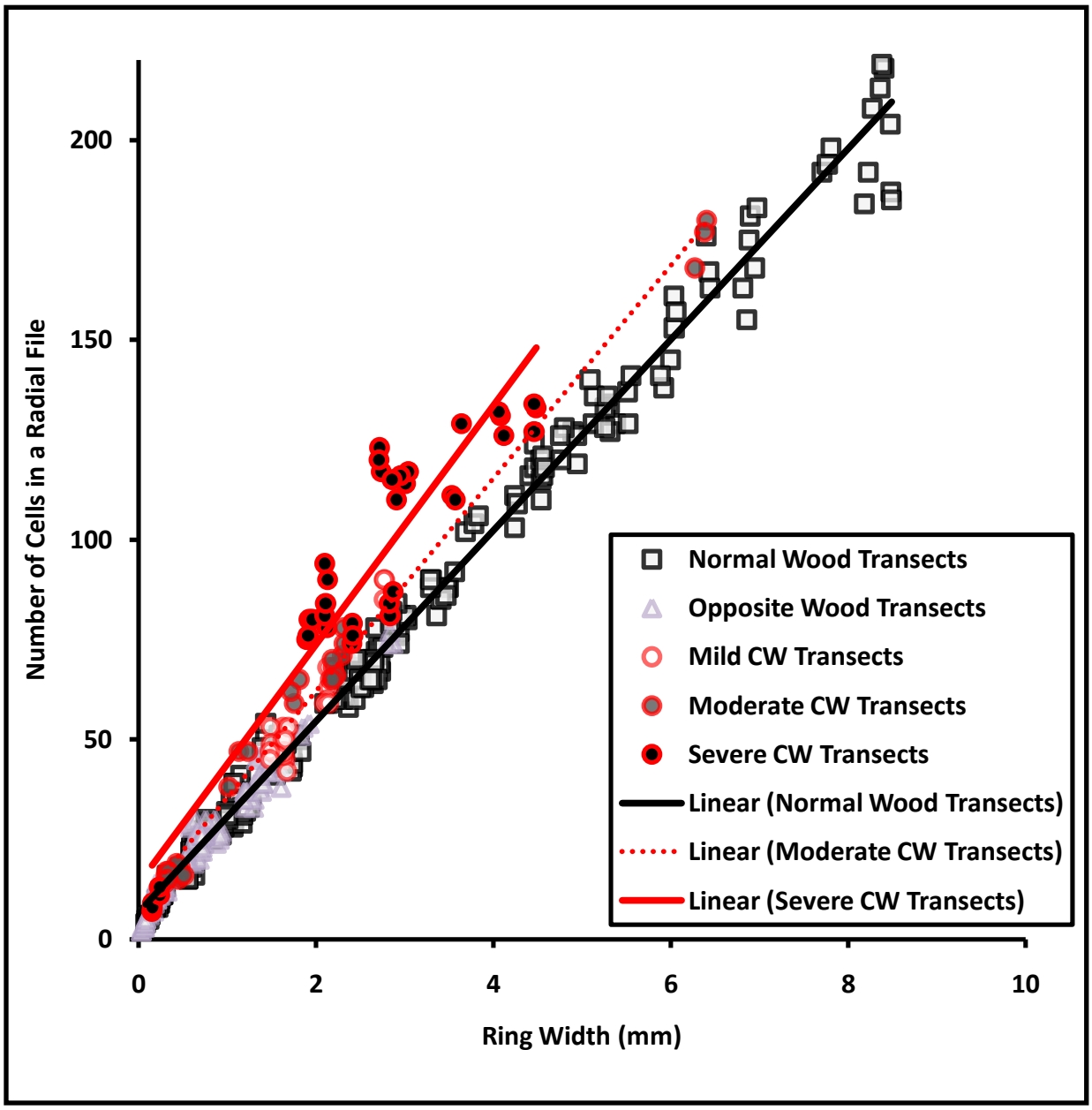

Figure 51. *Each point represents the total number of cells in a radial file (ring transect) by tree-ring width within each year examined.*

Appendix C4: Cell Geometry

The circularity of compression wood cells was significantly higher than all other cell types measured (0.92). However, circularity is sort of an abstract concept, so I decided to find circularity values of various equilateral (and equiangular) geometric shapes, and compare them to the cellular means (Table 10). Normal tracheid cross-sectional shape is usually described as boxy-to-hexagonal, and opposite wood is described as flattened, and indeed, the mean circularity of both normal and opposite wood cells was between a square and a hexagon, slightly more circular than a perfect pentagon. Compression wood cells, by contrast, were slightly less circular than a perfect heptagon. This increased circularity allows them to bear more weight load than a box-shaped cell. Another interesting but mostly pointless digression is that if you fit a perfect circle inside a perfect square so that only four points are overlapping, the circle occupies 78.54% of that square, which also happens to be the circularity measurement of a square.

Table 10. *Circularity values among equilateral geometric shapes and P. strobus cell types.*

Equilateral Shape	Circularity (0 – 1)	Cell Type and Mean Circularity (0 – 1)
Octagon	**0.948**	
Heptagon	**0.932**	**CW 0.924**
Hexagon	**0.907**	
Pentagon	**0.865**	**NW 0.867**
Square	**0.785**	**OW 0.87**

APPENDIX D: SPATIAL INVESTIGATIONS

Appendix D1: Direction of Tree Lean

A significantly positive correlation was noted between compression wood direction and the cosine of aspect (r = 0.8693) (Figure). All samples that had noticeable compression wood formation or eccentric radial growth were included in this analysis (n = 101). Those that had no compression wood or those that had no dominant directional trend were not included. Most trees (94%) leaned in the downhill direction, confirming the idea that trees are more likely to bend in the downhill direction when covered with ice (Figure 52). Microtopographical changes in the terrain, such as pit-and-mound topography were found to be a major cause of deviations from this trend.

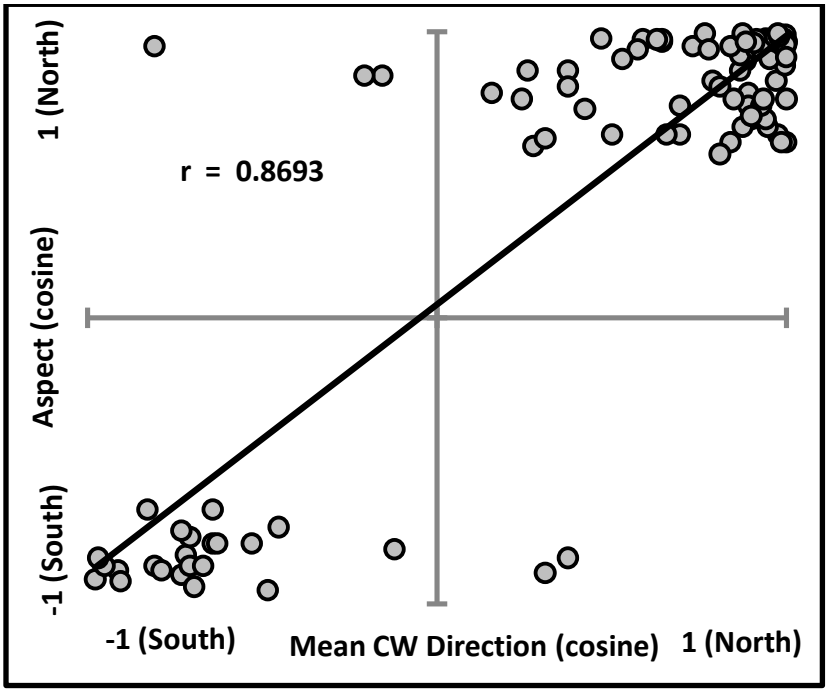

Figure 52. *Compression wood direction (x-axis) is positively correlated with aspect (y-axis), indicating that the direction of mean compression wood formation is downhill. A cosine transformation was used to normalize azimuth data.*

Appendix D2: Competition Index

Because focal tree diameter is the numerator in the equation for competition index (CI), the two variables are negatively related. This is Lorimer's original intention, because smaller diameter trees are more easily influenced by their larger neighbors than vice versa. The correlation between the two variables creates problems, however, when both are used in a regression model. Multicollinearity reduces the predictive power of the model, because the same range in variance is being predicted by both variables. Using the modified competition index classes from the compression wood analysis, we found the mean tree diameter in each class. Due to the negative correlation, smaller competition index classes contained larger trees (Figure 53).

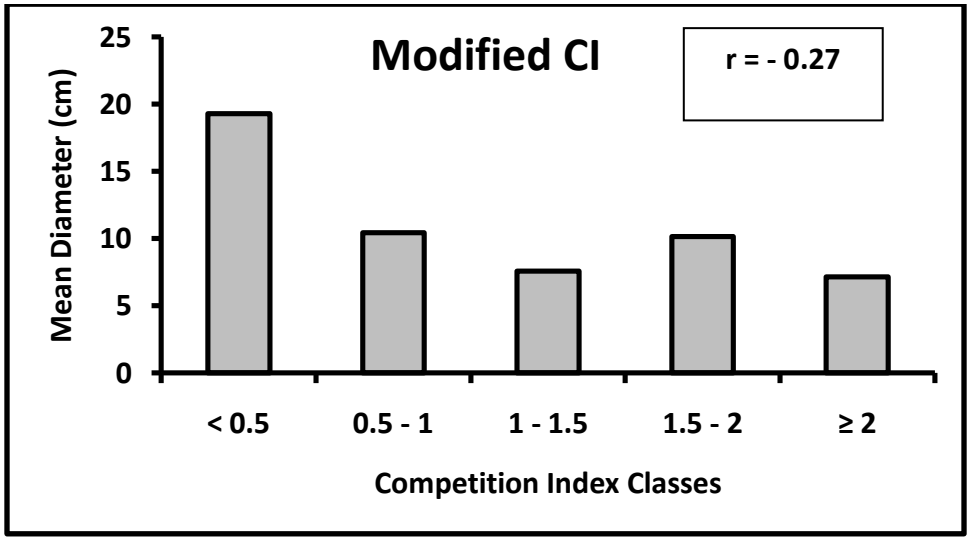

Figure 53. *A significant negative relationship was found between tree diameter and competition index class.*

Using the (x, y) coordinates of all *P. strobus* and their nearest neighbors (including all tree diameter data), we created an Excel spreadsheet that automatically finds the individual competition indices of all trees within a set radius from each focal tree. The search radius can be changed easily to observe changes in the summed CI. Set to a distance of 10 m from a focal tree, we found Lorimer's competition index for all study trees (n = 42) (Figure 54).

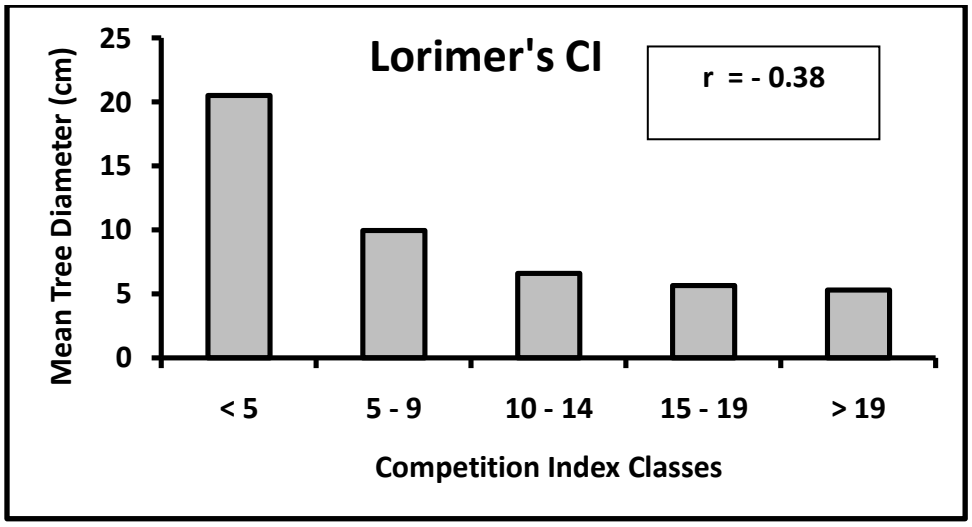

Figure 54. *A stronger negative correlation was found between summed competition index and tree diameter.*

Bear in mind that not all trees on the Fishburn site were originally sampled, so this dataset is not inclusive. However, repeating the same procedure as on the last page with the summed CI shows how summing many individual CI values intensifies the correlation with focal tree diameter (Figure 55). The relationship of CI and compression wood bears a strong resemblance to the relationship of tree diameter and compression wood, and this resemblance increases when CI values are summed.

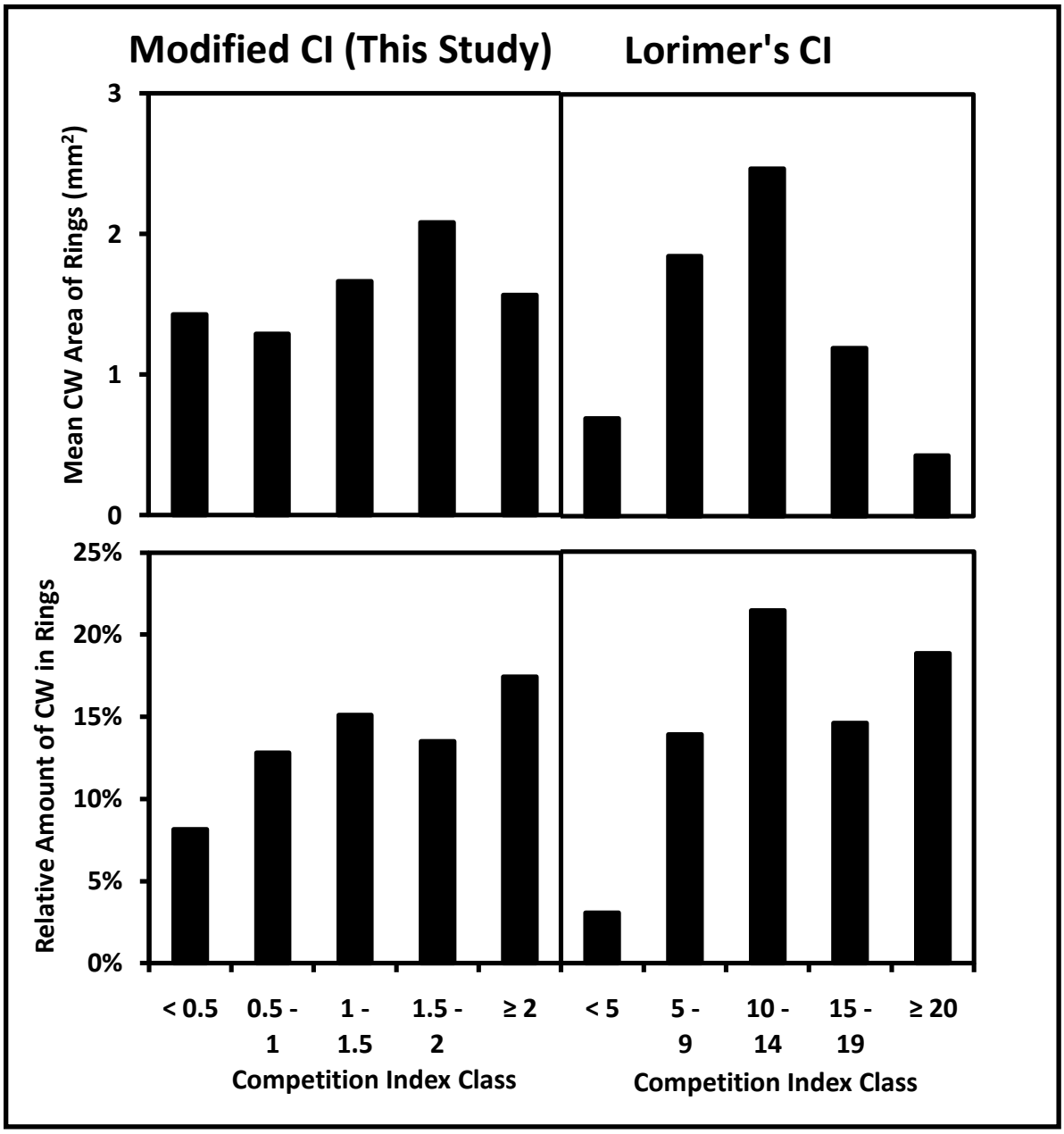

Figure 55. *The modified competition index (CI) used only a single neighboring tree, while Lorimer's original index summed all all CI values for trees within 10 m of a focal tree. The effect of summing many CI's increases its correlation with focal tree diameter.*

Appendix D3: Outlier Diagnostics

Two outliers were identified in the dataset which did not follow the same patterns of compression wood distribution. Upon investigation it was found that both of these trees occurred on very steep slopes (> 60%) and as a result, had formed unusually high amounts of compression wood which were obscuring other patterns among variables. They were removed from the dataset for multiple regression analysis, but a few graphs are included here to show the impact of their removal (Figure 56). Most of the compression wood area in the highest slope class of the graph on the left is from one large diameter tree with high compression wood area. The other outlier was on the southwest aspect, on a very steep slope, and skewed the results heavily due to the small sample size on that aspect.

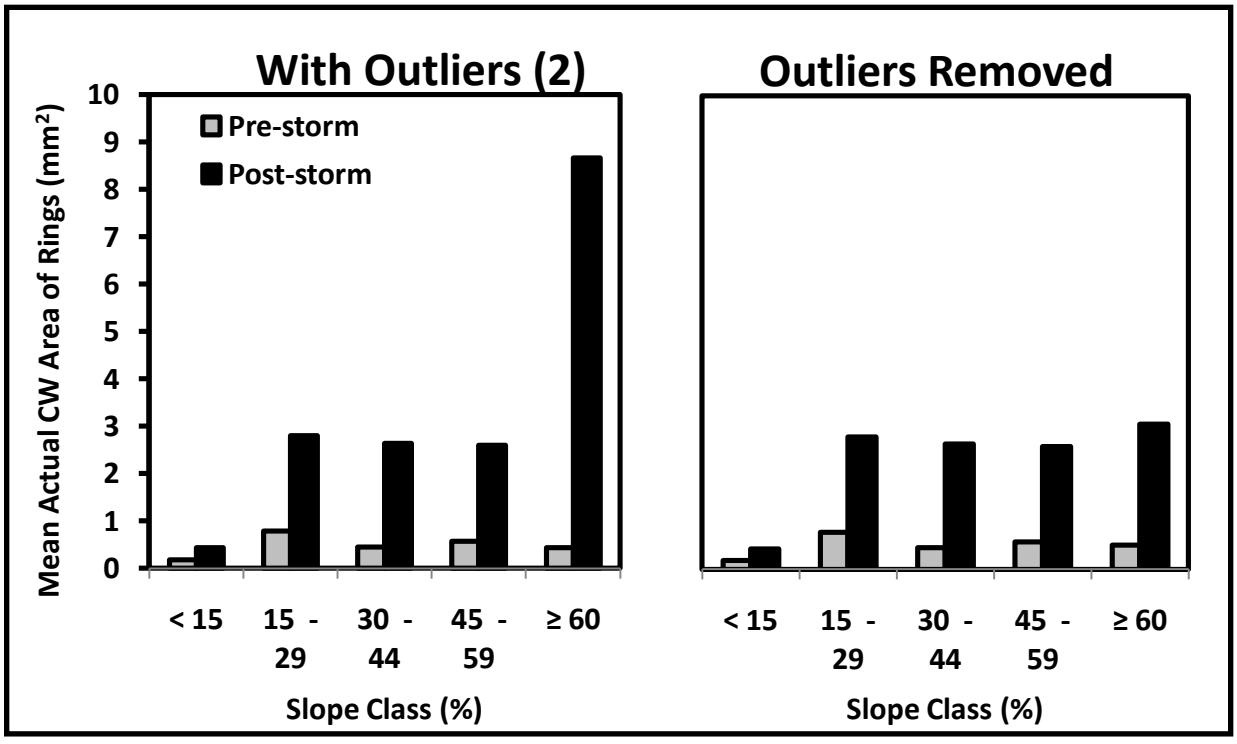

Figure 56. *Amount of compression wood formed by slope percentage class. Two outliers with extreme post-storm CW formation were located on very steep slopes (> 60%).*

APPENDIX E: Detailed Investigations in Compression Wood Formation

Appendix E1: Compression wood formation by diameter class through time

Dividing the trees on the northeast aspect into five diameter classes, and plotting mean tree diameter for every year of the cohort's lifespan, it becomes evident that the 6 – 9 cm (2007) diameter class had the highest post-storm compression wood (mean diameter was 4.6 cm in 1994), followed by the 10 – 13 cm class (mean 1994 diameter was 8.6 cm). This suggests that trees 4 – 8 cm in diameter require greater compressive forces to gain rigidity (Figure 57). It is also interesting to note that the most compression wood following the 1979 ice storm (2.5 cm of ice), formed in the 14 – 17 cm (2007) class, which was in the 4 – 8 cm diameter range at the time of the storm (Figure 57). From this analysis it seems that the 5 – 7 cm range is especially vulnerable to severe compression wood formation. Perhaps the diameter range of this wood is prone to plastic deformation in which cellular bonds are broken and reformed in the bent position, requiring greater compressive force to correct (Keckes et al. 2003).

Examining the same data, but with ring-width increments on the y-axis rather than cumulative tree diameter, we see that ice storms (1979 and 1994) caused growth releases in most diameter classes, except in the 6 – 9 cm (2007) class following the 1994 storm, which declined in mean ring width following ice damage. Relative compression wood area was highest (70%) in this size class and the 2 – 5 cm class, moderate (30%) in the 10 – 13 cm class, and low (< 10%) in tree-rings > 13 cm in diameter. Most juvenile trees (1968 – 1975) formed some compression wood to gain rigidity, but the smallest two diameter classes formed more throughout their lifetime, and extreme amounts after 1994 (Figure 58).

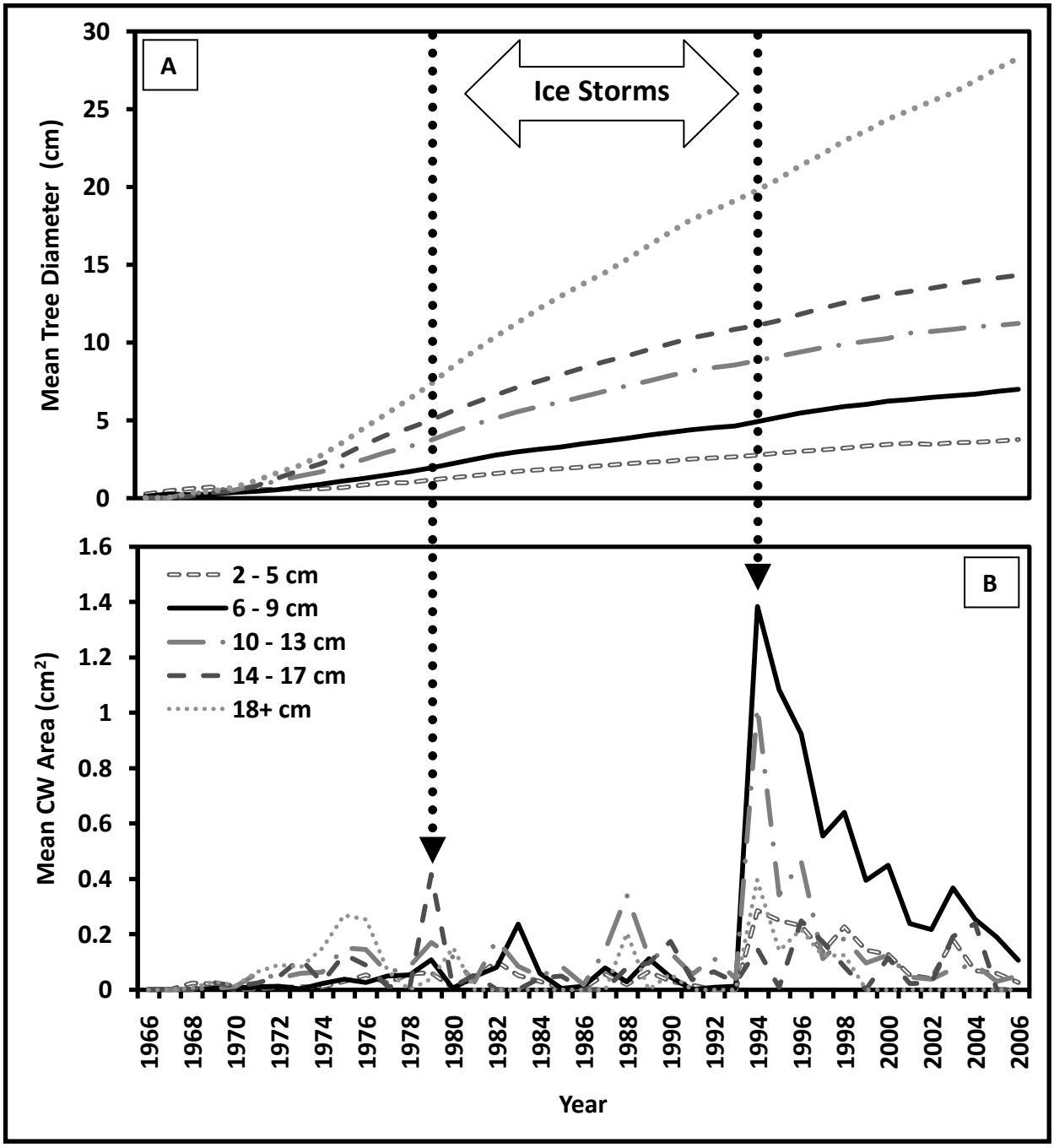

Figure 57. *Mean tree diameter in 5 classes* ***(A)*** *and mean compression wood (CW) area* ***(B)*** *by year. After 2.5 cm of ice was deposited in the 1979 storm, the 14 – 17 cm class (average 4.5 cm at the time) formed the most CW. After 8.5 cm of ice was deposited in the 1994 storm, the 6 – 9 cm class (average 4.6 cm at the time) formed the most CW, followed by 10 – 13 cm class (average 8.6 cm at the time).*

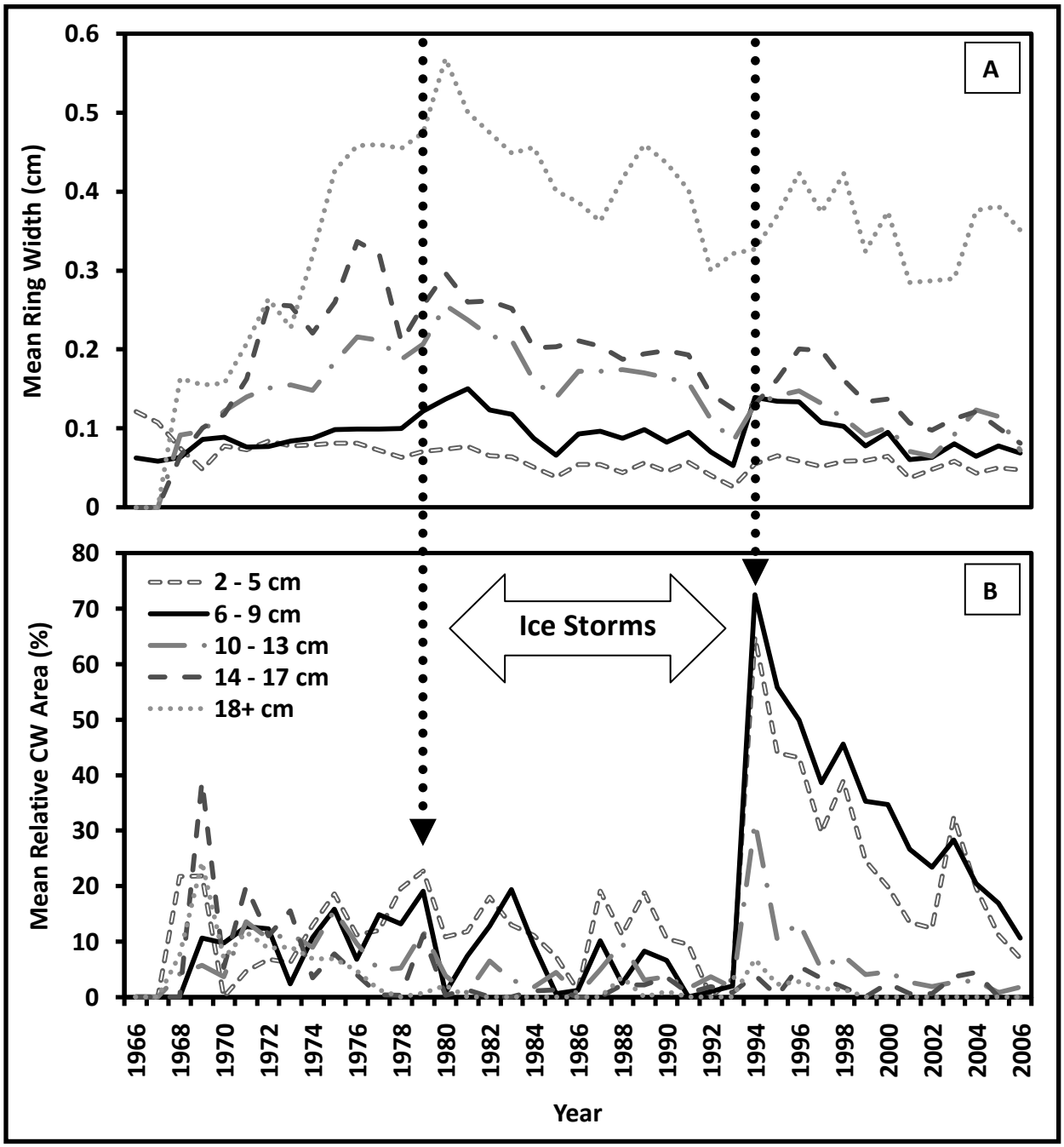

Figure 58. *Mean tree-ring width* ***(A)*** *and relative compression wood area* ***(B)*** *by year.*

Appendix E2: Spatiotemporal analysis of compression wood formation

To produce a general image of compression wood formation in different trees on the northeast aspect through time, we combined data from the three-dimensional stem map with data for total tree-ring cross-sectional area by year, and compression wood cumulative cross-sectional area by year (Figures 59 - 65: Time sequence). A bubble graph was created which contained all of the above data in separate series for each year and wood tissue type (1966, 1966cw, 1967 … 2005cw, 2006, 2006cw). In this graph, the (x, y) coordinates of each *P. strobus* tree on the northeast aspect were entered as (x, y) coordinates on the graph.

Elevation was represented as 1-m contour lines; drawn using z-coordinate data for each tree stem location on the northeast aspect. Bubble size data were cross-sectional area measurements (cm^2) for each series, scaled to 150. Whole tree-ring bubbles were represented as unfilled black circles, while compression wood bubbles were represented as filled red circles within the unfilled black circles, both at the same spatial location.

With all data series included, copies of this graph were duplicated for each year of the cohort's lifespan. The result is a series of identical graphs in every way except that the tree-ring and compression wood areas increase in bubble size as they continue to grow from year to year. Each of 38 consecutive graphs (1968 – 2006) was created in this manner, to observe geographical and temporal patterns in compression wood formation throughout the plot (Figures 59 - 65). See Figure 38 in the text for a more detailed description of the graph.

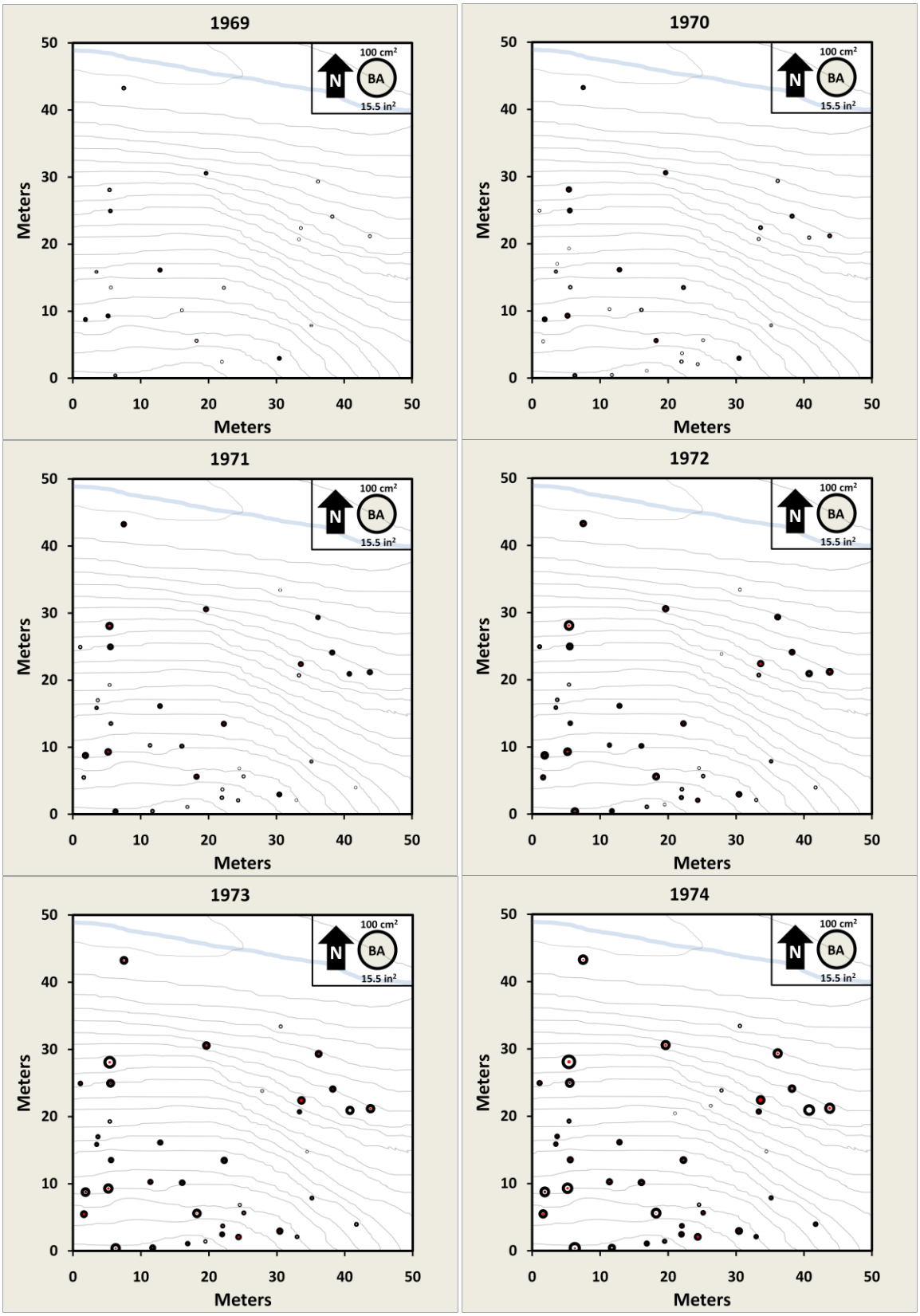

Figure 59. *Spatiotemporal compression wood distribution (1969 – 1974).*

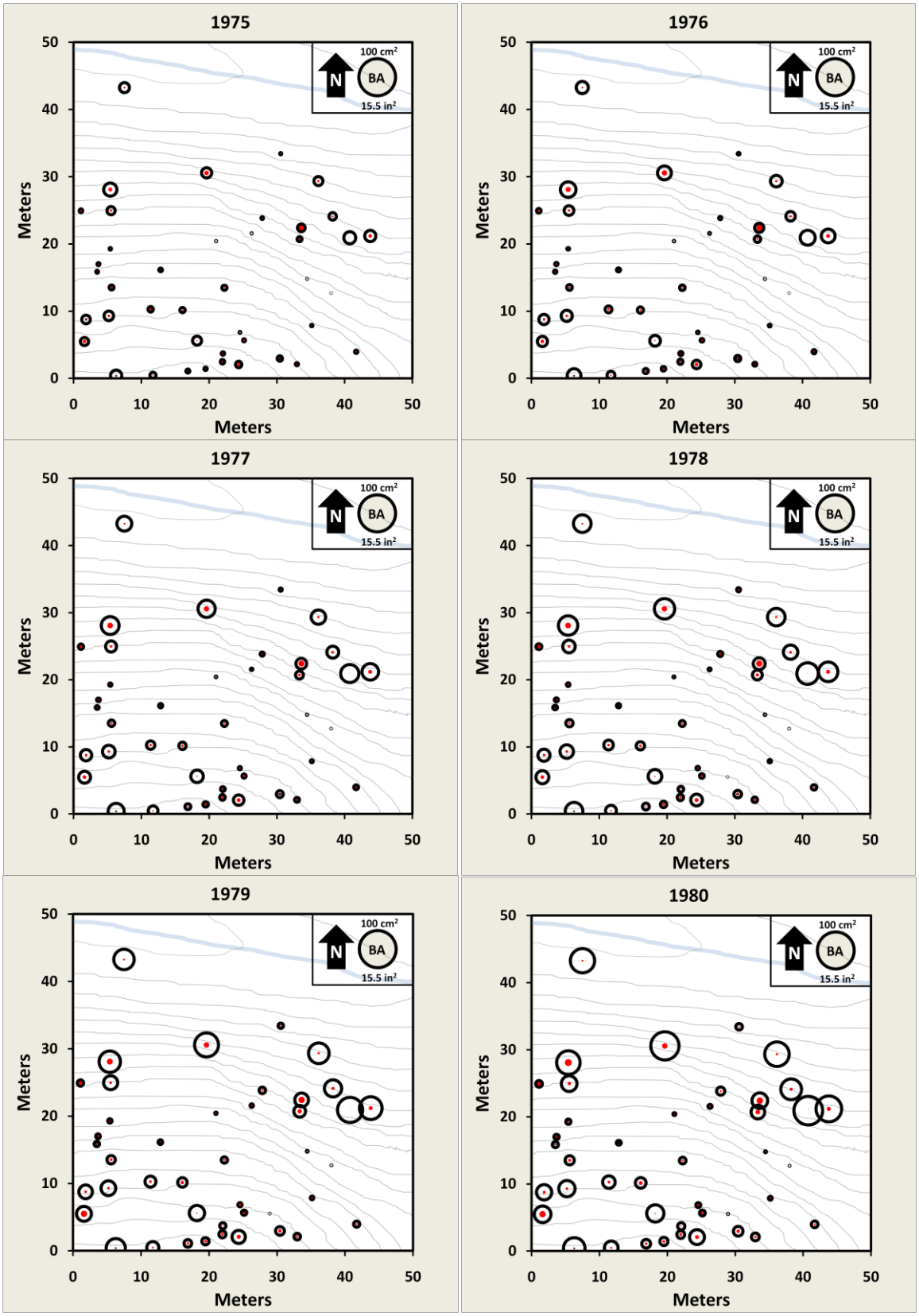

Figure 60. *Spatiotemporal compression wood distribution (1975 – 1980).*

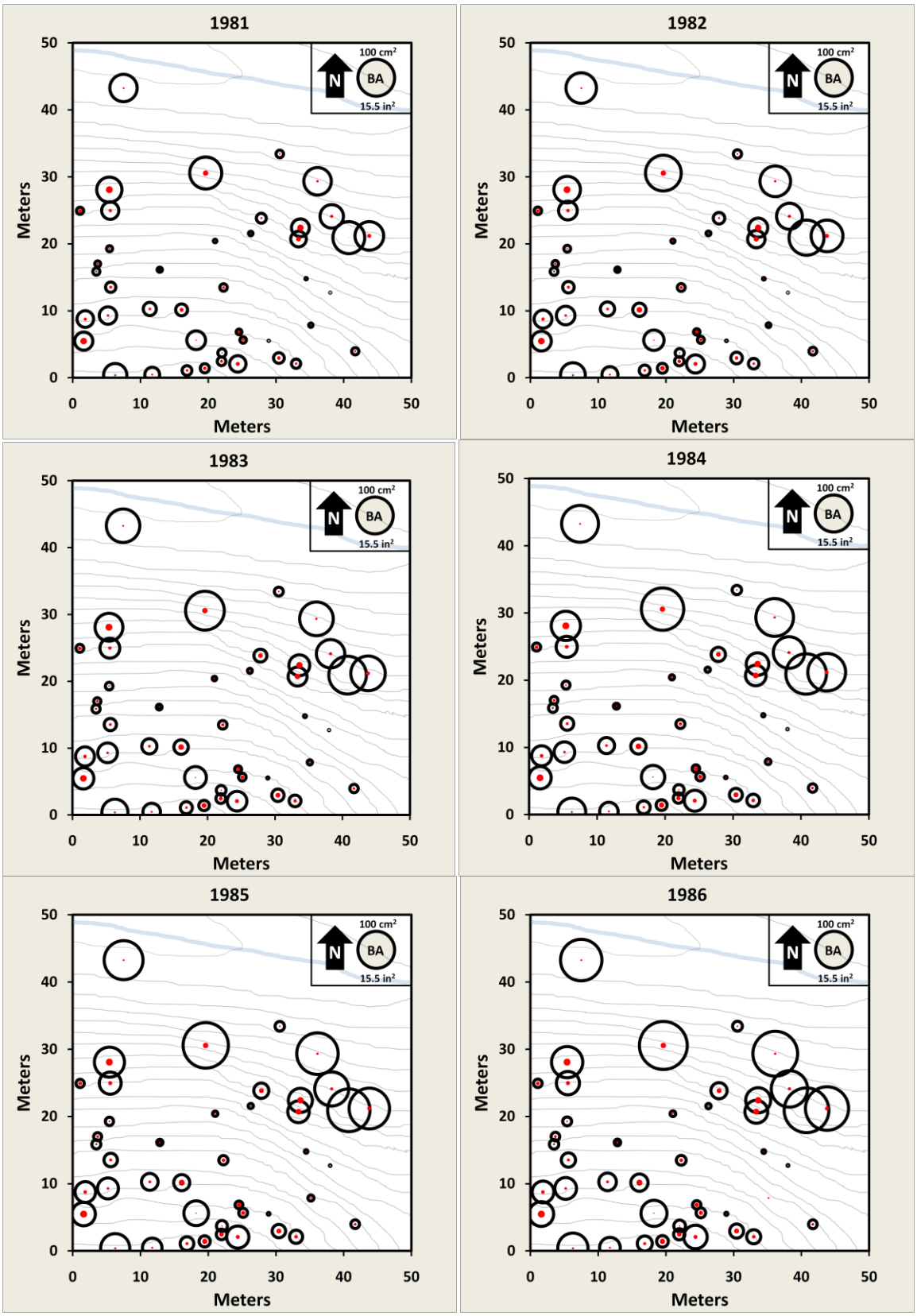

Figure 61. *Spatiotemporal compression wood distribution (1981 – 1986).*

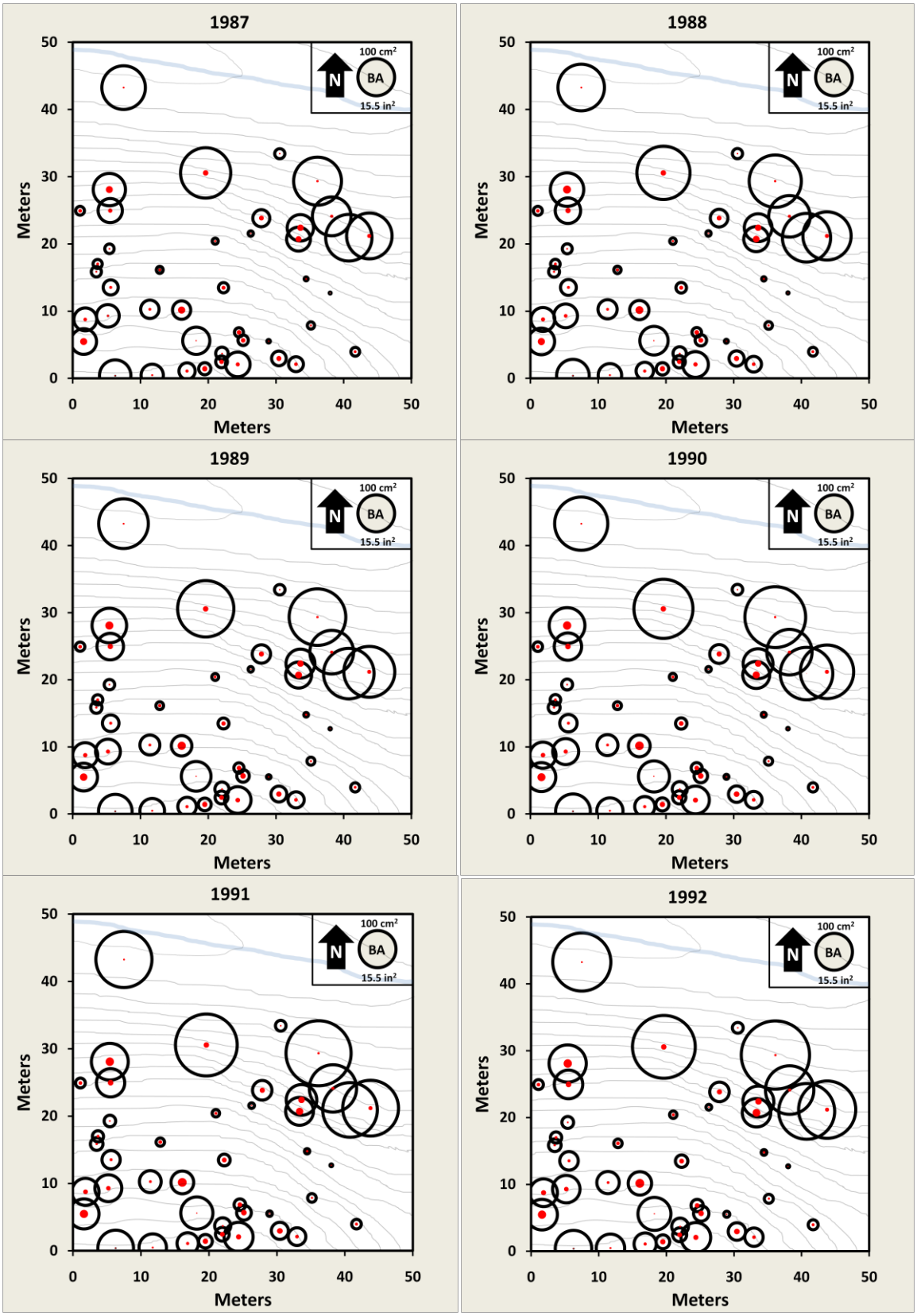

Figure 62. *Spatiotemporal compression wood distribution (1987 – 1992).*

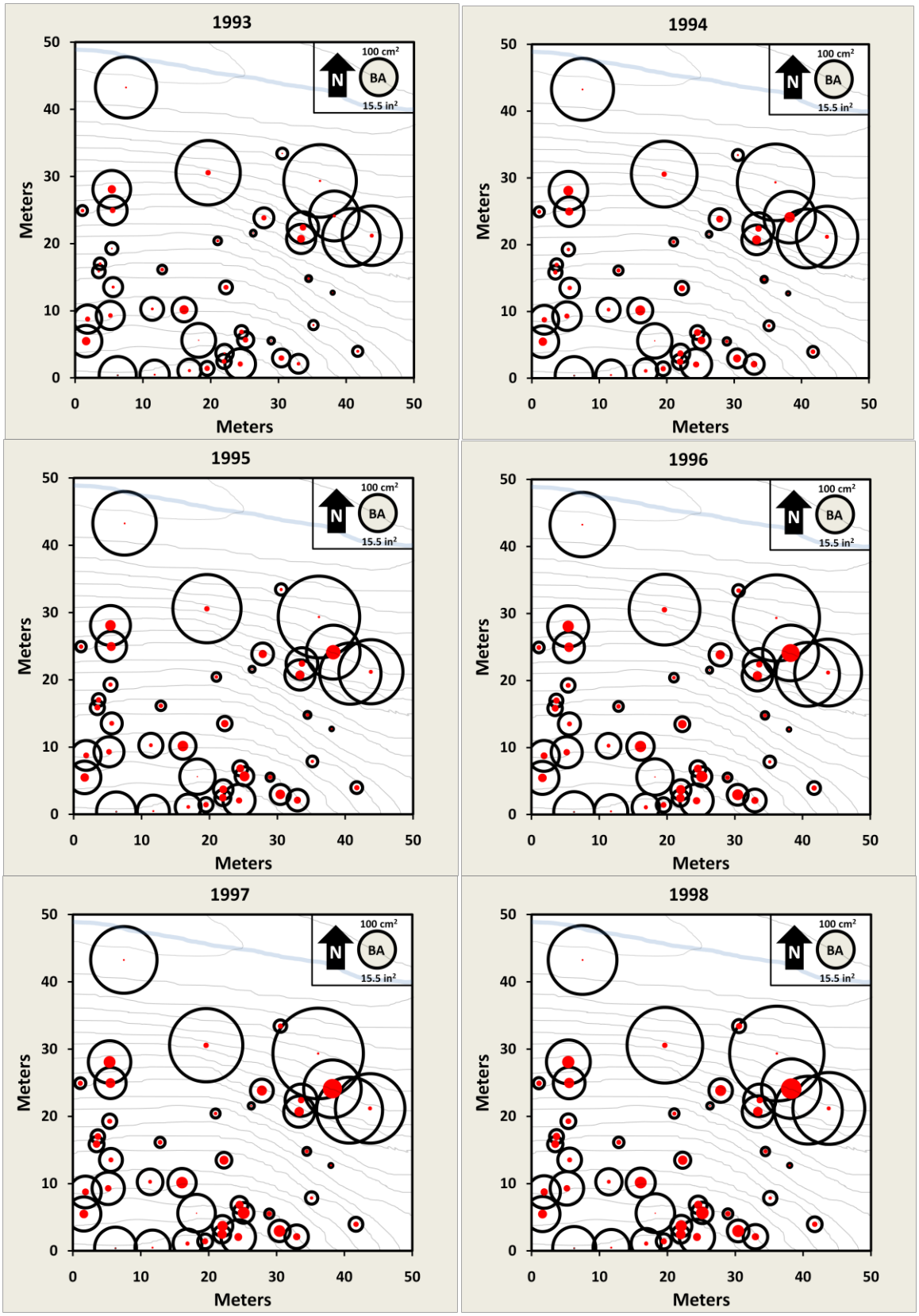

Figure 63. *Spatiotemporal compression wood distribution (1993 – 1998).*

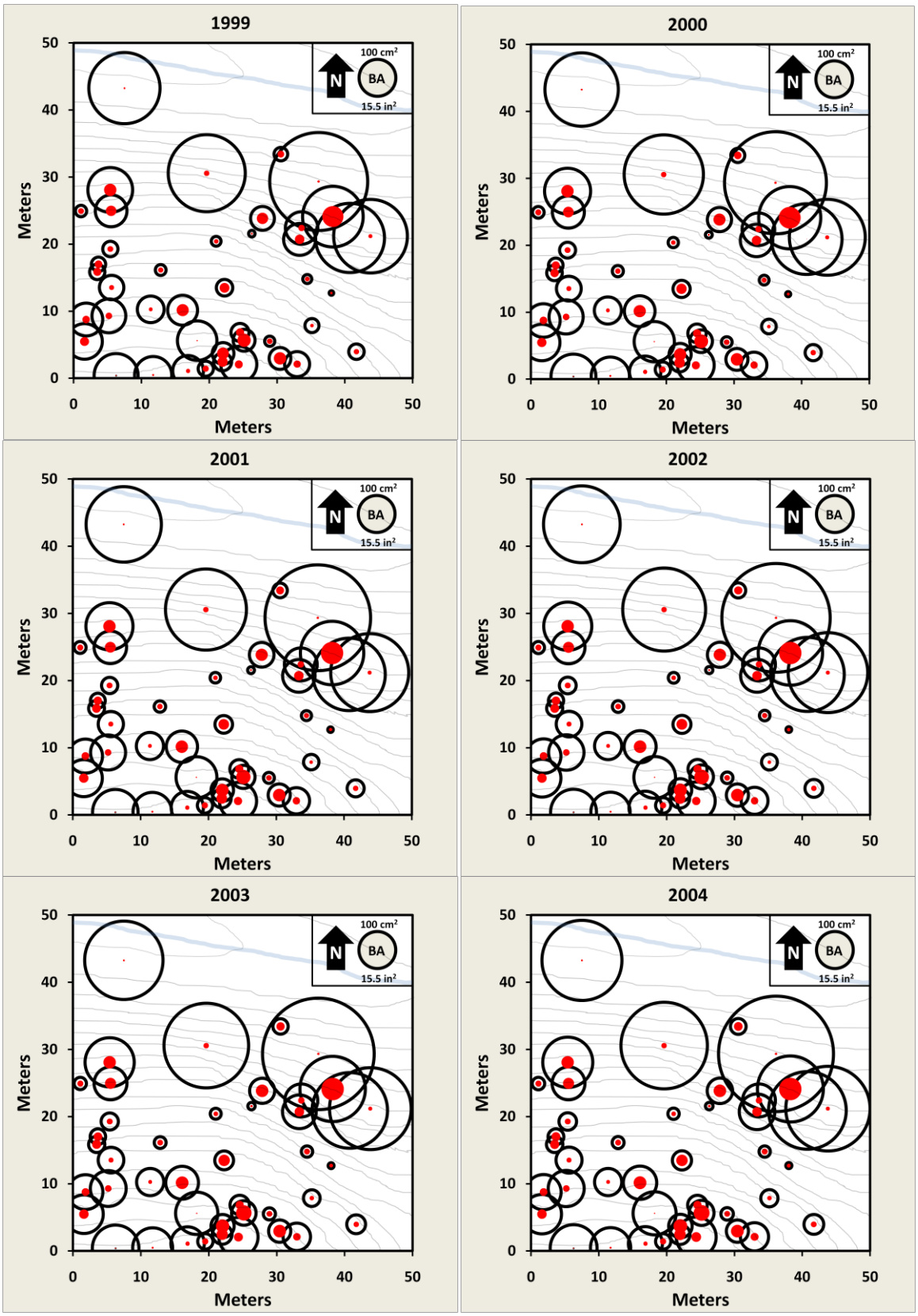

Figure 64. *Spatiotemporal compression wood distribution (1999 – 2004).*

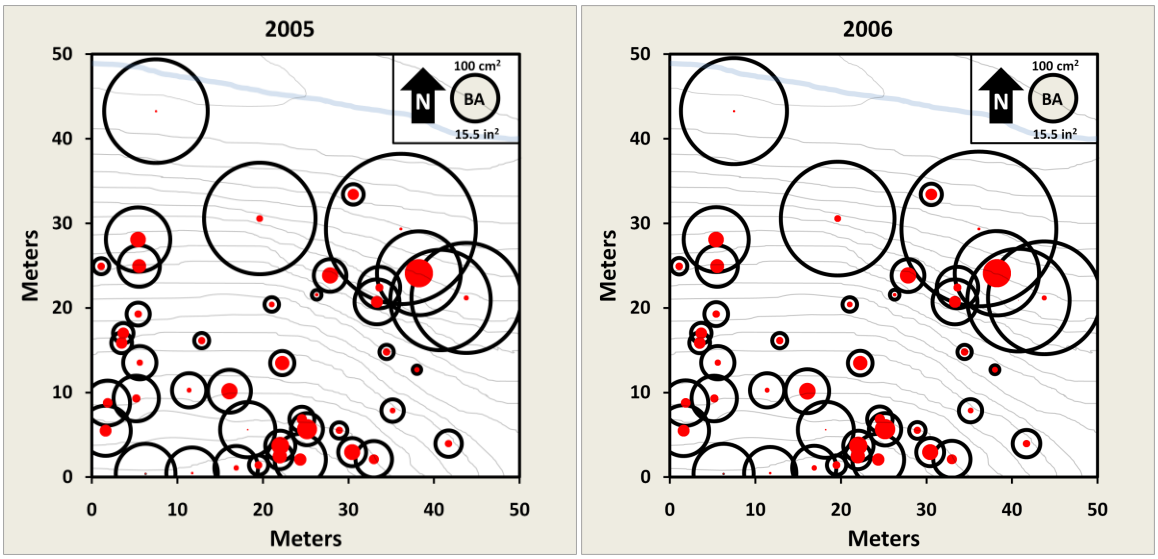

Figure 65. *Spatiotemporal compression wood distribution (2005 – 2006).*